CERN 74-8
10 April 1974

ORGANISATION EUROPÉENNE POUR LA RECHERCHE NUCLÉAIRE
CERN EUROPEAN ORGANIZATION FOR NUCLEAR RESEARCH

TOPICAL MEETING ON INTERMEDIATE ENERGY PHYSICS

Lyceum Alpinum, Zuoz, Engadin, Switzerland

4 - 13 April 1973

organized by

Schweizerisches Institut für Nuklearforschung (SIN) Villigen

co-sponsored by

The European Organization for Nuclear Research (CERN) Geneva

PROCEEDINGS

G E N E V A
1974

Copies are also obtainable from: SIN-Bibliothek,
CH 5234 Villigen, Switzerland

CERN - Service d'Information Scientifique - H/569 - 2600 - Avril 1974

PREFACE

This topical meeting follows the three SIN-schools:

1969 Leysin	Intermediate Energy Physics
1971 Zuoz	Pion Interactions at Low and Medium Energies (Co-sponsored by CERN)
1972 Zuoz	Weak Interactions and Nuclear Structure

Since we expect the first experiments at the SIN-meson factory to start in 1974, we decided to organize for spring 1973 a topical meeting rather than a traditional spring school. We thought such a topical meeting to be well adapted to the needs of information of experimentalists who are actively interested in or already engaged in preparations of new experiments at a new accelerator. The topics discussed at these meetings are represented in the "Plan of Sessions" in these Proceedings.

Each session consisted in an Introductury Lecture, a Progress Report and some "Working Group" Sessions or Seminars. The Working Group Sessions were led by experimentalists. These discussions were highly informal and touched mainly experimental questions concerning the corresponding experiments proposed at our accelerator.

We have not included the Introductory Lectures in this proceedings. Similar introductions can be found in the proceedings of the earlier SIN-schools. In this volume

we present only the Progress Reports and a few Seminars of the various sessions. There is, however, one exception. Since most particle- and nuclear physicists are not familiar with the elements of the applications of muons in solid state physics and physical chemistry, the introduction and the progress report on "Muon Depolarization in Solids" have been combined into one article.

W.E. Fischer

ACKNOWLEDGMENT

We take great pleasure in thanking Dr. Ad. Nadig, rector of the Lyceum Alpinum, and H.A. Zender from the Lyceum's administration, for their warm hospitality and their help in the technical preparation during the school.

We also thank the secretaries of SIN who co-operated in producing these Proceedings, and the CERN Document Reproduction Section for their work in reproducing these Proceedings. Special thanks to Mrs. E. Pedroni-Madlener who was in charge of the technical organization.

W.E. Fischer

CONTENTS

PLAN OF SESSIONS

I	A	Exotic Atoms	(Introduction)	J. Hüfner Univ. of Freiburg i.Br.
I	B	X-Ray Studies in Exotic Atoms	(Progress Report) (Manuscript not received)	J. Bailey Daresbury Lab.
I	C	New Effects in Muonium Atoms	(Working Group)	H.J. Leisi ETH
		Pionic Atoms	(Working Group)	H. Koch Univ. of Karlsruhe
II	A(1)	Muonium and Related Topics	(Introduction)	V. Telegdi Univ. of Chicago
II	A(2)	Muon Depolarization in Solids	(Introduction)	A. Schenck SIN
II	B	Muon Depolarization in Solids	(Progress Report)	K. Crowe Lawrence Berkeley Lab.
		Precession Experiments of Positive Muons in Ferromagnetic Materials		W.J. Kossler College William and Mary, Williamsburg
III	A	Nuclear Structure with Hadronic Probes	(Introduction)	C. Wilkin Univ. College London
III	B	Nuclear Structure with Hadronic Probes	(Progress Report)	N. Tanner Univ. of Oxford
III	C	Neutron-Nucleus Experiments	(Working Group)	K. Runge Univ. of Freiburg i.Br.
		Pion Production in Nuclei	(Seminar)	F. Lenz SIN

		π-Nucleus Experiments	(Working Group)	J. Domingo CERN C. Zupancic CERN
		Radiative Pion Capture	(Seminar)	P. Truöl Univ. Zurich
		Coulomb Interaction in Hadron-Nuclei Scattering	(Seminar)	L. Lesniak Univ. of Krakow
IV	A	Nucleon-Nucleon Scattering at Low and Intermediate Energies	(Introduction)	L. Lang ETH, Zurich
IV	B	Nucleon-Nucleon Scattering	(Progress Report)	J.A. Edgington Queen Mary College, London
V	B	Selected Topics in Weak Interection	(Progress Report)	J. Deutsch Univ. of Louvain
V	C	Weak Interaction of Pions and Muons	(Seminar)	C.W. Kim CEN Saclay
		μ-Capture and Muonic Atoms	(Working Group)	E. Zavattini CERN
LAMPF :		Status Report		K. Crowe Lawrence Berkeley Lab.
TRIUMF:		Status Report		D. Warren TRIUMF
SIN :		Status Report		J.P. Blaser SIN

NUCLEON-NUCLEON SCATTERING: PRESENT STATE AND FUTURE PROSPECTS

J.A. Edgington
Queen Mary College, London, England

'My purpose at this time is to note only omissions and deficiencies, and not to make any refutation of errors...; for it is one thing to set forth what ground lieth unmanured, and another thing to correct ill-husbandry in that which is manured.' (Francis Bacon, Advancement of Learning, 1605)

The field of nucleon-nucleon scattering has been heavily manured in the past years, and one may wonder whether the land is still productive; in this talk I shall assert that it is very fruitful, and that the new accelerators will provide rich fertiliser. In the main I shall restrict myself to the energy region accessible to the new accelerators, that is 200-800 MeV. I was asked to be controversial: I hope I have succeeded.

1. New lamps for old

In this section I compare the capabilities of the new facilities with those of the old. First, though, I shall summarise what is needed to improve the nucleon-nucleon experimental situation. If we look at Wilson's book (Wilson, 1963) we see that no significant technical advances have occurred in the last decade. In this time there has been only a marginal improvement in data quality, but a marked increase in sophistication of the analysis and interpretation. The number of energies at which 'complete' sets of experiments have been done has increased, but still the measurements remain overwhelmingly those of σ_t, $\sigma(\theta)$ and P. Polarised targets, developed for the πN system, have been relatively little used. The reason is the high specific ionisation of low energy protons, and the consequent difficulty in detecting the scattered particles, as well as problems of radiation damage. I am not too hopeful of dramatic improvements here, unless 'brute force' polarisation of hydrogen-rich compounds becomes feasible.

The other major 'standstill' area has been np experiments. Until recently neutron beams have been insufficiently intense for free np scattering, so quasi-free pn scattering on deuterium has been the rule. The Glauber corrections are frequently inconsistent; even now the theorists don't seem to have reached a consensus. The improvement programs at several machines have provided better neutron beams recently, but this is an area which will be pre-empted by the new facilities.

Let us now look at what these facilities will provide. Table 1 compares the external proton beams*. Major differences are the fixed energy at SIN, and the low macro duty-cycle at LAMPF. The latter has a very different rf structure, too. The fluxes at SIN and TRIUMF are similar, being determined by space-charge limitations; the nucleon fluxes at LAMPF could in principle be higher, but the nucleons derive from the H^- beam rather than the more intense H^+ beam. Perhaps the major difference is that LAMPF can explore the higher energy region where inelastic effects dominate. Also, because of the protons' higher energies, and hence lower ionisation, spin correlation experiments using polarised targets should be somewhat easier at LAMPF. Unfortunately, the polarised beam at LAMPF has lower priority than at the other two machines. At these it should be available soon after commissioning, albeit at much lower intensities than the design figure shown.

The proposed neutron beams are shown in Table 2. All come from quasi-free pn scatters in light targets, and the fluxes have been normalised to a distance of 10 m from these targets. The major difference here is the proposal, at TRIUMF, to produce the polarised beam by polarisation transfer from incident polarised protons. The higher polarisation and narrower energy bite may in some cases outweigh the lower flux.

In summary, the major advantages over present machines will be:

---

*Footnote: Parentheses indicate that the beam will not be available during initial operation.

(i) a factor of a hundred increase in intensity, allowing experiments of greater precision, or measurements of smaller cross sections than now;
(ii) the early availability of intense, highly polarised beams;
(iii) except at SIN, the energy will be variable (at TRIUMF, continuously; at LAMPF, in steps of 15 MeV);
(iv) excellent beam quality.Typical parameters will be energy resolutions of $\pm$ V3 %, and beam emittances of 1 cm mrad.

Two general comments are in order. Demand for time from meson users will be heavy. This will usually conflict with the operation of polarised ion-sources, so some thought will have to go into maximising efficiency. Second, the major limit on the quality of neutron experiments will be the background level in the experimental areas; adequate shielding is expensive but should not be skimped.

2. Phenomenology of elastic scattering

I now turn to the experiments that should be done, noting, as I have indicated, only omissions and deficiencies. Two recent articles (Signell, 1969; Moravcsik, 1972) have scrutinised the present data and, particularly, their interpretation; I shall often refer to these. Dr. Lang has discussed the relevance of the nucleon-nucleon problem to nuclear structure calculations; I refer you also to a recent review of the subject as seen by a member of the LAMPF nucleon group (Simmons, 1970).

I start with the elastic scattering of two nucleons, and in particular with the phenomenological treatment of data via partial wave analysis. This work has been done mainly by the Yale group (Seamon et al., 1968), Signell and co-workers at Michigan State, and the Livermore group (Mac Gregor, Arndt and Wright, 1968a, 1968b, 1968c, 1969 - hereafter referred to as MAW-VII - MAW-X, respectively). It is concluded (MAW-IX) that the isotopic spin 1 (I = 1) scattering matrix is well-determined up to 450 MeV, the I = 0 matrix is fairly well determined in the same energy region, but both, particularly the latter, are poorly known at higher energies. To see what experiments will clarify the situation we must look more closely at the partial wave analysis.

2.1 Energy dependence

Present scattering data are dominated by clusters of measurements made at some half-dozen fixed energy accelerators. At each energy separately various analyses give consistent results for the I = 1 phases. The I = 0 phases, found from np scattering, are less accurate and at some energies there are still several possible solutions. Nonetheless, there have been attempts to describe the totality of data using some energy-dependent form for the partial waves. The Livermore group, for instance, use a formula that correctly reproduces effects due to 1π, 2π, 3π, etc., production thresholds. The forms chosen include

one-pion exchange as a leading (not necessarily dominant) term, and are often constrained to give the correct low energy behaviour (effective range expansion).

There are clearly many possible forms that meet these requirements, none having any very sound theoretical justification (Signell, 1969). Figs. 1 and 2 show some results for an isovector (I = 1) and an isoscalar (I = 0) wave, respectively, and also the results of single energy analyses. The energy dependent fits naturally match the point fits reasonably well, there being few data elsewhere to constrain them, but have unnaturally small error bands. This is because no account is taken of any inexactness in the parameterisation of the energy dependence. Note, in this context, the difference between the Yale and Livermore isoscalar results. This difference is some measure of possible parameterisation errors. It is clearly enormous. Why then bother to do such energy dependent analyses?

I quote two reasons, from MAW-IX. A posteriori, they argue: 'Plausible energy dependent forms do exist, so that meaningful energy dependent analyses are feasible'. By this they mean that the χ^2 per degree of freedom is acceptable, being typically 1.05 to 1.1 for about 2000 datum points. But this numerical assessment implicitly assumes that the energy dependence chosen is not just plausible, but actually correct. Other forms may well give fits that are just as successful in a statistical sense, as the Yale analysis shows.

There is an a priori argument also: 'Phases obtained from single energy analyses often exhibit rather erratic behaviour when plotted as a function of energy. This behaviour

reflects either unknown systematic errors or else incompleteness in the data selection... We are led naturally to energy dependent analyses.' Logically, there is a third possible explanation of the 'erratic' behaviour; that it reflects real physics. To find out we now need, not more data analysis but better data, at more energies. But what data? The question can be answered, in general terms, as follows.

The I = 1 phases at each of seven energies are unique and well determined; partial waves of $\ell \leqslant 5$ are adequate to describe the data up to 425 MeV. We need measurements at closely spaced intervals, say 15 MeV, of quantities that can be determined to high precision. It doesn't matter if these data by themselves yield ambiguous solutions; the necessary discrimination exists already in the present data. The differential cross section and polarisation in pp scattering are the obvious candidates. The measurements are needed mainly above 200 MeV. In spite of the onset of inelastic effects above 400 MeV, they should be continued up to at least 650 MeV. The reason is as follows. Isotriplet phases above about 400 MeV couple strongly to the $\Delta(1238)$ resonance, and as yet there is no satisfactory prescription for including this inelasticity in the analysis. Isosinglet phases do not so couple and their inelasticity is small up to at least 600 MeV. Now, if we assume charge independence, simple formulae relate unmeasurable isosinglet amplitudes to directly measured np and pp quantities; for example

$$\sigma_{I=0}(\theta) = 2(\sigma_{np}(\theta) + \sigma_{np}(\pi-\theta)) - \sigma_{pp}(\theta) \qquad (1)$$

Thus the pp data at higher energies are useful for extracting the isoscalar amplitudes, and hence phase shifts, even if the isotriplet analysis is confused. As recent CERN measurements show (Albrow et al., 1970), the major needs are

for polarization data, and measurements of cross-sections at very small angles.

At present the isoscalar phase shifts are probably not unique and certainly not well determined (Signell and Holdeman, 1971). Historically, the measurements that finally removed ambiguities from the I = 1 analysis were those of triple scattering parameters. The new intense neutron beams make similarly precise np measurements possible. In principle, spin correlation parameters would probably do just as well (see Fig. 3, in which a well known I = 0 ambiguity at 330 MeV is sketched; measurements of either triple scattering parameters, or spin correlation parameters, are shown to resolve it). It seems a pity, though, having at great expense produced a worthwhile neutron beam, to fire it at a polarised target, when liquid hydrogen makes the experimenter's life easier. So I propose np triple scattering experiments to furnish a unique set of phase shifts, followed by precision cross section and polarisation measurements to find the energy dependence of the isoscalar phases.

A particularly interesting np angular region is that near 180^{o}. There is a very sharp backward peak here whose production mechanism is somewhat of a mystery. Data can be fit by forms such as

$$\frac{d\sigma}{dt} = \alpha e^{\beta t} + \gamma e^{\delta t}$$

with β having very large values (Fig. 4). There is the possibility of considerable structure at intermediate energies, and further data are urgently needed.

2.2. Charge independence

This is the hypothesis that nucleon-nucleon scattering amplitudes are determined only by the total isospin of the system. It was used in relation (1) above. Most partial wave analyses have assumed its truth, taking the isovector part of the np amplitude to be that found from pp scattering.

Dr. Lang has discussed the evidence that charge independence holds good at low energies. I would remind you that the measured scattering lengths a_{pp} and a_{pn} differ greatly. Many electromagnetic (hence non isospin conserving) corrections must be applied before one can say that charge independence holds (Moravcsik, 1972). Some of these corrections are intractable. Until they have been better handled we can say only that charge independence is not manifestly violated in the effective range approximation.

The effect of these corrections decreases with energy. This suggests that direct comparison of isovector phase shifts from np and pp scattering may be a useful test of charge independence. So far the experiments have been inadequate for any but the $^1S_0$ to be fitted to the np and pp data separately. Both the Yale and Livermore groups have done this. Once again the small quoted errors on the energy dependent solutions magnify any difference there might be between the two $^1S_0$ phases thus derived. The differences in solutions at fixed energies seem barely significant (see Fig. 5). It would be of great interest to measure np amplitudes sufficiently precisely for a similar isovector analysis to be done in all partial waves, independently of the pp data. For once fortune smiles, since any violation of charge independence will be small. Hence

computer minimisation searches can start from the pp phase shifts, which are unambiguous. The short range part of the two-nucleon interaction is of most interest (the long range part is quite sensitively tested by comparing the values of the pion-nucleon coupling constant given by the pp and np analyses separately; the agreement is good). This region is probed by the low partial waves. Of the simpler experiments, cross section and polarisation, the former may not be adequate as in the np system it is dominated by the $I = 0$ amplitudes. Hence we need precise np polarisation measurements, and the subsequent extraction of the isovector P wave phase shifts. Once more, though, I must advertise the need for better calculations of the electromagnetic corrections, before any conclusions about charge independence can be drawn.

2.3 Charge symmetry

Since only neutral particles can be exchanged in the pp and nn systems, effects due, for example, to the $\pi^{\pm} - \pi^{0}$ mass difference are absent. Thus these better calculations are not needed if we wish to test the weaker hypothesis of charge symmetry. It should be a relatively simple matter to evaluate the corrections that remain. Motivated by the desire to discriminate between different potential models, Signell and co-workers (Miller et al., 1969) have calculated the neutron-neutron scattering length a_{nn} for several different models, all of which fit a_{pp} equally well. They find that all the potentials yield similar values of a_{nn} and conclude that its measurement is not a good way to discriminate between models. One can invert the argument; a measurement of a_{nn} which disagrees with their calculated values is prima facie evidence for the breakdown of charge

symmetry, because of the model-independence of the calculated value.

At present a_{nn} can be determined only poorly, mainly from three-body break-up reactions. The errors, amounting to perhaps ± 1 fm, are largely in the theoretical three body analysis and are unlikely to be much reduced. One would like to perform free nn scattering experiments. I suggest that these may soon (within a decade) become possible.

For long they have seemed utterly remote; few people seriously believed, for instance, that a proposal to detonate simultaneously two atomic devices (Moravcsik, 1964) was practicable. Moravcsik's work was valuable, however, in indicating that even very imprecise measurements of the energy-dependence of the total nn cross section could pin down the effective range parameters rather precisely. Even measurements to about 10 %, for example, would determine a_{nn} to ± 1 fm.

Though high-flux beam reactors provide sufficient neutrons, a rather more convenient source is needed. The novel ideas come from fusion research work. Calculations (Kidder, 1972) suggest solid pellets of deuterium/tritium, adiabatically compressed by converging laser pulses, could attain central temperatures and densities that would sustain thermonuclear reactions. These devices would be intense sources of 'thermal' neutrons ('thermal' here corresponding to about 10^8 K and implying energies of tens of keV). As an example of what may be possible, Winterberg has considered a similar device utilising fission reactions also (Winterberg 1973). He conceives a pellet of U^{235} similarly compressed by converging laser beams. Central densities reach hundreds of times normal density, and the critical mass is thereby

reduced to a small fraction of a gram. The neutron yield is enhanced if the pellet is encased in a deuterium/tritium blanket which acts as a neutron reflector plus fusion source. Winterberg finds that less than 1 MJ of laser energy would produce a pulse of some 10^{22} neutrons, in a volume of about 1 cc, moving outward with velocities 10^{9} cm s^{-1}. Other devices, involving d-d or d-t reactions in dense plasmas, have been proposed. Some are even in operation. These and other possible neutron sources are discussed by Persiani (1972). The majority are pulsed devices, and attainable neutron yields should reach 10^{15} neutrons per pulse without going beyond known physical principles.

With such sources nn scattering would become feasible. Two ideas are sketched in Fig. 6. The first shows two such devices firing in synchronism; allowing 10 m of collimated flight path for the neutrons, one gets about one nn scatter per pulse in the 100 cm^2 interaction region. Neutron energies range up to 14 MeV so the effective range parameters could be determined according to Moravcsik's prescription. Supposing only one neutron source to be available, it could operate in the path of a neutron beam from one of the new machines, thus studying nn scattering at higher energies. Typical reaction rates are however only one per hundred pulses, even for a Winterberg-type device. In this latter case a <u>low</u> duty-cycle factor is required, to allow synchronisation of source and beam pulses; so my estimate relates to LAMPF, the only pulsed machine. For obvious reasons physicists working at Los Alamos are more likely to have access to such a neutron source than those at SIN or TRIUMF. I am told that technical prospects in this field are bright (Boyer, 1973).

2.4 Some conjectures on the dynamics

Dr. Lang has discussed the attempts to describe phenomenological partial wave analyses by means of potential or boson exchange models. Clearly these models have great practical utility. But what is their heuristic value? The potential models in particular have taught us little about strong interaction physics, and their justification, in their non-relativistic form at least, is being increasingly questioned (see Moravcsik, 1972). Here I shall concentrate on one particular aspect of all potential schemes, the use of a repulsive core.

The 'hard core' was invented (Jastrow, 1950) to explain the qualitative difference between pp and np cross sections above 300 MeV, as revealed by the early experiments on the Berkeley synchrocyclotron. Jastrow comments on the arbitrary nature of the short range repulsion, and indeed such sudden potential steps of the size commonly used (hundreds of MeV) are intuitively unpleasing. The concept has remained valuable for two reasons. First, several phase shifts ($^1S_0$, $^3S_1$(?), $^3P_0$) become negative at similar energies, indicating that the long and intermediate range attraction in these partial waves becomes a repulsion at a radius of ≈ 0.5 fm. Second, the exchange of heavy bosons, particularly the ω, has been invoked as a mechanism for providing such a repulsive core. Unfortunately such an assumption seems erroneous, as has been stressed by Signell (Signell, 1969); boson exchange models work moderately well at intermediate energies, but they are silent about separation distances less than $\sim$ 1 fm.

There have been several recent attempts to exorcise the hard core. I shall mention two of these. Following

Blankenbecler and Sugar, Gross has developed a relativistic wave equation with the special feature that one of the two interacting particles is restricted to its mass shell (Gross, 1972). He claims that such a formalism, with pion and heavy meson exchanges, always produces repulsive cores which arise as a natural dynamical consequence of Lorentz invariance. For simplicity he takes the non-relativistic limit and compares the effective potential of the resultant Schrödinger's equation with the Reid soft-core potentials. The agreement is quite impressive (Fig. 7) though final judgement must await solution of the fully relativistic equation, and comparison with phase shifts. As usual, Gross parametrises the two-pion exchange terms by a fictitious boson, but the mesons invoked, and their coupling constants, are otherwise conventional.

Another approach that offers a link with high energy phenomenology is the attempt by a Russian group (Neudatchin et al., 1973) to eliminate the repulsive behaviour of the phase shifts altogether. Their work stems from an application of Levinson's theorem, which relates the total change in a phase shift as a function of energy to the total number, n, of bound states of the interacting particles in that partial wave:

$$\delta(0) - \delta(\infty) = \pi n$$

Some years ago Swan showed that, in evaluating n, one must count not only the physical bound states but also those which would occur were it not for the operation of the exclusion principle (Swan, 1955). Thus, for example, in n-^{3}He scattering the singlet S-wave solution possesses one bound state, ^{4}He, whereas the triplet S-wave solution has none because of the Pauli principle. Nonetheless the

experimental data demand that in both cases we take $\delta(0) = \pi$ ($\delta(\infty)$ may conventionally be set equal to zero). Neudatchin et al., noting that all experimental phase shifts are arbitrary up to an integer number of π, have proposed that there exists one 'forbidden bound state' in the $^1S_0$ partial wave of the composite nucleon-nucleon system. Thereby $\delta(0) = \pi$, and the customary phase shifts are all raised by π. The consequence is that the $^1S_0$ phase does not change sign; the apparent hard core becomes an artifice of the exclusion principle, operating, they hazard, on the quark constituents of the composite system. Fig. 8 shows the $^1S_0$ phase shift according to this hypothesis, evaluated for an attractive Yukawa-like potential with three free parameters, plus one pion exchange. The agreement with conventional analyses is qualitatively good. Also, applying this formalism to the electron disintegration of the deuteron (an S-wave process at threshold) they appear to have resolved a puzzling discrepancy between experiment and theory (see Fig. 9). The experimental need is for precise elastic phase shifts, as a function of energy, up to about 1 GeV.

It is appropriate here to discuss another conjecture motivated by high energy phenomenology. Astbury (Astbury, 1973) has drawn attention to some suggestive correlations that appear when a variety of hadron-hadron total cross sections are plotted against the cm momentum, p^*, of the particles. Fig. 10 shows the 'bumps' in $\sigma_t(\pi p)$, when plotted thus, and their assignment to nucleon isobars. Astbury notes that Kp, $\bar{p}p$, pp and pn cross sections similarly show bumps, to a greater or lesser degree, at the same p^* values. He postulates that these effects may be due to 'mesonic' or 'baryonic' quark interactions of the $\bar{q}q$ or qqq type, irrespective of the hadron in which the quarks are bound

(Fig. 11). The simplest test of this conjecture is, surprisingly, in low and intermediate energy NN scattering. The lowest nucleon isobars (Δ(1238), N(1520) and N(1688)) occur at p* values corresponding to 113, 440 and 690 MeV, for np or pp scattering. Precision (better than √2 %) total cross section measurements should reveal structure at these energies. Near 100 MeV in np scattering the situation is intriguing, with possible structure in a region overlapped by separate measurements (Fig. 12). Similar structure may exist at the higher energies but present experiments are confused (Fig. 13); the pp channel is further confounded by threshold effects due to Nπ production. The 100 MeV region is currently being investigated at Harwell; if structure is found, further experiments at higher energies become compelling. It would be amusing if the first substantive evidence for quark sub-structures were to come from intermediate energy machines.

3. Symmetries of the strong interaction

Conventional wisdom has it that strong interactions are invariant under P and T. In fact the evidence that this is so **is** surprisingly weak (Thorndike, 1965). Thorndike estimated that the strengths of suitably-defined P- and T-violating parameters could be as much as 70 % and 7 %, respectively, of their maximum possible values. Since then nucleon-nucleon scattering experiments have improved the latter limit marginally, the former a little more. Experimental tests of P and T have been virtually restricted to nuclear physics, where T-violating amplitudes in certain electromagnetic transitions have been shown to be less than 1 % (e.g., Holmes et al., 1973). No such precision holds for strong interactions, and the nucleon-nucleon system

would seem a convenient and appropriate place to rectify this.

3.1 Parity conservation

Since parity is not conserved in the weak interaction any mixture of a weak Hamiltonian H_W into the strong interaction may produce violation. The mechanism for this is the exchange of pseudoscalar or vector mesons, that is, mainly π, ρ, σ, ϕ. The magnitude of this effect must be known before any conclusions about the strong interactions are drawn; fortunately an exhaustive review of the relevant theory has recently appeared (Fishbach and Tadic, 1973). These author's predictions of parity-violating effects are restricted mainly to the circular polarisation of gamma rays from excited nuclear states, such a polarisation being rigorously zero if parity is conserved. An interesting and simple case is the reaction $n + p \rightarrow d + \gamma$, for which a circular polarisation of $\sim 10^{-8}$ is predicted. A recent measurement by the Leningrad group, made in a most ingenious manner, gives a polarisation of $-(1.3 \pm 0.45) \times 10^{-6}$ (Lobashov et al., 1972). The clear discrepancy is unexplained, though it is unlikely that theorists will willingly attribute it to a breakdown of parity conservation in the strong interactions! This illustrates the difficulty of estimating, even to an order of magnitude, the strength of any admixture of H_W into H_{strong}.

Turning to nucleon-nucleon scattering at intermediate energies, parity violation is manifest as a mixing of partial waves of angular momentum ℓ, $\ell \pm 1$. Thus mixing parameters analogous to the (parity-conserving) ε -parameters are introduced; for example, in the I = 1 system the $^1S_0$

and $^3P_0$ states can mix via a parameter we may call ζ_0, following Thorndike.

$$\langle {}^3P_0 | T | {}^1S_0 \rangle \sim \sin 2\zeta_0 \exp i(\delta({}^3P_0) + \delta({}^1S_0)) \qquad (2)$$

All we can presently say is that ζ_0 is no more than 10 % of that value ($\pi/4$) which maximises this expression (Gucker and Thorndike, 1971). In an ideal world, data have no systematic errors; one could therefore introduce ζ_0, like the ε-parameters, into the partial wave analysis and estimate it from the data. The world being non-Utopian, it is more sensible to measure directly quantities which are sensitive to parity violation, due for example to an non-zero ζ_0. Suitable quantities are the asymmetry following scattering of a longitudinally polarised beam, and the up-down asymmetry following scattering of a vertically-polarised beam. The reduction of systematic errors is probably easier in the first case than the second.

Simonius (1972) has proposed a similar experiment with the aim of studying parity violation due to the H_W mentioned above. He calculates the effect to be small (in terms of the formalism above, $\zeta_0 \sim 10^{-7} - 10^{-8}$). The observed asymmetry is shown by Eqn. 2 to depend on the phase shifts in the partial waves concerned; for the $^1S_0$ - $^3P_0$ case, their sum decreases above $\sim$ 50 MeV (see MAW-X), so the asymmetry also falls. Note, however, that the phase shift sum rises again, to large negative values, above 400 MeV; this may be a suitable region for experiments. Simonius' work shows that H_W is of negligible importance, compared with the precision (1 %?) for which one would aim, in searching for parity violation in H_{strong}.

3.2 Time reversal invariance

The discovery that K_L^o decay violates CP has stimulated research in this field. Both electromagnetic, and weak interactions other than K-decay, have been shown to be invariant under time reversal to precisions of the order of 1 %. The corresponding limit is nearly an order of magnitude poorer for the strong interactions. In the case of nucleon-nucleon scattering there seem excellent prospects of improving it considerably.

The situation was most recently reviewed by Bilen'kij et al. (1968). The effect of a breakdown of T-invariance is basically that the direct and time-reversed transition amplitudes differ; thus the scattering matrix is unsymmetric. The off-diagonal elements are related by equations such as

$$\langle {}^3P_2|T|{}^3F_2\rangle - \langle {}^3F_2|T|{}^3P_2\rangle = -2\sin 2\varepsilon_2 \sin\lambda_2 e^{i(\delta({}^3P_2)+\delta({}^3F_2))}$$

Here ε_2 is the (parity-conserving) maxing parameter coupling the ${}^3P_2$ and ${}^3F_2$ states; a non-zero value of λ_2 violates T, but not P. Similar equations hold for parity-violating couplings, for example that of the ${}^3P_0$ and ${}^1S_0$ states (Eqn. 2). Note that a maximal violation of T corresponds to a value of $\pi/2$ for the relevant λ-parameter.

There are two immediate experimental consequences of a breakdown of T. First, the polarisation P, produced when an initially unpolarised nucleon beam scatters at an angle θ, is no longer numerically equal to the analysing power observed when such a beam is rescattered through the same angle (Fig. 14). Secondly, the relationship between the triple scattering parameters

$$\frac{A + R'}{A' - R} = \tan \theta$$

is modified by the inclusion of an additive T-violating term to the right hand side. The first of these consequences has been more frequently checked, with the conclusion that $\sin\lambda_2 \leqslant 0.07$ (95 % confidence level). The second consequence was checked by Handler et al. (1967), in pp scattering at 430 MeV, and they found $\sin \lambda_2 \leqslant 0.06$. In both tests the assumption is made that there is no T-violation in the term coupling the $^3F_4$ and $^3H_4$ partial waves. Note that all these tests have been confined to pp scattering, that is, the I = 1 system.

Supposing parity to be conserved, or only weakly violated, one needs to study those partial waves that are mixed by the ε-parameters, and Eqn. 2 tells us that experiments will be most sensitive at energies for which these parameters are large. Moreover the sensitivity increases, the larger the sum of the individual phase shifts. Of the four coupling parameters needed in analyses up to J = 4, only the isoscalar parameter ε_1, coupling $^3S_1$ to $^3D_1$, meets both these requirements, and that above 200 MeV. Thus the np system, at energies above 200 MeV, is indicated as suitable.

Bryan and Gersten (1971) have studied the predictions of a specific model for T-violation due to Sudarshan. This model invokes heavy meson exchanges to mediate the hadronic current of the weak interactions: the vector and axial-vector parts are represented by ρ and A_1 exchange, respectively. These meson exchanges contribute to H_{strong} also. CP (and hence T) violation is got by assuming that both direct and derivative coupling of the A_1 occurs (such couplings, when both are present, automatically remove the

symmetry from the scattering matrix). Bryan and Gersten predict a large T-violating effect in np scattering above ~150 MeV, but very little at lower energies or in pp scattering. The reason is basically similar to the arguments outlined above. T-violating exchange forces due to the heavy A_1 are of short range, hence are probed mainly by low angular momentum states at high energies. The coupled states of J = 1, $^3S_1$ and $^3D_1$, are therefore favoured more than the states of higher J. Whether or not this particular model has any merit, the fact remains that, if T is violated, it is likely to be in the relatively unknown short range part of the nucleon-nucleon interaction.

In principle either (P - **A**) or (A + R')/(A' - R) can be measured. In the former case the absolute polarisation is needed, and this is more difficult to measure for neutrons than for protons. Protons can be scattered off carbon, and as long as the scattering is elastic (hence involving spin-1/2 - spin-zero scattering only) no T-violation can occur; thus no circular arguments are involved*. On balance a measurement of the triple scattering parameter in np scattering seems subject to fewer systematic errors.

---

*Footnote: A major virtue of polarised proton beams from the meson factories is their good energy resolution; there should be no difficulty in finding their polarisation precisely by p-C scattering, as the ground state scattering, and that to excited states, should be easily separable. The equality of asymmetry and polarisation in the p-C elastic scattering is due solely to parity conservation.

4. Off-shell amplitudes

This is perhaps the most interesting area in nucleon-nucleon scattering (Signell, 1969; Moravcsik, 1972). The off shell behaviour is useful on the one hand, for its importance in many-nucleon system, and, on the other, for the constraints it imposes on any theory of the interaction. It exerts, for instance, a profound effect on the binding energy of nuclear matter, to the extent of as much as 20 MeV per nucleon (Haftel and Tabakin, 1971). It provides the only means of deciding between different potential models which give equally good fits to the elastic scattering data, the class of so-called 'phase equivalent' potentials. That these two aspects are intimately related is clear, for example, from the sensitivity of the binding energy to the precise choice of potential (Miller et al., 1969), or alternatively the phase shifts, even the high energy ones (Chong et al., 1972).

All inelastic processes are influenced to some extent by off-shell effects, but some are more sensitive, experimentally simpler, or more tractable theoretically, than others. Possible processes at intermediate energies involve electromagnetic transitions (bremsstrahlung, np capture) and strong interactions (pion production, few-nucleon studies). I discuss these in turn.

4.1 Bremsstrahlung

These experiments are technically the most challenging that I shall discuss. Both theory and measurement have grown from virtually nothing, a decade ago, to mature respectability.

The amplitude for the process $N + N \rightarrow N + N + \gamma$ can be expanded in powers of k, the photon momentum

$$M = M_{-1}/k + M_0 + M_1 k + M_2 k^2 + ...$$

Low observed, 15 years ago, that both M_{-1} and M_0 depend only on the elastic amplitudes; all the off-shell behaviour is in terms of higher order in k. Consequently, when the cross section is expanded in powers of k, the first two terms contain no off-shell information (Burnett-Kroll theorem). Thus the most interesting region for off-shell behaviour is that of high k.

How high it is difficult to say. The maximum value of k increases as the opening angle between the two outgoing nucleons decreases from 90^o. For example, at 62 MeV, with outgoing nucleons detected at $\pm 30^o$, the gamma ray can take away up to 26 MeV; the ratio $\xi = k_{max}/E_{inc}$ (which is 26/62 = 0.42 in this case) may be taken to define the degree to which the interaction is off-shell. Until recently one could summarise the state of proton-proton bremsstrahlung very simply (Halbert, 1971) - between 3 MeV and 200 MeV, and for ξ less than about 0.45, all experiments agreed very well with 'theory'. The 'theory' is usually based on either a potential or a one-boson-exchange model. As one might expect, for small ξ only purely on-shell terms need be considered. For larger ξ, discrepancies of up to 20 % appear unless the (model dependent) off shell effects are included. However, the actual model dependence appears to be very small. Differences between the predictions of various phase-equivalent potentials are typically $\sim$ 1 %, much smaller than the experimental precision.

The air of complacency is now dissipating rapidly, as the

result of a recent measurement at 52 MeV. Here a value of ξ = 0.56 was attained by observing the outgoing protons at $\pm 8\frac{1o}{2}$. The cross section predicted is in excess of 100μb sr^{-2}, to be compared with a measurement of (-4 ± 16) μb sr^{-2}, (Sanada et al., 1972). The discrepancy is unexplained. Clearly ppγ is by no means dead, at least at large values of ξ. Measurements up to the pion threshold, ~300 MeV, should, can, and probably will be made.

By comparison with ppγ, few measurements of npγ have been made. This is a pity because npγ is expected to be more sensitive than ppγ to off-shell differences between the various phase equivalent potentials (McGuire, 1970). The experiments are much more difficult, neutron beams being less intense than proton beams, and the problems of unwanted background are even harder to overcome. Results of the two experiments reported to date are shown in Figs 15 and 16, along with predictions of a potential model and a one-boson exchange model. Clearly nothing very significant can yet be said about the comparisons. More data, again up to at least the pion threshold, is needed.

To do these experiments well, high data acquisation rates plus superlative rejection of unwanted background are needed. The former can be achieved with proportional counter arrays. The latter may require detection of the gamma ray as well as both nucleons; this is less difficult at the higher energies and constitutes a return to the so-called 'Rochester' trigger system. Another useful device is a solid hydrogen target. Fig. 17 shows one which has already been used at Harwell in an experiment on small angle pp scattering. The advantage is the target's lack of walls which, however thin, are difficult to ignore completely in these measurements. Such a target is presently

being used in an experiment on np capture, to which process I now turn.

4.2 np capture

The process n + p → d + γ is related to its inverse, γ + d → n + p, by detailed balancing. A recent flurry of activity saw quite a few measurements of these two reactions near nucleon energies of 600 MeV, and gamma ray energies of 300 MeV, respectively. These energies correspond to production of the Δ(1238) in the cm. The measurements were motivated by suggestions that the γNΔ vertex might exhibit some breakdown of time reversal invariance, thus invalidating the detailed balance arguments. No such breakdown was observed.

Apart from this recent work, measurements of the capture reaction are sparse. There are many, precise, measurements at thermal neutron energies, but virtually none elsewhere. For the photodisintegration reaction, cross section and polarisation measurements exist up to 50 MeV gamma ray energy (= 100 MeV nucleon energy), and again above 170 MeV (= 340 MeV nucleon energy). So there are no np capture data, either direct or deduced, between 100 and 340 MeV.

Why should there be? because np capture is fundamentally a simpler process to calculate than bremsstrahlung. The two body behaviour restricts the off-shell intermediate states, over which integration occurs, to those in which two nucleons can couple directly to the deuteron. To the extent that the deuteron wave function and the 'half off shell' amplitudes are well known, the calculation is exact. In spite of this there are several glaring discrepancies

between prediction and observation. First, the measured thermal capture cross section is 8 % higher than the theoretical one:
σ_{exp} = 334.2 $\pm$ 0.5 mb, σ_{th} = 309.5 $\pm$ 5 mb. The calculation is fairly easy since only S-waves are involved, so something is basically wrong. Adler (1972), for instance, has proposed that the $^3S_1$ continuum state of the free neutron and proton, and the deuteron ground state (also $^3S_1$ primarily), may not be orthogonal. He finds that an essentially complete overlap of wave functions between these two states is sufficient to bring about agreement. Unfortunately for convention, such non-orthogonality of two states of the same quantum numbers but different energies implies that the strong interaction Hamiltonian is non-Hermitian. Whatever the fate of this conjecture, capture measurements at other than thermal energies are urgently needed, and are indeed being done at existing synchrocyclotrons.

Another discrepancy is found between the excitation functions for photodisintegration, as evaluated by, for example, Partovi (1964), and as measured (e.g., Baglin et al., 1973). An example is shown in Fig. 18. The electrodisintegration cross section, referred to earlier (Fig. 9), is another area of disagreement.

Most present data come from photodisintegration because intense gamma ray beams have been available whereas neutron beams have not. The situation will now change, with the added benefit that the neutron energy resolution will be much better than that of the bremsstrahlung gamma rays. Techniques may resemble those of bremsstrahlung experiments, but advantage can be taken of the kinematic requirement that the deuteron emerge in a narrow forward

cone. Thus, though cross sections are low, $\sim$ 10 μb, all the events can be detected. Given the present state of theory, experiments will be most useful up to the pion threshold.

4.3 Pion production

This reaction also involves the two nucleons being off-shell. However little information on their off-shell behaviour is likely to emerge directly. The reason is the strong interaction of the pion itself, which, besides being dynamically obscure, makes a perturbation treatment, such as is used for the electromagnetic terms in bremsstrahlung, impossible.

One has to look elsewhere for the immediate utility of pion production experiments. At the energies we are concerned with, single pion production is virtually the only inelastic process that occurs. Cross sections for two pion production are negligible below 1 GeV. The one pion production is dominated by the influence of the $\Delta(1238)$. Based on this, a very simple model due to Mandelstam (1958) has been surprisingly successful in fitting data, principally the total cross sections, up to $\sim$ 750 MeV. Better data on the angular distributions, energy spectra and, particularly, the polarisation, would test and constrain the model quite well.

Whether the Mandelstam model is completely adequate or not, it does provide a phenomenological framework by which to treat the inelasticity in the partial wave analyses. Until someone has made an attempt at such an integrated analysis, detailed consideration of the measurements needed, and

their precision, is premature. But clearly pion production in general should have high priority.

An interesting sub-set of possible experiments are those involving π-production very near threshold, leading to deuteron formation. The cross section goes as

$$\sigma_{NN \rightarrow d\pi} = \alpha\eta + \beta\eta^3$$

where η is the cm pion momentum in units of $m_\pi c$. The dynamics which determines α is very sensitive, both to the NN potential used and to the D-state probability of the deuteron. Thomas and Afnan (1971) have discussed the sensitivity explicitly, for values of P_D between 1 % and 9 %. The determination of α and β is another low cross section (≈ 200 μb) experiment that could usefully be consindered along with bremsstrahlung or np capture measurements.

4.4 The deuteron

The deuteron has an honourable history, but since it told us about the existence of tensor forces it has been strangely silent. We don't even know its D-state percentage very well. Its use in the field we are discussing has really been rather limited. It has mainly been used as a carrier of 'quasi-free' neutrons. Thus at high energies most of the 'np' measurements have really been pd measurements, with the Glauber recipe being used to correct for shadowing effects. Further refinements to this correction have begun to appear in the literature (Atwood and West, 1972; Dumbrajs, 1970) but they are probably too late, as most experiments in future will use the lovely neutron

beams we eagerly await.

Break-up reactions of the type n(d,nnp) may leave two of the three outgoing particles in close proximity at a low relative energy, so that their interaction can be studied in the final state. Following some success in fitting pp and pn effective range parameters this way, the same thing has been attempted for the nn system. The main problem is that the values deduced depend rather critically on the way the interaction is handled. Fadeev-type approximations require separable potentials, which are certainly not as good as some others in fitting elastic scattering data. There is hope of progress at higher energies ($\sim$ hundreds of MeV) because the time that the third particle spends near the other two is reduced, and its interference minimised. Noyes in particular is hopeful that such experiments will be useful (Noyes, 1972) but others are less tranquil (Moravcsik, 1972). If one forgets about attempts to fix the low energy parameters, and concentrates on information that can be got about the off-shell behaviour, the outlook is brighter. The amount by which one can go off-shell is very much larger than in bremsstrahlung, owing to all three particles being massive. Even with our present limited knowledge of the dynamics, large differences are apparent between predictions of the various potential models (Morlet et al., 1972). With the large, automated data acquisition systems coming into use, these measurements should and will be extended.

5. Summary

In these remarks I have covered only a fraction of the topics open to me. Even so, not all the experiments I've

mentioned can be done at once. In Table 3 I have listed those measurements which, in my opinion, should have high priority. I have included only those for which both a tried technique, and adequate means of interpretation, exist. Some I have listed are likely, you may think, to yield only null results. That is no reason to neglect them. I started with a quotation from Bacon, and shall finish with another:

'If a man will begin with certainties, he shall end in doubts; but if he will be content to begin with doubts, he shall end in certainties.'

References

R. J. Adler, Phys. Rev. 169, 1192 (1968); 174, No. 5 (1968), erratum

R. J. Adler, Stanford Linear Accelerator Centre Report SLAC-PUB-1035 (1972)

M. G. Albrow et al., Nucl. Phys. B23, 445 (1970)

A. Astbury, RHEL report RPP/H/103, (1973)

W. B. Atwood and G. B. West, Stanford Linear Accelarator Centre Report SLAC-PUB-1081 (1972)

J. E. E. Baglin et al., Nucl. Phys. A201, 593,(1973)

S. M. Bilen'kij, Dubna Report P2-3716 (1968); CERN translation 68-9

K. Boyer, Astronautics and Aeronautics 11, 28 (1973)

R. Bryan and A. Gersten, Phys. Rev. Letters 26, 1000 (1971)

K.-F. Chong et al., Physics Letters 38B, 132 (1972)

O. V. Dumbrajs, Dubna Report P2-5444 (1970): CERN translation 71-22

E. Fishbach and D. Tadic, Physics Reports 6C, 125 (1973)

F. Gross, Stanford Linear Accelerator Centre Report SLAC-PUB-1138 (1972)

E. J. Gucker and E. H. Thorndike, Phys. Rev. D4, 2642 (1971)

M. I. Haftel and F. Tabakin, Phys. Rev. C3, 921 (1971)

M. L. Halbert, 'Review of Experiments on Nucleon-nucleon Bremsstrahlung' (Contribution to Gull Lake Symposium, 1971)

R. Handler et al., Phys. Rev. Letters 19, 933 (1967)

M. J. Holmes et al., Nucl. Phys. A199, 401 (1973)

R. Jastrow, Phys. Rev. 79, 389 (1950), Kidder, University of California report UCRL-74040 (1972)

V. M. Lobashov et al., Nucl. Phys. A197, 241 (1972)

M. H. MacGregor, R. A. Arnat and R. M. Wright, Phys. Rev. 169, 1128 (1968a)

M. H. MacGregor, R. A. Arnat and R. M. Wright, Phys. Rev. 169, 1149 (1968b)

M. H. MacGregor, R. A. Arnat and R. M. Wright, Phys. Rev. 173, 1272 (1968c)

M. H. MacGregor, R. A. Arnat and R. M. Wright, Phys. Rev. 182, 1714 (1969)

J. H. McGuire, Phys. Rev. C1, 371 (1970)

S. Mandelstam, Proc. Roy. Soc. A24, 491 (1958)

M. D. Miller et al., Phys. Letters 30B, 157 (1969)

M. J. Moravcsik, University of California report UCRL-7854 (1964)

M. J. Moravcsik, 'The Interaction of two nucleons' (Rep. Prog. Phys. 35, 587, 1972)

M. Morlet et al., Nucl. Phys. A191, 385 (1972)

V. G. Neudatchin et al., Phys. Letters 43B, 13 (1973)

H. P. Noyes, 'Nuclear Forces and the Three Nucleon Problem' (Lectures at the 3rd Physics Summer School Mexico, 1971)

F. Partovi, Ann. Phys. 27, 79 (1964)

P. J. Persiani, Argonne National Laboratory Memorandum AP/CTR/TM-2 (1972)

J. Sanada et al., Tokyo University Report TUENS-6 (1972)

R. E. Seamon et al., Phys. Rev. 165, 1579 (1968)

P. Signell, 'The Nuclear Potential' (In 'Advances in Nuclear Physics'Vol. II, ed. Baranger and Vogt, Plenum Press, 1969)

P. Signell and J. Holdeman, Phys. Rev. Letters 27, 1393 (1971)

J. E. Simmons, LAMPF preprint LA-4640 (1970)

M. Simonius, Phys. Letters 41B, 415 (1972)

P. Swan, Proc. Roy. Soc. 228, 10 (1955)

A. W. Thomas and I. R. Afnan, Phys. Rev. Letters 26, 906(1971)

E. H. Thorndike, Phys. Rev. 138B, 586 (1965)

R. Wilson, 'The nucleon-nucleon interaction' (Wiley, 1963)

F. Winterberg, Nature 241, 449 (1973)

EXTERNAL PROTON BEAMS.

	ENERGY MeV	INTENSITY		TIME STRUCTURE	
		UNPOL.	POL.(80%)	MACRO.	MICRO.
SIN (H^+)	580	100 μa	100 na	C.W.	5ns/44ns
TRIUMF (H^-)	200-525	100 μa	100 na	C.W.	5ns/44ns
LAMPF (H^-)	200-800	100 μa	(?)	6%	1/4 ns/5ns

Table 1

EXTERNAL NEUTRON BEAMS.

	UNPOLARIZED		POLARIZED		
	ENERGY MeV	INTENSITY (into 10^{-6}sr)	ENERGY MeV	POLARIZATION	INTENSITY (into 10^{-6}sr)
SIN	540 ± 40	5×10^{7} s^{-1}	(450 ±60	0·30	4×10^{6} s^{-1})
TRIUMF	520 ± 15 (variable)	8×10^{6} s^{-1}	512 ± 5 (variable)	0·63	10^{4} s^{-1}
LAMPF	745 ± 5 (variable)	6×10^{6} s^{-1}	530 ± 30 (variable)	0·35	2×10^{6} s^{-1}

SIN beams by scattering from Be/C; the others by scattering from LD_2.

TRIUMF polarized beam produced by polarization transfer from $p\vec{t}$ on LD_2.

Table 2

HIGH PRIORITY ELASTIC SCATTERING EXPERIMENTS.

	PP		
1.	$\sigma(\theta)$ at small angles. } $P(\theta)$ }	200 - 650 MeV	Deduce energy-dependence of I=1 phase shifts.
2.	Asymmetry in scattering of longditudinally polarized beam.	> 400 MeV	Test of P conservation.
	NP		
3.	$\sigma(\theta)$ near 180°	200–800 MeV	Explore backward peak.
4.	Triple scattering parameters.	200–650 MeV	{ Define I=0 phases. { Test of T invariance
5.	$P(\theta)$, $A(\theta)$	200–650 MeV	{ Extract I=0 and I=1 phases separately. { Test of T invariance.
6.	σ total.	~100, 440, 690 MeV	Search for quark substructure.

HIGH PRIORITY INELASTIC SCATTERING EXPERIMENTS

1.	$pp\gamma$	200–300 MeV	Off shell behaviour (high E_γ)
2.	$np\gamma$	200-400 MeV	——— " ———
3.	np capture nfp capture	200-400 MeV	σ total, $\sigma(\theta)$, asymmetry.
4.	Pion production	300-800 MeV	Data needed for complete partial wave analysis.
5.	$pp - \pi^+ d$ } $np - \pi^0 d$ }	Threshold	P_D of deuteron
6.	p (d, npp) n (d, nnp)	200-400 MeV	Far off shell behaviour.

Table 3

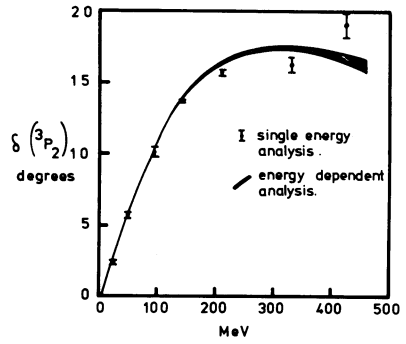

Fig. 1

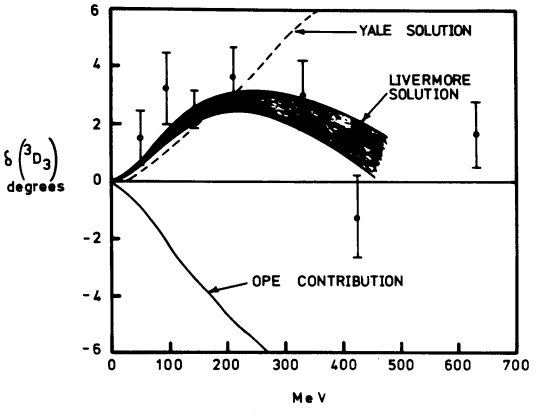

Fig. 2

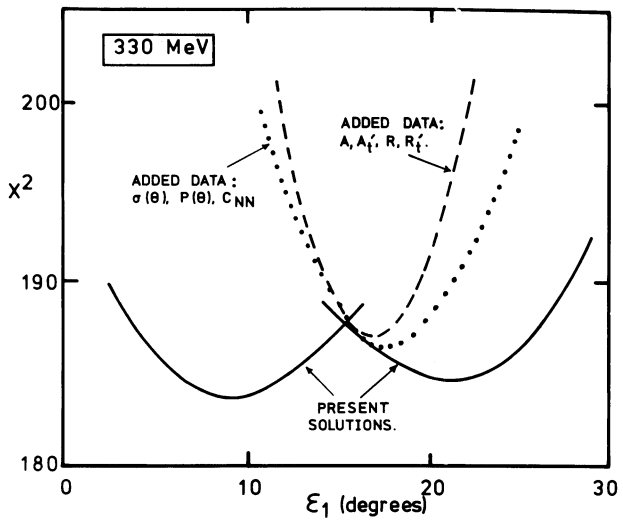

Fig. 3

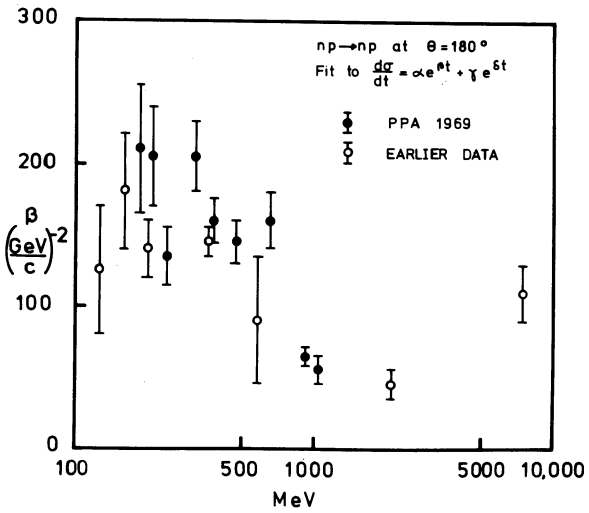

Fig. 4

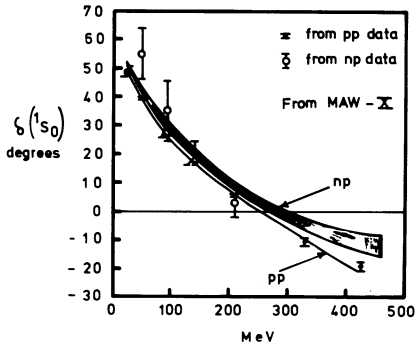

Fig. 5

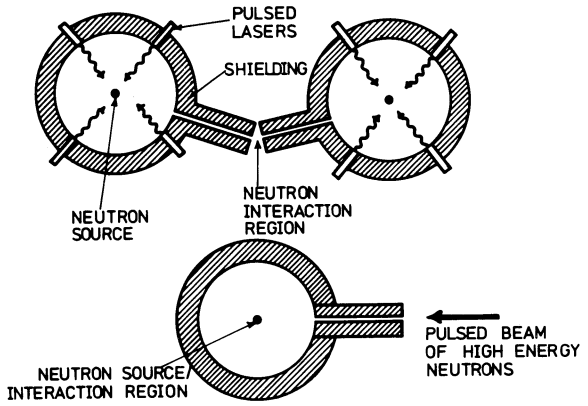

Fig. 6

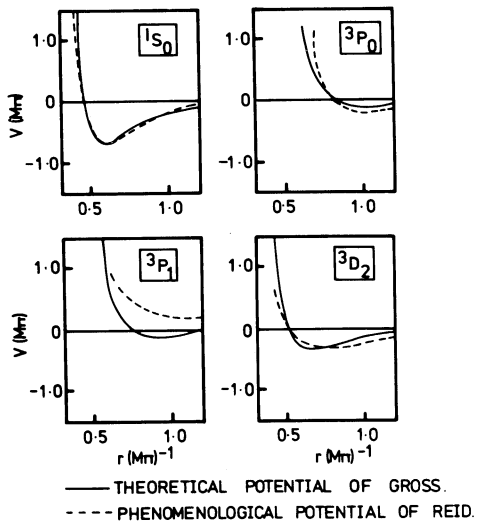

Fig. 7

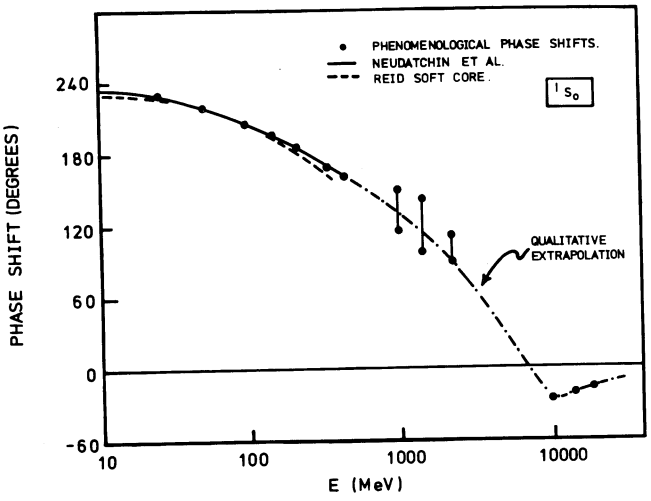

Fig. 8

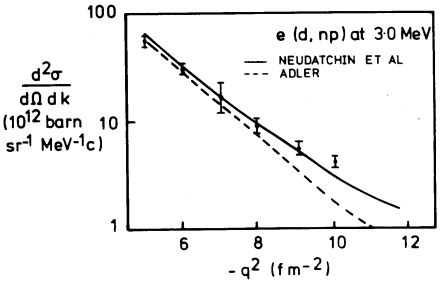

Fig. 9

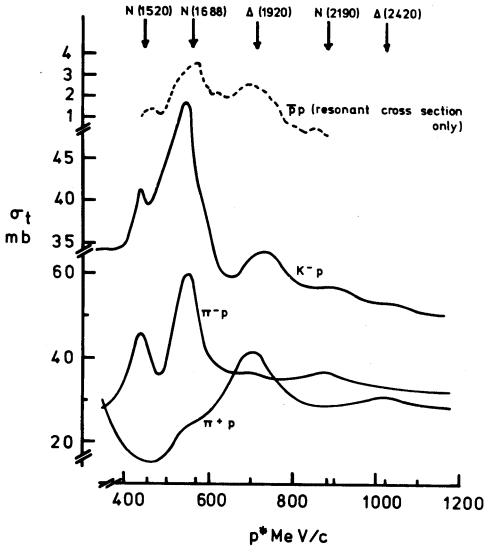

Fig. 10

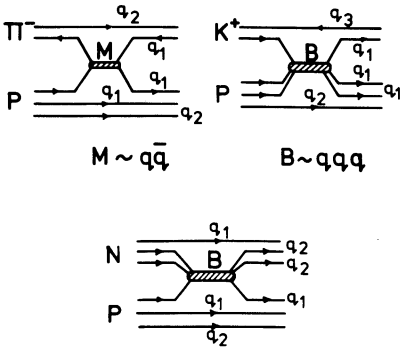

Fig. 11

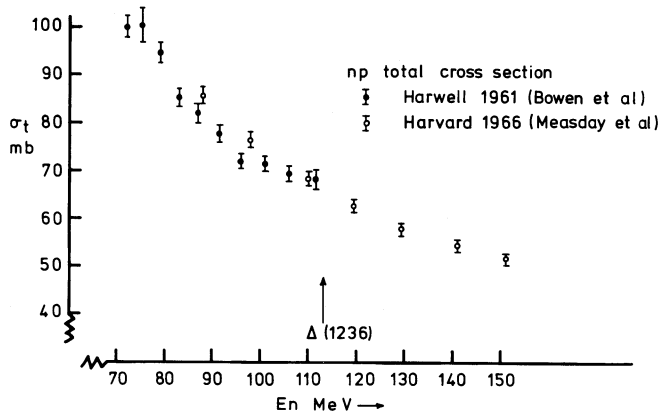

Fig. 12

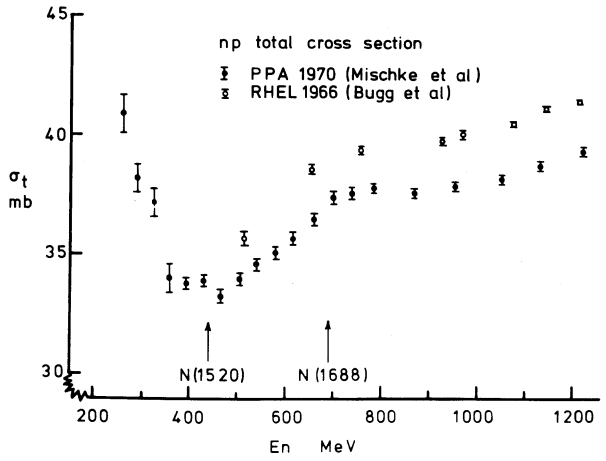

Fig. 13

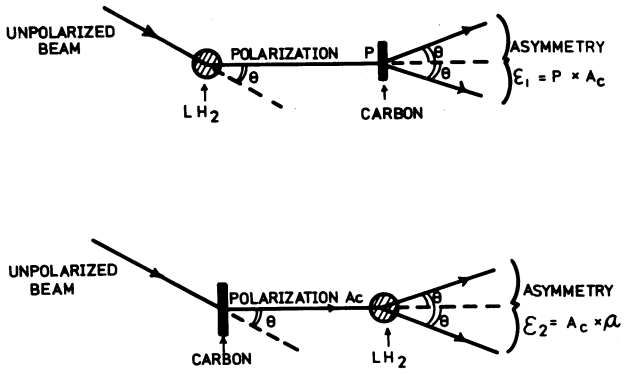

IF T IS VIOLATED $\varepsilon_1 \neq \varepsilon_2$

Fig. 14

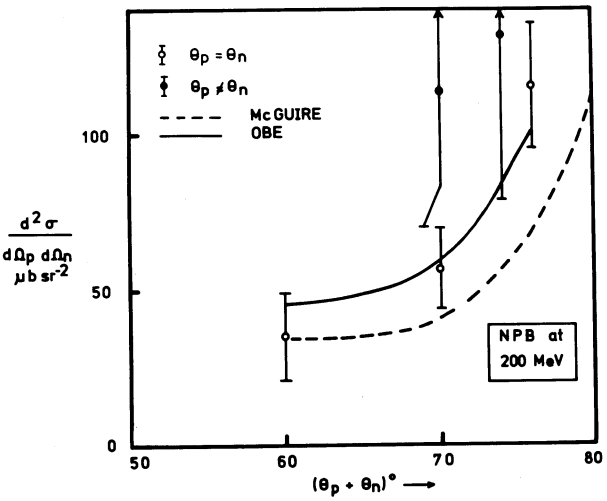

Fig. 15

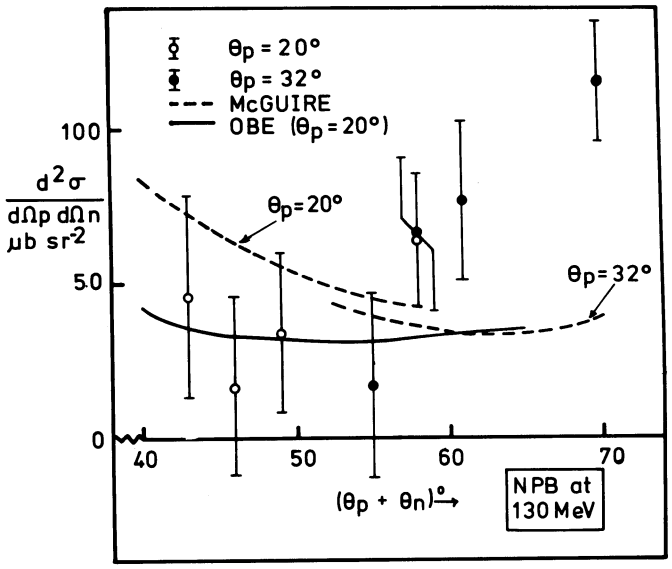

Fig. 16

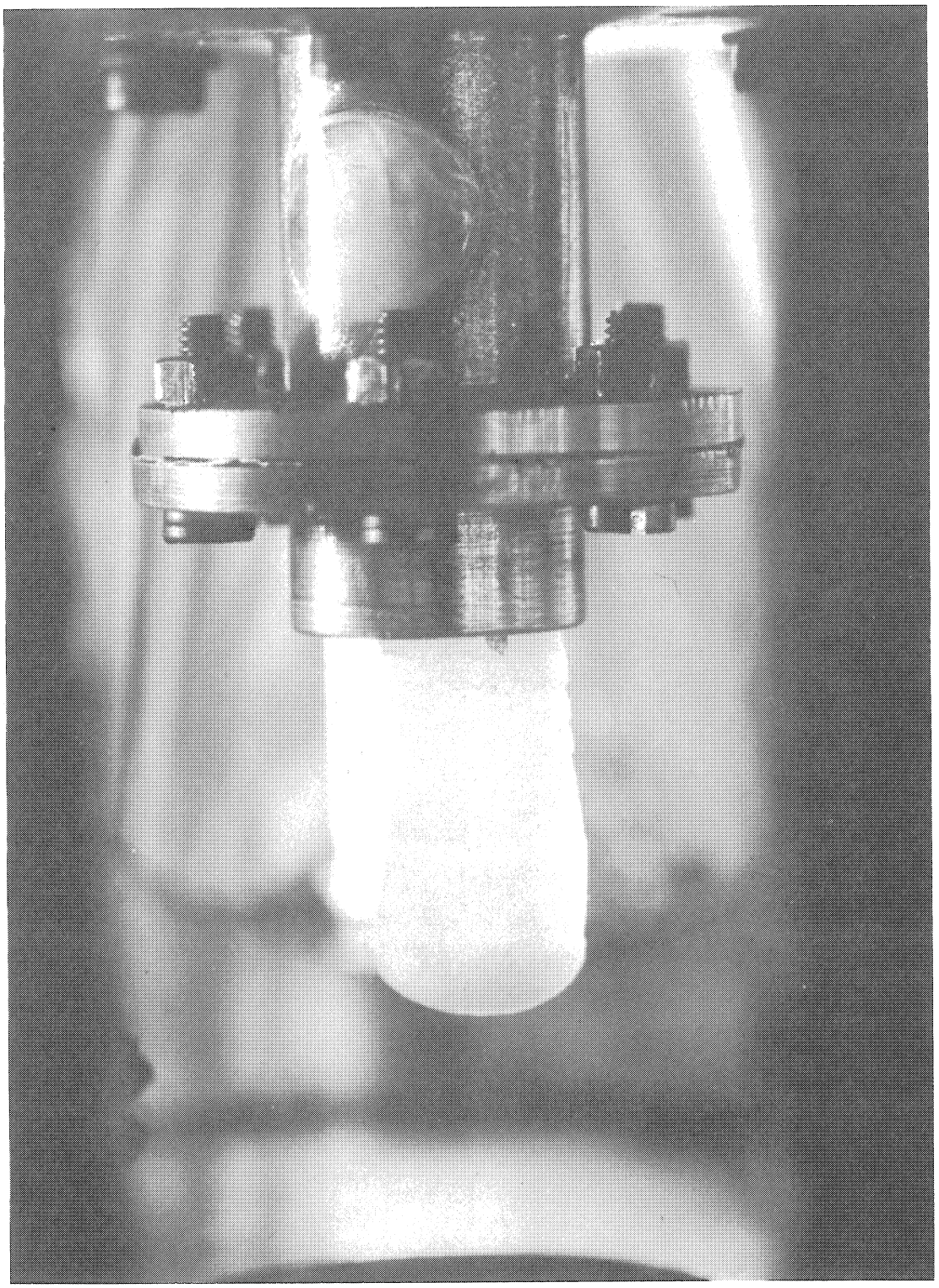

Fig. 17

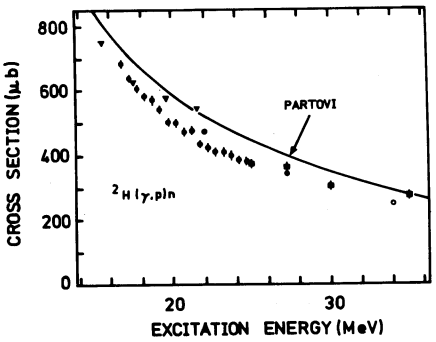
800
600
400
200
0
CROSS SECTION (μb)
PARTOVI
^{2}H (γ,pn)
20
30
EXCITATION ENERGY (MeV)

Fig. 18

THE PRESENT AND FUTURE OF NUCLEAR STRUCTURE WITH HADRONIC PROBES

N.W. Tanner
University of Oxford, England

Most of this lecture will be concerned with the scattering of medium energy pions by nuclei in anticipation of an increase in intensity of about three orders of magnitude from the meson factories. The future of pion nuclear physics, in the strictly experimental sense, can be read from the lists of proposals at SIN, TRIUMF, and LAMPF, but the interesting and much more difficult question is what these measurements are likely to yield from unambiguous analysis? It does not seem very useful to labour once such-and-such a measurement which is established by hand waving to be sensitive to so-and-so property (often short range correlations!) if so-and-so is obscured by other effects. At present the interpretation of nuclear properties is limited by the experimental data which is often inaccurate and/or insensitive and sometimes incomprehensible, but in the near future the inadequacies of analysis are likely to become much more apparent. So far we have learnt the pattern of pion production and absorption, and scattering and charge exchange, and can even describe these phenomena qualitatively but little in the way of new nuclear properties has been extracted.

At GeV energies the eikonal approximation of Glauber (see e. g. Wilkin 1971 for a review and references (1)) appears to offer a foolproof method for the analysis of π-nucleus

scattering. The example of π-d scattering (2) shown in Fig. 1 is typical of the kind of agreement observed between experimental data and Glauber calculation, and this is at an energy of 770 MeV where the high energy approximations might not be fully satisfied. The curve in Fig. 1 is in fact a prediction not a fit as the deuteron wave function is known well enough from other evidence and the pion-nucleon scattering amplitudes are also well established. It is of interest to note that the high energy π-d (as well as p-d and e-d) scattering did actually reveal a nuclear property of some interest viz. the d-wave form factor for the deuteron. (Early calculations, to the everlasting shame of the scattering experts, omitted the d-wave component of the deuteron ground state and predicted a deep interference minimum). For the investigation of nuclear properties the ideal pion energy is in the region 2 to 2.5 GeV/c where the π-N cross-section is sensibly energy independant and the momentum transfers of interest, say ~ 500 MeV/c, are obtained at a small scattering angle. In practice there is likely to be a serious shortage of energy resolution except in the particular cases of scattering from deuterium which provides a detectable recoil there by identifying elastic events, and from He^4 which has no excited states below 20 MeV. Accurate measurements of πd and πHe^4 elastic and summed inelastic could be very instructive providing the Glauber approximation is very good, a fact which it seems must be established experimentally from π-d scattering and which at present is certainly not known to better than 5 %. In passing it should be mentioned that the summed inelastic scattering (3) from a nucleus A is, assuming closure, proportional to

$$\left\{ 1 + (A-1)\, C\,(q) \right\}$$

in the single scattering approximation (which is the leading

term of Glauber), where C(q) is the Fourier transform of the two body correlation function. This direct appearance of the correlation function looks very interesting but the dynamical part of (A-1) C(q) is at most (4) about 0.1 or 0.2 and it would require very accurate measurements and a religious belief in Glauber to determine C(q).

At medium energies, mostly in the range 200 $\pm$ 100 MeV, resolution is less of a problem and there exists a useful body of experimental data (5) concerning $\pi^{\pm}$ elastic scattering from He^4, C^{12}, O^{16} and Ca^{40}, and an extensive literature seeking to interpret this data. The example shown in Fig. 2, $\pi^+ O^{16}$ elastic at 270 MeV, was chosen deliberately to mislead: The Glauber calculation due to Lesniak and Lesniak is practically a perfect fit to the data and invites the conclusion that any scattering theory which predicts so accurately must be true. More often the prediction is quite accurate in the forward direction but fails by perhaps a factor of two in the region of the second maximum - which still looks quite respectable on logarithmic graph paper. The example shown in Fig. 3 is typical. There is no shortage of competition for the Glauber prescription, including the optical potential of Kisslinger (local and non-local), other forms of multiple scattering series and, for inelastic scattering, simpler approximations such as the impulse (single scattering) approximation and black disk diffraction. Many of the variants were described by Wilkin (1) and for more recent work reference might be made to the papers of Schmidt (6) and of Gibbs (7). At the risk of a broad generalization it might be said that all of these scattering prescriptions are qualitatively successful but that none has returned any nuclear information of any value. The small angle scattering is largely fixed by the size of the nucleus (fed in from electron scattering data), the wavelength of the

pions, and the "blackness" of the nucleus which is consequent on the large πN cross-sections near 200 MeV. Nuclear properties become more interesting in the region of the second maximum, but it is just in this region that the scattering prescriptions become uncertain. It is not without significance that nearly all analyses of scattering have been made in terms of simple harmonic oscillator wave functions, and it is difficult to have enough confidence in the scattering formalisms to ascribe a misfit to an inadequacy of the nuclear wave function.

The difficulties of pion-nucleus scattering near 200 MeV are deepseated and non-trivial:

(i) Pions of this energy are patently relativistic and there is no clear method for representing the known πN scattering amplitudes by a potential as a first step towards building up a multiple scattering series.

(ii) The πN scattering is resonant which introduces serious difficulties into π-nucleus scattering which are unknown in proton-nucleus scattering.

(iii) Pions are absorbed in a literal way, $\pi 2N \rightarrow 2N$, which is not simply related to πN scattering and has caused great difficulty.

The consequence of these peculiar problems is that the scattering prescriptions have been extrapolated from high energy or from low energy without any control over the accuracy of the approximations. It is certainly possible to proceed in this empirical way, adjusting parameters to fit experimental data, and perhaps elaborating the prescription to cope with the more sophisticated experiments such as double charge exchange ($\pi^{\pm}$, $\pi^{\pm}$) and correlation measurements ($\pi,\pi\,\gamma$) etc., but there is no certainty of extracting more than a

set of "effective parameters" (c. f. the DWBA industry of low energy physics)

This view may be unduly pessimistic but it does seem unlikely that the underlying dynamical problem of multiple scattering by a relativistic resonant particle subject to absorption will be solved by studying complicated systems such as πC^{12}. It is much more likely that a solution (of some kind or kinds) to the scattering problem will be based on a very detailed analysis of πd scattering. At present there is little experimental data on which to work. The total cross-section data of Fig. 4 comes from old bubble chamber measurements and is not sufficiently accurate to be of great value. There are also some bubble chamber measurements of elastic scattering but only the measurement of Pervitt et al. (9b) at 142 MeV (shown in Fig. 5) and of Norem (9c) at 183 MeV have sufficient statistical accuracy to be useful. In addition there is a counter measurement (9d) at 256 MeV, Fig. 6, with some idea of the energy dependence, Fig. 7, and a measurement (9e) of πd elastic at 50 MeV by Ingram et al. yet to be published. The measurement at 256 MeV was obtained using a deuterated scintillator as target which also served to detect the recoil deuterons, and the measurement at 50 MeV by resolving elastic from inelastic pions by pulse height from a scintillator. Neither of these methods can be easily extended to provide a systematic set of data over the resonance, but it is already clear that the existing scattering approximations cannot claim better than factor of two accuracy (8, 9d, 10). Higher intensities will allow thinner targets and/or better spectrometers and we can confidently predict good measurements of πd scattering both elastic and inelastic, and we can at least hope for a better formulation of the scattering theory.

For conventional nuclear structure studies of matrix elements

or more generally form factors, between nuclear states low energy pions of about 50 MeV offer the best prospects. At 50 MeV the πN cross-section is small, c. 10 mb, and multiple scattering is relatively unimportant for light nuclei. To a respectable first approximation (11) it should be possible to treat π-nucleus scattering on the basis of single scattering of a non-relativistic, non resonant πN system subject to considerable absorption via π2N → 2N. Supposing the absorption problem can be handled it should be possible to extract interesting nuclear physics out of pion inelastic and charge exchange scattering. In general πN scattering can be written (12) as four terms

$$f = \tfrac{1}{3}(2f_3 + f_1) + \tfrac{1}{3}(2g_3 + g_1)\,\vec{\sigma}\cdot\vec{n}$$

$$+\tfrac{1}{3}(f_3 - f_1)\,\vec{\tau}\cdot\vec{t} + \tfrac{1}{3}(g_3 - g_1)(\vec{\sigma}\cdot\vec{n})(\vec{\tau}\cdot\vec{t})$$

where $\underline{\sigma}$, $\underline{\tau}$ are the spin and isospin of the nucleon, $\underline{t}$ is the isospin of the pion, $\underline{n}$ is the unit vector normal to the scattering plane, and f_{2T} and g_{2T} are the spin-non-flip and spin-flip scattering amplitudes for the πN system in a state of total isospin T. It is incidental but important that these scattering amplitudes are not at present well determined at 50 MeV but presumably this deficiency of the πnucleon data will be rectified by the same high intensity that will allow the πnucleus measurements to be made. In the single scattering approximation (1) the πnucleus scattering amplitude is

$$F_{fi}(q) = \langle f | \sum_{j=1}^{A} f_j(q)\, e^{iq r_j} | i \rangle$$

$$= A \bar{f}(q)\, S_{fi}(q)$$

where q is the momentum transfer, $S_{fi}(q)$ is an inelastic form factor, and $\bar{f}$ is an appropriate average over the A nucleons.

It is possible to construct selection rules for nuclear excitation governing spin S and isospin T, $\Delta S = 0, 1$ and $\Delta T = 0, 1$ corresponding to the four terms of f above, with some angle, i. e. q, dependance from the π-N scattering. Spin-flip with or without isospin-flip is proportional to sin θ, and assuming present knowledge of phase shifts (13) $(2 f_3 + f_1)$ is roughly proportional to $\cos\theta$, and $(f_3 - f_1)$ is large at backward angles. All of the nuclear physics is contained in the form factors $S_{fi}(q)$ which are often known near $q = 0$ from β- and γ-transitions. Pions of 50 MeV ($\sim$130 MeV/c momentum) can cover the range from zero to 250 MeV/c, if indeed there is enough form factor left at 250 MeV/c to be measured, for excited states of the target nucleus and, by charge exchange, for the states of the neighbouring nuclei with $Z \pm 1$. It is likely that most of the interest will be in the complex of spin isospin giant resonances at 20 to 30 MeV excitation in light nuclei. Judging from the properties of the well known electric dipole resonance a resolution of 50 KeV will be required for an adequate study of detail. This should not be impossible for inelastic scattering of charged pions using a magnetic spectrometer but it is difficult to imagine how resolutions better than several MeV can be achieved for neutral pions from charge exchange with a practical counting efficiency. It may however be possible to study the interesting case N^{14} (π^-, π^o) C^{14}, which is the inverse of the celebrated slow β-decay $C^{14} \rightarrow N^{14}$, as the first excited state of C^{14} is 6 MeV above the ground state. This is a $\Delta S = 1$, $\Delta T = 1$ case with a nuclear (i. e. β-decay) form factor $S_{fi}(q)$ which is very nearly zero at $q = 0$ but which should be non-zero for larger q (corresponding to a second forbidden G-T matrix element in β-decay). A great deal of effort has been expended arranging wave functions that would ensure $S_{fi}(0) = 0$ for C^{14} β-decay and it would be

of more than trivial interest to examine the properties of the wave functions at $q \neq 0$.

The only existing experimental inelastic data near 50 MeV are total (4π) cross-sections obtained by detecting secondary nuclear radiations (9i, 14) or residual β-activity (15, 16). Hilscher et al. (9i) observed the excitation of C^{12} with 70 MeV pions and obtained $\sim$ 16 mb for the 4.4 MeV state ($J^{\pi} = 2^{+}$, i. e. $\Delta S = 0$, $\Delta T = 0$, $\Delta L = 2$ in the simplest description) and <1 mb for the 15.1 MeV state ($J^{\pi} = 1^{+}$, $\Delta S = 1$, $\Delta T = 1$, $\Delta L = 0$) which is consistent with the expectation that spin-flip scattering should be weak: the spin-flip amplitude is proportional to $\sin\theta$ and near 90^{o} where the amplitude is large the momentum transfer is $\sim$ 200 MeV/c and the nuclear form factor S_{fi} is small.

Pion inelastic scattering is not the only way of studying nuclear form factors with a preference for exciting the collective giant resonance states. Mu-capture, π-radiative capture, and electron inelastic scattering all tend to excite the same states with much the same dependance on form factors. Neutrino spectroscopy is a practical impossibility so μ-captive is not very interesting, but radiative capture (16) of stopped π^{-} determines the charge exchange form factor, albeit at only one value of $q \simeq 120$ MeV, but with resolution problems which, while still difficult, are less severe than those encountered with neutral pions. Electron inelastic scattering can do all (non-charge-exchange) things but with a resolution limited by bremsstrahlung to >0.1 % and with a background due to bremsstrahlung of two or three times the signal. Marvels of analysis (17) have been achieved with such data but it is not clear that it will be possible to disentangle the complicated structure of the collective states at $\sim$25 MeV excitation with electron alone.

Summary

Predicting the future with an intensity increase by a factor 10^3 imminent is likely to be a fairly unreliable exercise, but we can be fairly confident that whatever is to be learnt about nuclear structure physics will come from precise measurements and detailed analysis; not from instant discoveries. Pion scattering where it is easy c. 200 MeV is not likely to be very revealing except in two respects:
(i) the scattering problem itself which is best studied in the framework of the πd system, and (ii) simple spectroscopy of double charge exchange, $(\pi^{\pm}, \pi^{\mp})$ and (p, π^{-}), which reactions allow the study of the energy states of strange nuclear species such as Be^5 and C^{18}. Nuclear properties will be more easily extracted from low energy (c. 50 MeV) pion scattering and, in the case of high momentum properties, from high energy (c. 2 GeV) scattering.

Nothing has been said here of pion absorption except as a complicating nuisance to the scattering. The experts have promised us two-hole states of nuclei and short range correlations and even delivered these things, but the problems are formidable and at present the arguments read more like plausible explanation of experiments rather than analysis for hard facts. It is difficult to be optimistic about this field.

References

1. C. Wilkin, CERN Yellow Report 71-14, Lectures at Spring School, Zuoz, 1971

2. G. Alberi and L. Bertocchi, Nuovo Cimento 63A, 285, 1969

3. A. Kerman, H. Mc Manus, and R. Thaler, Ann. of Phys. (N. Y.) 8, 551, 1959

4. Unpublished estimates of C. W. Wong, 1968

5. Most of the experimental data of π-nucleus scattering may be found in the following references:

(a) He^4 elastic	M. M. Bloch and D. Koetke Nuclear Physics B5, 451, 1968
(b) He^4 elastic	Crowe et al. Phys. Rev. 180, 1349, 1969
(c) He^3 and He^4 elastic	Falomkin et al., Lett. Nuovo Cimento 5, 1121, 1972
(d) He^4 elastic	Kolynk et al. JINR-P-1-6693, Dec. 1972
(e) C^{12} elastic	Edelstein et al. Phys. Rev. 122, 252, 1961
(f) C^{12} elastic, inelastic, and total	Binon et al. Nucl. Phys B17, 168, 1970 B33, 42, 1971 B40, 608, 1972
(g) C^{12} elastic	Scott et al. Phys. Rev. Lett. 28, 1209. 1972
(h) C^{12} total	Clough et al. RPP/NS 9, Feb. 1973
(i) C^{12} inelastic	Hilscher et al. Nucl. Phys. A158, 593, 1970
(j) C^{12} inelastic	Scipione et al. Phys. Lett. 42B, 489, 1972
(k) O^{16} elastic	Rohlin et al. Nucl. Phys. B37, 461, 1972

(l) O^{16} elastic — Bercan et al. Phys. Rev. Lett. 29, 1031, 1972

(m) Ca^{40} elastic — Bercan et al. unpublished

(n) Total cross-sections — Ignatenko et al. Dokl. Akad. Nauk. USSR 103, 395, 1955

(o) Total cross-sections — Gabathuler et al. CERN, unpublished

(p) Reaction cross-sections — Abashian et al. Phys. Rev. 104, 855, 1956

(q) Reaction cross-sections — Allardyce et al. Phys. Lett. 41B, 577, 1972

6. C. Schmidt, Nucl. Phys. A197, 449, 1972

7. W. R. Gibbs, Phys. Rev. C5, 755, 1972

8. W. R. Gibbs, Phys. Rev. C3, 1127, 1971

9. Experimental measurements on πd scattering at medium energies:

(a) Total cross-section — See ref. 8

(b) Elastic 142 MeV — Pewitt et al. Phys. Rev. 131, 1826, 1963

(c) Elastic 183 MeV — J. H. Norem Nucl. Phys. B33, 512, 1971

(d) Elastic 256 MeV — Gabathuler et al. Nucl. Phys. to be published

(e) Elastic 50 MeV — Ingram et al. U.B.C., Vancouver

10. C. Carlson — Phys. Rev. C2, 1224, 1970

11. Ref. 5a gives an application of the single scattering approximation to πHe^4 elastic at 24 MeV.

12. J. Hamilton and W. S. Woolcock, Rev. Mod. Phys. 35, 737, 1963

13. Herndon et al., UCRL 20030 πN, 1970

14. Alster et al., Phys. Rev. Lett., 28, 313, 1972

15. Chivers et al., Nucl. Phys A126, 129, 1969

16. Zaider et al, TAUP-352-73, Tel-Aviv, 1973

17. P. Truoel, Lecture at Zuoz Spring School, April 1973

18. H. Theissen, "Spectroscopy of Light Nuclei by Low Energy (<70 MeV) Inelastic Electron Scattering" in "Springer Tracts in Modern Physics", Vol. 65, 1972

Figures

1. Elastic scattering of pions of 770 MeV by deuterium and the prediction of the Glauber approximation (2).

2. Elastic scattering of π^+ by O^{16} at 270 MeV. The Glauber prediction is due to Lesniak and Lesniak (5k).

3. Elastic scattering (5f) of π^- by C^{12} at 280 MeV. The Glauber prediction is due to Wilkin (1).

4. Total cross-sections for $\pi^{\pm}$d from old bubble chamber data (8).

5. Elastic scattering of πd at 142 MeV. The experimental points are from the measurement of Pewitt et al. and the curve from Gibbs' multiple scattering calculation (8).

6. Elastic scattering of πd at 256 MeV with a double scattering prediction (9d).

7. Energy dependance of πd scattering in the backward direction (160°), compared with the prediction of a double scattering calculation (9d).

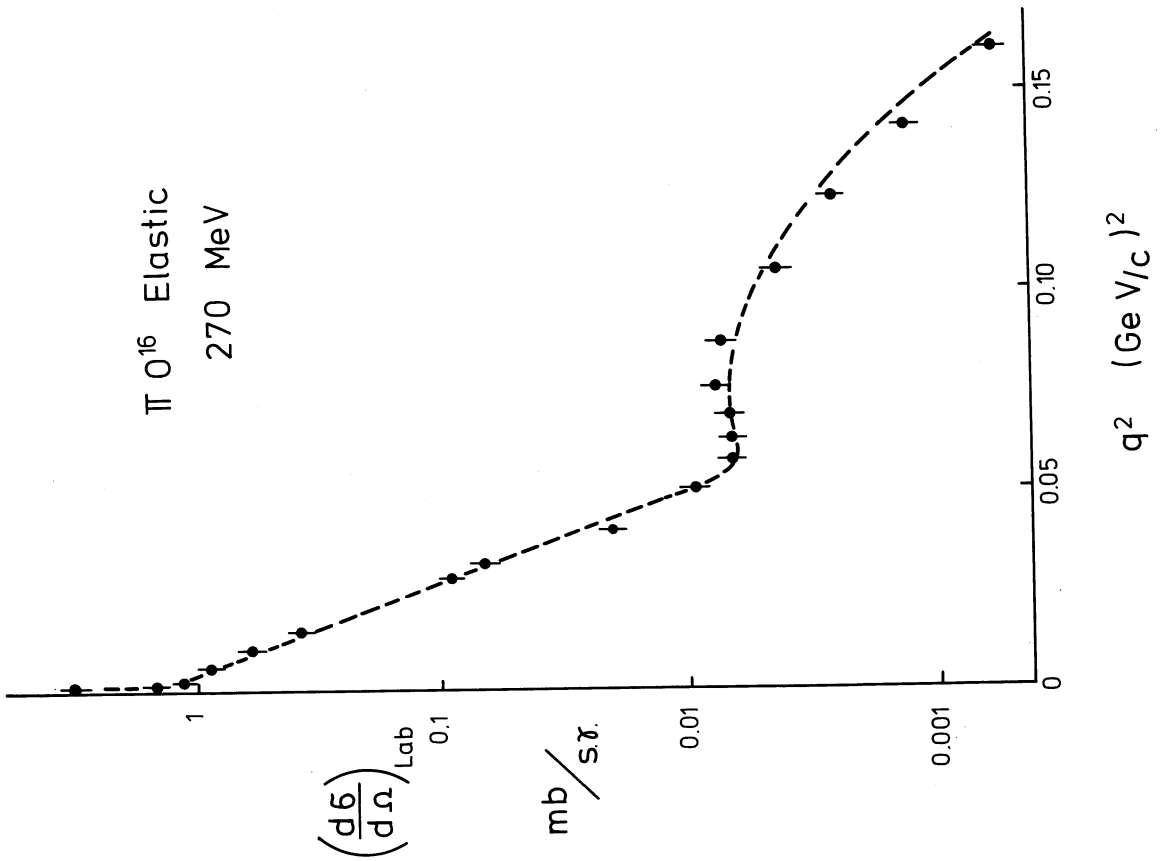
π O16 Elastic
270 MeV
(dσ/dΩ)Lab
mb/s.r.
1
0.1
0.01
0.001
0
0.05
0.10
0.15
q2 (Ge V/c)2

Fig. 2

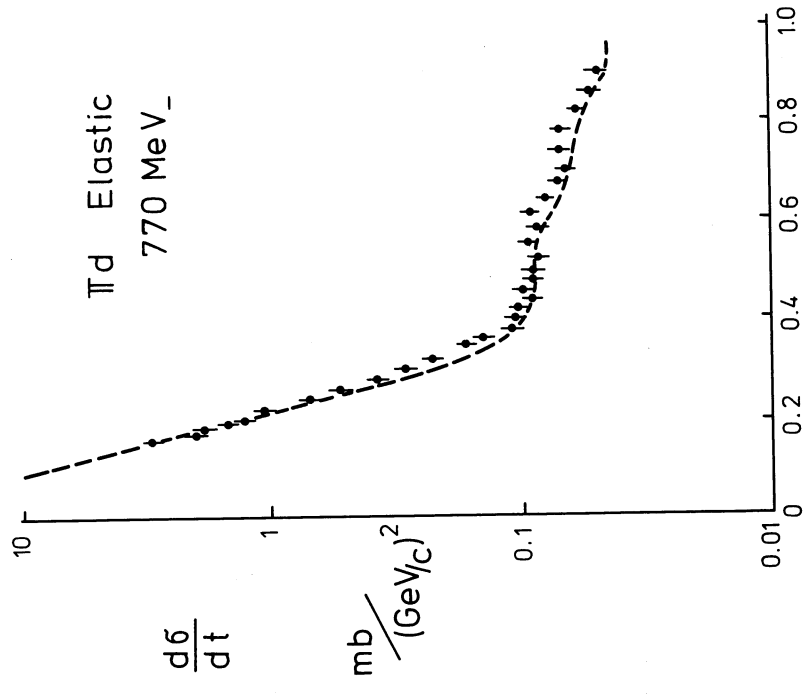
π d Elastic
770 MeV
dσ/dt
mb/(GeV/c)2
10
1
0.1
0.01
0
0.2
0.4
0.6
0.8
1.0
q2 (GeV/c)2

Fig. 1

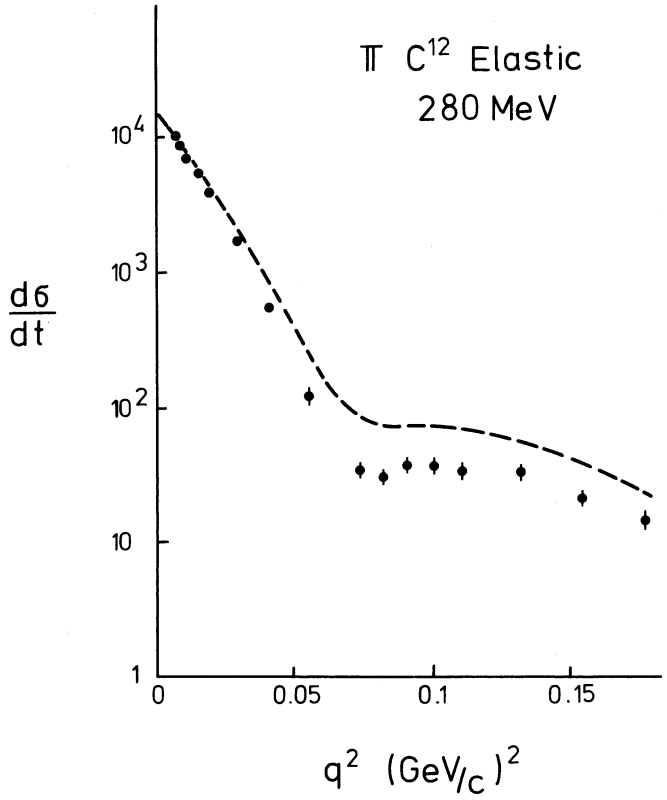
π C12 Elastic
280 MeV
dσ/dt
10^4
10^3
10^2
10
1
0
0.05
0.1
0.15
q^2 (GeV/c)^2

Fig. 3

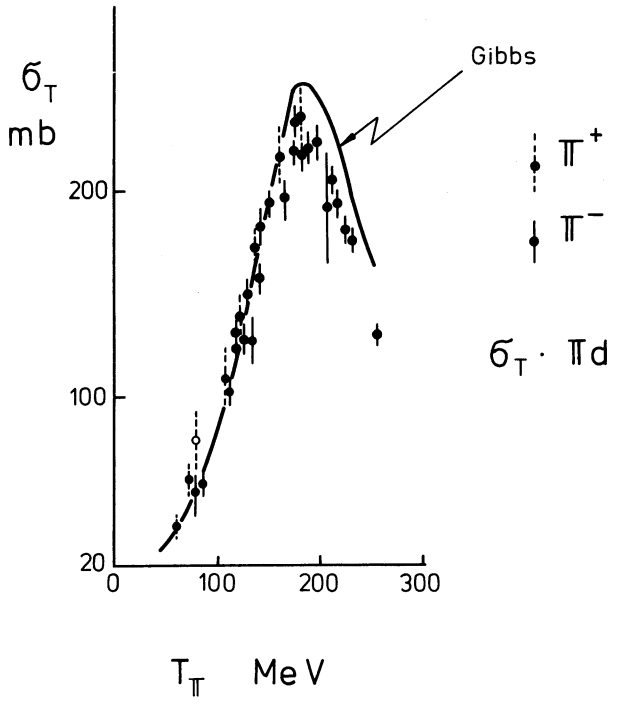
σT
mb
Gibbs
π+
π−
σT · πd
200
100
20
0
100
200
300
Tπ MeV

Fig. 4

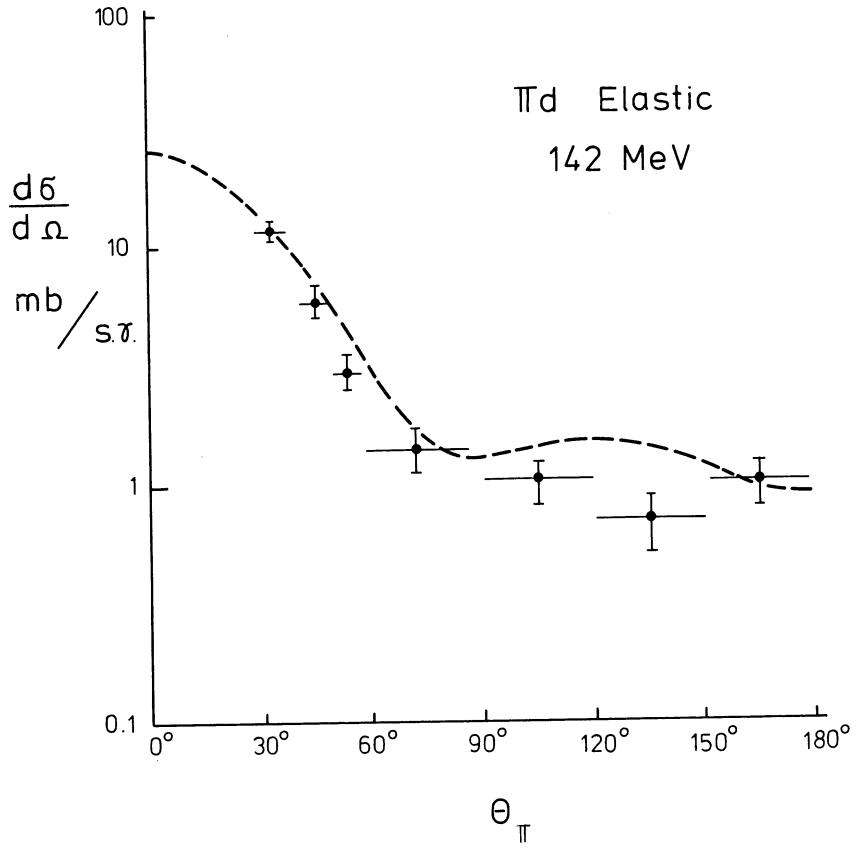
πd Elastic
142 MeV
dσ/dΩ
mb/s.r.
100
10
1
0.1
0°
30°
60°
90°
120°
150°
180°
Θπ

Fig. 5

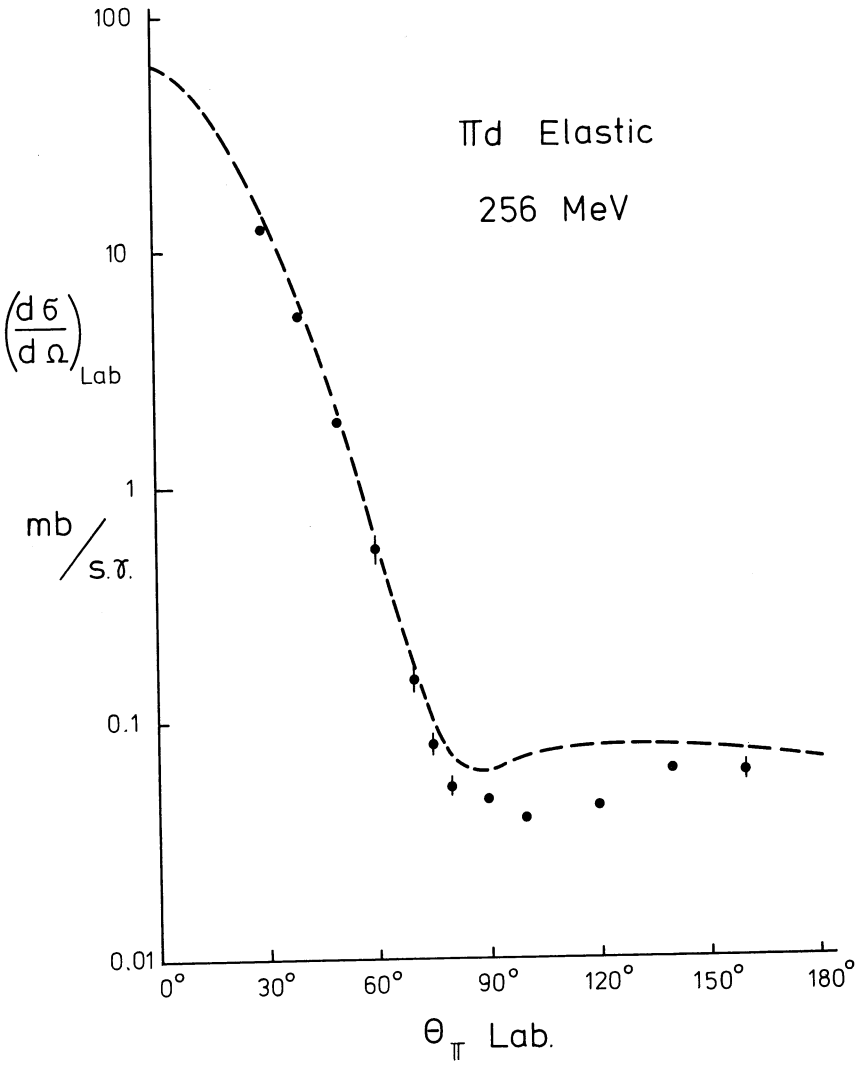
πd Elastic
256 MeV
(dσ/dΩ)Lab
mb/s.r.
100
10
1
0.1
0.01
0°
30°
60°
90°
120°
150°
180°
Θπ Lab.

Fig. 6

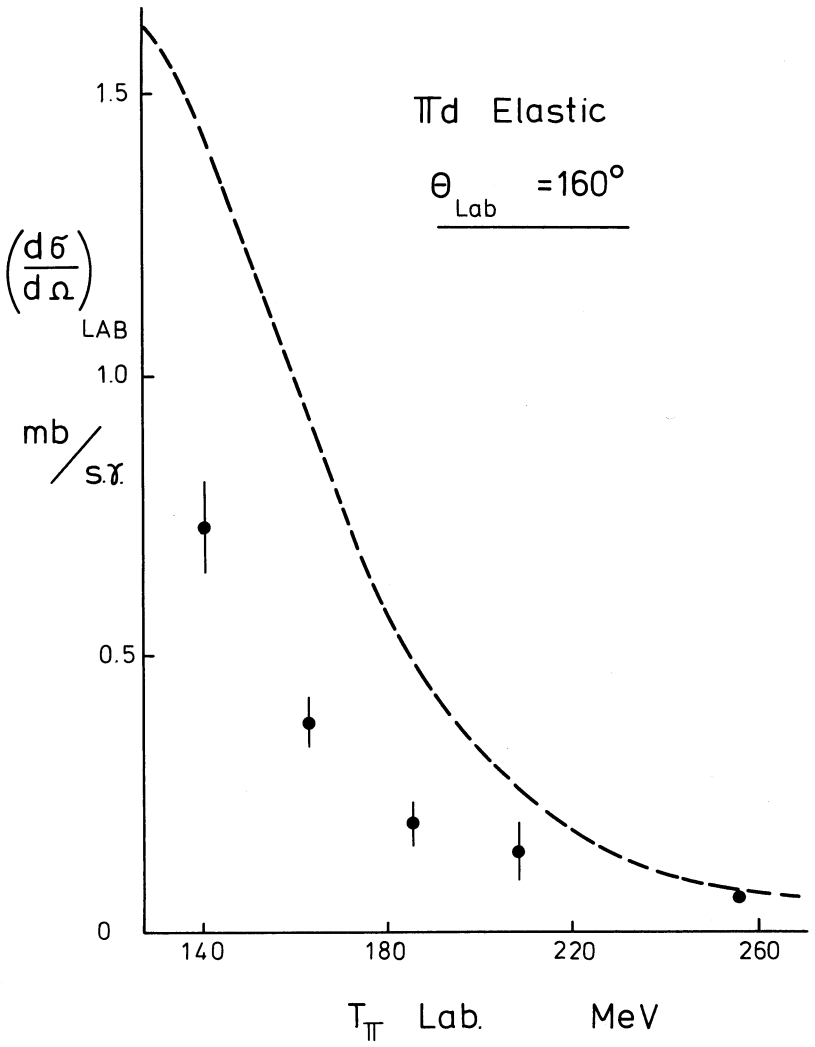
πd Elastic
θ Lab =160°
(dσ/dΩ) LAB
mb/s.r.
1.5
1.0
0.5
0
140
180
220
260
T π Lab. MeV

Fig. 7

NUCLEAR STRUCTURE INFORMATION FROM PARTICLE-EMISSION IN MUON CAPTURE

J. Deutsch
University of Louvain, Belgium

A. Neutron-emission

A.1. Evaporation

experiment: Jahnke et al., Helv. Phys. A 45 (72) 49
Evseev et al., Sov. J. Nucl. Phys. 15 (72)639

Theory: P. Singer, Nuovo Cim. 23 (62) 669
B. Mc Donald et al., P.R. 139 (65) B 1253

A.2. Giant resonance

excitation in muon-capture

compare e. g.

Igo-Kemenes et al.
Phys. Letters 34B (71) 286

Ullrich et al.
Nucl. Phys. A123 (69) 641

R. Leonardi
Bologna preprint

H. Uberall
Colorado Meeting on Muon Physics, 1971

A.3. Direct emission

i) the asymmetry-problem for review of the situation see

Evseev et al.
Yadern. Fiz. 15 (72) 939

an alternative solution: measurement of neutron helicity:

Devanathan et al.
Ann. Phys. (N.Y.) No. 2 (72) 428

ii) the neutron spectrum and the momentum distribution of the capturing proton:

nucleon correlations:

M. G. Huber
Ann. der Physik 5 (70) 239

K. Chang et al.
Z. Phys. 240 (70) 195

Phys. Letters 32B (70) 536

Phys. Letters 29B (69) 265

J. W. Morris et H. J. Weber
Phys. Rev. Letters 27 (71) 1299

W. Weise et al.
Z. Phys. 236 (70) 176

Lett. Nuovo Cim. 4 (70) 541

Dillig et Huber
Asilomar Meeting 1973

W. Weise et al.
Nucl. Phys. A162 (71) 330

Phys. Letters 38B (72) 301

B. Proton-emission

B.1. Inadequacy of the evaporation-mechanism

C. Ishi
Progr. Theoret. Phys. 21 (59) 663

to be compared to:

D. Kotelchuk and J. V. Tyler
Phys. Rev. 165 (68) 1190

Capture on surface-clusters:

P. Singer
Phys. Rev. 124 (61) 1602

Capture on virtual pions:

M. Bertero et al.
Nuovo Cim. 52 (67) 1379

B.2. Proton-proton correlation ?

B.3. Muon-capture in deep proton shells

review of deep shell exploration

M. Riou and Ch. Ruhla
Progr. Nucl. Phys. 11 (70) 195

S. Pittel et N. Austern
Phys. Rev. Letters 29 (72) 1403

RADIATIVE PION CAPTURE

P. Truöl
Physik-Institut der Universität Zürich, Switzerland

My subject, radiative pion capture, has not been talked about in the introductory sessions on π-nucleus interactions, because it falls in the category of seemingly ununderstood absorption processes. I will try to do my best in the next few minutes to convince you, that we have here on the contrary a theoretically rather well treated, experimentally accessible tool, which does provide us with new type of nuclear structure information. The reason for this is, that radiative pion capture, i.e. the process

$$\pi^- + N(A,Z) \longrightarrow N^*(A,Z-1) + \gamma$$

is an electromagnetic process and occurs, contrary to most of the other pion absorption modes on a single nucleon in the nucleus, the elementary process being

$$\pi^- + p \longrightarrow n + \gamma$$

This process is the inverse reaction to photopion-production, for which the amplitudes are at least near threshold reasonably well known. If one starts with the most general, Lorentz-invariant matrix element, takes further the nonrelativistic limit near threshold, one ends up with a Hamiltonian characterising the interaction, of the form:[1)]

$$H = 2\pi i \left(1 + \frac{m_\pi}{m_p}\right) \sum_{j,\lambda} e^{-i\vec{k}\vec{r}_j} \tau_j^{(-)} \Phi_\ell^n(\vec{r}) \cdot$$

$$\cdot \left\{ A\vec{\sigma}_j\hat{\varepsilon}_\lambda + B(\vec{\sigma}_j\hat{\varepsilon}_\lambda)(\vec{q}\vec{k}) + C(\vec{\sigma}_j\vec{k})(\vec{q}\hat{\varepsilon}_\lambda) + \right. \qquad (1)$$

$$\left. + iD\vec{q}(\vec{k}\wedge\hat{\varepsilon}_\lambda) + E(\vec{\sigma}_j\vec{q})(\vec{q}\hat{\varepsilon}_\lambda) \right\} \delta(\vec{r}-\vec{r}_j)$$

Here

$\vec{\sigma}_j$	is the nucleon spin
$\hat{\varepsilon}_\lambda$	the photon polarisation unit vector
$\vec{k}$	the photon momentum
$\vec{q}$	the pion momentum
$\tau_j^{(-)}$	the isospin-operator changing a proton into neutron
Φ_ℓ^n	the pion wave function in orbit (n, l)

Near the threshold the pion-momentum is small and the whole expression reduces to the first term, the electric dipole part. The interaction is sufficiently weak that one may apply the impulse approximation, when one studies the process on nucleons bound in a nucleus. This means that we treat the nucleus as an ensemble of single nucleons, take the transition operator between the single particle wave functions of the nucleons in the initial and the final state and sum over all nucleons. If we keep for simplicity only the leading term in the Hamiltonian and further restrict ourselves to a spin 1/2 - nucleus and capture from a 1s-Bohr orbit, as say ^{3}He, we get the following expression for the transition-rate:

$$\Lambda(^3He(\pi^-,\gamma);1S) = \frac{1}{4\pi}\frac{k}{m_\pi} A^2 \left(1-\frac{k}{m_3+m_\pi}\right)\left(1+\frac{m_\pi}{m_N}\right)$$

$$\times \frac{1}{2J_i+1}\sum_{\substack{M_i,M_f\\ \lambda}} \int \frac{d\Omega}{4\pi}\hat{k}\left|\langle J_f M_f|\sum_{j=1}^{A}\hat{\varepsilon}_\lambda \vec{\sigma}_j \tau_j^+ e^{-i\vec{k}\vec{r}_j}\phi_0^1(\vec{r}_j)|J_i M_i\rangle\right|^2 \quad (2)$$

If one factors out the pion-wave function, which is justified since it varies only very little over the nuclear volume, replaces it by its value at the origin, makes a further correction for distortion and the extended charge distribution, the remaining part of the matrixelement is just the familiar Gamow-Teller-matrixelement appearing β-decay. The difference lies only in the appearance of the retardation phase $e^{-i\vec{k}\vec{r}_j}$. It doesn't appear in β-decay since the equivalent quantity to the photon momentum, the neutrino momentum is almost zero. We may stress the connection with the Gamow-Teller-matrixelement by writing the integral as the β-decay matrixelement multiplied by a formfactor, which contains the variation with the momentum transfer. The momentum transfer in the radiative μ-capture is $q^2 = 0.954\ m^2$. The matrixelement of the axial current also appears in μ-capture process, here with $q^2 = 0.547\ m^2$. Besides the transitions to or from the bound states, found also in β-decay, the electric dipole part will also induce transitions into the giant-resonance region to the different types of collective excitations known from the Goldhaber-Teller model. This was first realized for μ-capture through the work of Walecka, Foldy, Ueberall and others[2]. In radiative pion-capture we have the possibility to directly observe these transitions, if we only measure the photon spectrum with high enough resolution. Besides the primary

interest of a nuclear physicist, which is to use the fact that the interaction is known well enough that by comparison with experimental rates nuclear model wave functions can be tested, there is another aspect, which I want to mention briefly. The constant A in the Hamiltonian, which in the impulse-approximation is the value of the electric dipol multipole amplitude in pion-photoproduction at threshold has the value[3]

$$A = 4\pi\,(E_{0+}^{(\pi^-)}) = 4\pi * (3.15 \pm .06) * 10^{-2}\ m_\pi^{-1} \qquad (3)$$

Now one can obtain its value also using PCAC and soft-pion techniques[4]. It is then related to the pion-decay constant f_π and the ratio of the axial-vector to vector coupling constants for the nucleon:

$$A = 4\pi\,\frac{g_A}{g_V}\,(\alpha/4\pi)^{1/2} * 1/f_\pi = 4 * 3.23 * 10^{-2}\ m^{-1} \qquad (4)$$

$$A = 4\pi\,(2\alpha)^{1/2}\,g = 4\pi\,(\alpha/4\pi)^{1/2}\,(g_r/m_n)\,2^{-1/2} = 4\pi * 3.44 * 10^{-2}\ m_\pi^{-1}$$

(g_r = rationalized π-N-coupling constant = 13.64) (5)

The same value is obtained in the original Kroll-Rudermann-derivation[6]. Now measuring is capture rates in light nuclei, where the formfactor could be taken via the elementary particle treatment from other processes, one could basicly test the soft-pion results and a few corrections of higher order in m_π/m_n discussed by M. Ericson and collaborators[7].

Since the constants do not differ very much, one finds in praxis very little difference between the soft-pion calculations and the impulse approximation, if the parameters of the nuclear wave functions are chosen such that the other reactions involving the axial-vector and vector form-factors are represented well or if one takes the form-factors from experiment by some suitable extrapolation[8] technique, as is done in soft-pion calculations. However, the soft-pion results apply only to capture from an 1s-orbit.

Now let me give a very brief account of the existing data and then turn to ^{6}Li and ^{12}C to bring out in detail the ingredients which are needed for a fruitful comparison of theory and experiment. All data shown with one exception were measured by the Crowe-group in Berkeley[9] using a pairspectrometer, which I will describe towards the end, when I intend to discuss ways to improve the present experimental situation.

Figure 1 shows the data for $A \leq 4$. The results can be summarized as follows:
^{1}H: With a hydrogen-target one measures resolution and efficiency of the instrument by means of the reactions $\pi^- p \rightarrow n \pi^0$ and $\pi^- p \rightarrow n\gamma$. I might point out, that the discrepancy between the Panofsky-ratio, which is defined as the ratio of mesonic to radiative capture at rest, when calculated from the difference of the singlet and triplet pion-nucleon scattering length as given by phase-shifters and the π^- - multipole amplitude from pion-photoproduction,

which gives P = 1.85-2.02[10] and the experimental value of P = 1.533[11] is still unresolved. Only measurements of the Panofsky-ratio in flight between say 5 and 50 MeV will probably settle this question.

From the $\pi^- p \to n\gamma$ transition the resolution is found to be 2 MeV FWHM at 130 MeV for the Berkeley spectrometer.

^{2}H: The deuterium data are from an old experiment by Ryan[12] and are shown merely to remind you, that the most accurate determination of the n-n scattering length comes from the measurement of radiative pion capture in deuterium[12a].

^{3}He: The Helium-3-data are new and show all three channels predicted Messiah in 1952[23]:

1) the $t\gamma$ - line at 135.8 MeV
2) the $dn\gamma$ and $pnn\gamma$ continuum with endpoint energies 129.8 and 127.7 MeV
3) the $t\pi^0$-continuum with $53 \leq E_\gamma \leq 86$ MeV

We extract a Panofsky-ratio of 2.8±.2. We further find some evidence for possible broad resonance structures in ^{3}He. The Panofsky-ratio in ^{3}He has been quoted as the prime test case for soft-pion calculations. We already had the expression for the radiative capture. The Hamiltonian to be used in an impulse-approximation calculation for mesonic capture is of the following form:

$$H = 2\pi i \left(1 + \frac{m_\pi}{m_N}\right) A \sum_{j=1}^{A} \delta(\vec{r} - \vec{r}_j)\, \Phi_\mu^\ell(\vec{r})\, \tau_j^{(-)}\, e^{i\vec{q}_0 \vec{r}_j} \qquad (6)$$

with $A = \frac{\sqrt{2}}{3}(a_1 - a_3)$

The capture rate becomes

$$\Lambda(^3He(\pi^-,\pi^0)^3H) =$$

$$= 4\pi A^2 |\Phi_1^0(0)|^2 \frac{q_0}{m_\pi}\left(1-\frac{\omega_0}{m_3+m_\pi}\right)|M_F|^2 |F_V(q^2\cong q_0^2 = 0.054 m_\pi^2)|^2 \qquad (7)$$

With the radiative rate given previously we may express the Panofsky-ratio in ^3He in terms of the equivalent quantity in Hydrogen.

$$P_3 = \frac{1}{9}\frac{(a_1-a_3)^2}{|E_{0^+}^\pi|^2}\frac{q_0}{k}\cdot\frac{m_\pi+m_3-q_{03}}{m_\pi+m_3-k_3}\left|\frac{F_V}{F_A}\right|^2$$

$$= P_1 \cdot f_{kin} \cdot \frac{F_V(q^2=0.054 m_\pi^2)/g_V}{F_A(q^2=0.945 m_\pi^2)/g_A} \qquad (8)$$

$$= 1.53 \cdot 1.11 \cdot (1.76 \pm 0.18) = 3. \pm 0.3$$

The soft pion result is equivalent to replacing[13]

$$\frac{k_1}{q_1}P_1 = (a_1-a_3)^2/9|E_{0^+}^\pi|^2 \quad \text{by} \quad \frac{m_\pi^2}{8\pi\alpha f_\pi^2} \quad \text{with } P_3 = 2.7 \qquad (9)$$

^4He: ^4H does not have a bound state, but the shape of spectrum can be nicely described by assuming the excitation of three broad T = 1 resonances with $J = 2^-$ at 3.4 MeV above the ^3He + n threshold; $J = 1^-$ at 5.1 MeV and $J = 1^-$ at 7.4 MeV.

Most of the experimental effort was concentrated on 1p-shell nuclei with $4 \leqslant A \leqslant 16$. Here the sensitivity to nuclear structure is most clearly seen. There a three features common to the photonspectra, which are shown in Figure 2:

1) Transitions to bound states, the

$$^{6}Li \rightarrow {}^{6}He: \quad {}^{12}C \rightarrow {}^{12}B; \quad {}^{16}O \longrightarrow {}^{16}N$$

transitions are seen as well as a minor bump for the $^{14}N \rightarrow {}^{14}C$ transition, which is known for its anomalously high log (ft)-value for an allowed Gamow-Tellerβ-decay (9 instead of 3 as expected). In the Nitrogen-case a second transition to a $J = 2^-$-state at 7.0 MeV is separated, for ^{6}Li a contribution from the 1.8 MeV-state is found, in Oxygen and Carbon several bound states close to ground-state of ^{16}N and ^{12}B resp. are not resolved.

2) Transition into the giant resonance region, mainly to 2^- states, first identified in ^{12}C, later in ^{16}O and now also confirmed by our latest data for ^{14}N and maybe also in ^{6}Li.

3) A continuum component from quasi-direct capture leading to the separation of a neutron from the recoil nucleus. This process is theoretically described by a pole-model with single proton-exchange, as demonstrated by Figure 3[14].

With the proton-separation energy, or which is equivalent the average excitation energy of the recoil nucleus and the coupling-constant at the nucleus-vertex as a free parameter the general shape of the continuum is described very well for a wide range of nuclei including medium and heavy mass nuclei, which are shown in Figure 4. It is clear, that while for light nuclei the resolution is barely sufficient to resolve some final states this is not the case for the heavier nuclei. Returning to the 1p-shell

nuclei, it is appearant, that though the pole-model seems to be a good description of the low energy part of the spectrum, it is doubtful whether it can be used to calculate the non-resonant background in the resonance region. For example interference between the continuum and resonance contributions is neglected. Furthermore, the relatively simple case of deuterium shows how final state interactions do influence the spectral shape especially near the neutron-breakup threshold, which are not considered, too. The comparison between experiment and theoretical calculations for the giant resonance region, which all fail to discuss the continuum, is therefore only qualitative. Figure 5 shows the ^{12}C-spectrum again, with an incoherent subtraction of the pole model contribution compared to a theoretical curve[15]. Table I gives the detailed numerical account for all p-shell nuclei; including the transitions to bound-states, for which a much more accurate comparison with theory can be made, since experimentally no nonresonant background has to be subtracted and better wave functions for theoretical calculations exist. The agreement between data and theory is satisfactory within the limits set by the accuracy of pionic X-ray measurement. This is particularly remarkable, since we find that the experimental rates (we always measure the fraction of pions inducing such a transition), vary over a range of 1000 from 6.9% for ^{3}He to .008% in ^{14}N. I will discuss ^{6}Li as an example, for what enters into the detailed comparison between theory and experiment.

Before I do that let me just insert a remark on ^{14}N - ^{14}C. If we had only the dominant $\vec{\sigma}\hat{\xi}$ term in the Hamiltonian,

we should expect the same kind of suppression of the matrix element as in β-decay, which is mainly due to the small overlap of the nuclear wavefunction, namely by a factor of 10^6. That the reduction is only about 40 if we compare to ^{6}Li is mainly due to the higher terms in the Hamiltonian proportional to the momentum transfer, which become especially important for capture from a 2p state. With the dominant contribution eliminated we have here the rather unique situation that small parts of the Hamiltonian, usually contributing only a few % can be investigated together with higher momentum components of the nuclear wavefunction. This example shows that we really learn a lot of nuclear physics here. Furthermore, we have another bound state, which allows us to get rid of some of the uncertainty arising from the pionic - x - ray data.

Now let us turn to ^{6}Li.

In order to compare experiment and theory, we need two quantities

1) the probability, that a pion gets absorbed from a given Bohr-orbit into the nucleus $\omega(n,l)$
2) the total strong absorption width of each orbit

$$\Lambda_a(n,l)$$

which are connected by the expression

$$\omega(n,l) = P(n,l)\Lambda_a(n,l) / (\Lambda_a(n,l) + \Lambda_x(n,l) + \Lambda_A(n,l))$$

Where P (n,l) is the population of state (n, l) and Λ_x, Λ_A are the X-ray and Auger-transition rates.

The fraction of pions undergoing radiative capture at each orbital is

$$\frac{\omega(n,\ell)\Lambda_\gamma(n,\ell)}{\Lambda_a(n,\ell)} \qquad (11)$$

the total fraction the incoherent sum over all orbitals

$$R_\gamma = \sum_{n\ell} \frac{\Lambda_\gamma(n,\ell)}{\Lambda_a(n,\ell)}\,\omega(n,\ell) = \frac{\Lambda_\gamma(1s)}{\Lambda_a(1s)} \sum_n \omega(n,s) + \frac{\Lambda_\gamma(2p)}{\Lambda_a(2p)} \sum_n \omega(n,p) \qquad (12)$$

Now we may compare the different theoretical calculations for Λ_γ^{1s} and Λ_γ^{2p}. The results are given in Table II. We see that the different impulse approximation calculations[16] agree well with each other and with experiment, when the parameters of the wavefunctions, like the p-shell-harmonic oscillator size parameter are chosen such, that other experimental quantities like the charge radius, the β-decay matrixelement and μ-capture rates, the radiative width of the anologous state to the ^{6}He-ground state in ^{6}Li are fitted well also. Soft pion calculations[17] deal only with 1s-capture, but yield between 10 and 20% higher values for the 1s-capture rate. Especially Delormes[18] calculation, which uses especially high corrections to the soft pion amplitude, already yields a 1s-capture fraction higher than total experimental number. The errors for the theoretical calculations are entirely due to pionic-x-ray data. ^{6}Li is due to the Virginia measurements for the capture schedule[19] one of the more favourable cases. The main errors come from Γ_{1s} and $\omega(1s)$. Fortunately last week I was told by Prof. Backenstoss, that they remeasured Γ_{1s} for

^{6}Li, with an error less than 10%. We get now the following result .319±.044 % theoretically vs. .306=.035% experimentally. It is of uttermost importance for us that capture schedules, widths and yields especially for the lighter nuclei will be remeasured, including He^{3}, for which we know nothing and ^{4}He where we know things with 40% error bars. The situation is not much better for ^{12}C, the only other nucleus where a capture schedule is known, but where the 2p-widths disagree by more than a factor of two.

Let me not further discuss the results, but rather indicate what I think the future might bring us.

From the preceding it is clear that we may improve the experiments as follows: First two easy things, which, however, both require accurate X-ray-measurements, if anything more than counting peaks is attempted:

1) a wider range of nuclei
   This could be done with the existing apparatus, i.e. a resolution of 2 MeV. We think of the targets ^{3}H, ^{9}Be, ^{7}Li, ^{10}B, ^{209}Bi. I might add ^{11}B, because we can do the giant-resonance search proposed by Deutsch[20] for μ^--capture, too.

2) Higher statistics experiments
   The total branching ratio for radiative μ-capture is 2%, the acceptance about 10^{-5} and pion beams have an intensity of about $2 * 10^{5}\,sec^{-1}$, giving about 150 events an hour, so that 20 000 events is about the practical limit for any given target. That this is not enough, I will demonstrate with a blown-up version of the ^{3}He

spectrum, shown in Figure 6, which contains about this many events. One would really like to know whether the deviations from the pole model are indications of resonances in the A=3 system or not.
The next step is not that easy:

3) Better resolution
In ^{16}N, ^{12}B, ^{6}Li we either did not resolve or had trouble resolving the different bound states, in the medium range nuclei the spectrum appears structureless precisely for the same reason. For a better understanding the experimental apparatus is shown in Figure 7. It should really have been shown at the beginning. The resolution is mainly determined by the spatial resolution of the detectors for the electron-positron pair. In the present experiment we have wire-chambers with 1 mm wire distance, but wound under 12^{o} to the horizontal coordinate, so that we have a resolution of ± 2.5 mm. This can be improved and will be improved with MWPSC to ±1.0 mm in a similar setup at SIN. We think we get 0.8 MeV with the same kind of radiator and an acceptance of about 2 to 4 times the Berkeley value. With a smaller radiator we think that 0.5 MeV is about the lower limit. We are investigating a proposal of Zupancic, which is to use szintillator (say NaI) as converter to recover part of the resolution lost due to the energy loss in the radiator. This is not expected to yield more than a factor of two in resolution, rather it allows one to use a thicker radiator with constant resolution.

The first experiment, one should do is to remeasure

the photon spectrum from radiative capture in deuterium to redetermine the n-n-scattering length. High resolution is extremely important here, since the influence of the scattering length and effective range is only noticeable in the very high end of the γ-spectrum, that is in the region between 131 and 131.5 MeV. Though we do have here the cleanest n-n-final state except maybe in $\mu^- d \rightarrow nn\nu_\mu$, the present theory used to extract the scattering length is believed to have an uncertainty of 1 fm. With increased precision, one then is forced to reexamine the calculatins by Bander, McVoy, Watson and Stuart[21], from the late 50's.

4) Coincidence experiments

All the things I mentioned so far can with a little patience certainly be done cheaper at Berkeley or at the improved SC than at SIN or Los Alamos, not to mention that the low intensity of the old accelerators was somehow compensated by the fact, that they were in cities socially somewhat more attractive, thereby quaranteeing the for good experiments so necessary peace at home for the physicist. There is one class of experiments which is to be done only at meson factories, and these are the coincidence experiments. (The very personal style has not been touched by the editor.)

If we start with 10^8 π^-'stop in the target, take the average acceptance of the pair-spectrometer between 100 and 130 MeV of about $8 * 10^{-5}$, than we have, if 1% of all π^-'s make radiative transitions $10^8 * 8 * 10^{-5} * 10^{-2} = 80$ radiative events per sec.

Basically, we can do all the experiments in coincidence with a radiative capture, which would be possible detecting only the other particle at intensities a 1000 times less than existing ones. Let me consider the different classes.

a) Coincidence with the pionic-X-ray preceeding the capture. This is really the experiment of prime interest because selecting an event preceeded by an $2p \rightarrow 1s$ -X-ray will assure that we have capture from a 1s-state. We then loose all the problems with capture schedule, model dependence of 2p-capture, higher terms in the Hamiltonian and might then check PCAC and soft-pion calculations directly.

How does the rate come out for our ^{6}Li-model case: $10^8 \pi^-$ stop in the target, of which 0.3% make transition to ^{6}He ground-state and 0.18% make transition to ^{6}He ground-state from 1s. 26% is the yield for the $2p \rightarrow 1s$ X-ray, $1.2 * 10^{-4}$ is the detection efficiency for the high-energy γ-ray. We have therefore $10^8 * 1.8 * 10^{-3} * 1.2 * 10^{-4} * .26 = 5.6$ sec^{-1} X-rays into the full solid angle with a γ detected.

The energy of the X-ray is 27.8 keV, if we select two Silicon-diodes with 0.80 cm^2 at a distance of 10 cm we have an acceptance of

$$\frac{2*8}{100} * \frac{1}{4\pi} = 1.3*10^{-3}$$ and a rate: $7*10^{-3}$ sec^{-1} or 21

events/hour.

b) Coincidence with neutron

The neutron γ-angular correlation was shown by Raiche and Werntz[22] for the ^{4}He case to be different for 1s and 2p-capture, it also may tell you about the spin of the decaying excited state from giant-resonance multiplets. The angular distribution will have the typical shape given by the combination of Clebsch Gordon-Coefficients and Legendre-Polynomials, whereas the quasidirect process preferentially decays with and neutron back to back. If we place 10 neutron-counters at 2 m, having an aerea $20*100 = 2000$ cm^2 we have a solid angle per counter of .05. With 1.5 nsec resolution we have an energy resolution of 4 MeV at 40 MeV and .5 MeV at 10 MeV, if we use time of flight with the start signal given by the photon. The rate per counter (efficiency .20) comes out to be, if no correlation is assumed whatsoever, $5*10^{-2}*5.6\frac{1}{4}*.2 = 4.5*10^{-3}$ sec^{-1} or 16/hour per counter. With some patience one might be able to do the deep-shell capture experiment Deutsch was talking about in his lecture.

Lastly I should again refer to Zupancic's remark on detecting the second high energy photon to do π^0-spectroscopy. Presently, we have only seen charge exchange at rest for Hydrogen and He^3. For other nuclei, where it is energetically possible like d, ^{6}Li, ^{14}N, ^{40}Ca, ^{209}B upper limits have been set:

d	$(3\ 4) * 10^{-3}$
^{6}Li	0.4%
^{14}N, ^{40}Ca, ^{209}Bi	0.5%

I wish to express my thanks to K.M. Crowe and H.W. Baer of the Berkeley group for their help in the preparation of this seminar. Most of the figures and both tables are taken from their recent review article[28].

References

1) J. Delorme, T.E.O. Ericson, Phys. Letters 21,98 (1966)
D.S. Anderson, J.M. Eisenberg Phys. Letters 22, 164 (1966)

2) L.L. Foldy, J.D. Walecka, Nuovo Cimento 34,1026 (1964)
H. Ueberall, Nuovo Cimento Suppl. 4, 781 (1966)

3) G. Ebel et al. Nucl. Phys. B33, 317 (1917)

4) H. Pietschmann et al. Phys. Rev. Letters 19, 1259 (1967)
N. Ericson, A. Figureau, Nucl. Phys. B3, 609 (1967)

5) M.L. Goldberger, S.B. Treimann, Phys. Rev. 110, 1178 (1958)

6) N.M. Kroll, M.A. Rudermann, Phys. Rev. 93, 233 (1954)

7) M. Ericson, M. Rho, Phys. Reports 5C, 58 (1972)
M. Ericson, A. Figureau, Nucl. Phys. B11, 621 (1969)

8) Following C.W. Kin, H. Primakoff, Phys. Rev. 139B, 1447 (1965) one usually takes $F_A(q^2)/F_A(o)$ $F_M(q^2)/F_M(o)$

9) J. Bistirlich, K.M. Crowe, A.S.L. Parsons, P. Skarek, P. Truöl, Phys. Rev. Letters 25, 689 (1970) (^{12}C)
Phys. Rev. Letters 25, 905, (1970) (^4He)
Phys. Rev. C5, 1867 (1972 (^{16}O, ^{24}Mg, ^{40}Ca)
H.W. Baer, J. Bistirlich, K.M. Crowe, A.N. de Botton, J.A. Helland, P. Truöl, The Few Body Problem in the Nuclear Interaction, I. Slaus ed. p. 805, North-Holland, Amsterdam (1972) (^6Li, ^3He)

10) Using the expressions in G. Kälen, Elementarteilchenphysik, Kap. 6.2, Hochschulstaschenbücher, Mannheim (1965) and the data from the compilation of ref. 3

11) V.T. Cocconi, T. Fazzini, G. Fidecaro, H. Legros, W. Merrison Nuovo Cimento 22, 494 (1961)

12) J.W. Ryan, Phys. Rev. 130, 1554 (1963)

12a) R.M. Salter et al., The Feco Body Problem in the Nuclear Interaction, J. Slans ed., p. 112, North-Holland, Amsterdam (1972)

13) P. Pascual, A. Fujii, Nuovo Cimento, 65A, 411 (1970) erratum Nuovo Cimento 67A, 135 (1970)

14) L.G. Dakhno, Yu. D. Prokoshkin, Sov. Jour. Nucl. Phys. 7, 351 (1968), for a recent more detailed discussion of this model see H.W. Baer, K.M. Crowe, Proc. Int. Conf. on Photonuclear Reactions and Applications, Asilomar (1973)

15) F.J. Kelly, H. Ueberall, Nucl. Phys. A 118, 302 (1962)

16) J.D. Vergados, H.W. Baer Phys. Letters, B41, 560 (1972)
F. Roig, P. Pascual, preprint G.I.F.T. (Spain) April 1972
W. Maguire, C. Werntz, Nucl. Phys. A 205, 211 (1973)

17) L.P. Fulcher, J.M. Eisenberg, Nucl. Phys. B 18, 271 (1970)
D. Griffiths, C.W. Kim, Phys. Rev. 173, 1584 (1968)

18) J. Delorme, Nucl. Phys. B 19, 573 (1970)

19) W.W. Sapp et al. Phys. Rev. C5, 690 (1972)

20) J. Deutsch, Proc. SIN-Spring School, Zuoz (1972)

21) K.M. Watson, R.N. Stuart, Phys. Rev. 82, 738 (1951)
M. Bander, Phys. Rev. 134, B1053 (1964)
K. McVoy, Phys. Rev. 121, 1401 (1961)

22) K. Raiche, C. Werntz, Phys. Rev. C4, 2003 (1971)

23) A.M.L. Messiah, Phys. Rev.87, 639 (1952)

24) S. Skupsky, Phys. Letters 36B, 271 (1971); Nucl.Phys. A 178, 289 (1971)

25) J.D. Vergados, Proc. Int. Conf. on Photonuclear Reactions and Applications, Asilomar (1973)

26) J.D. Murphy et al., Phys. Rev. Letters 19, 714 (1967)

27) C. Werntz, private communication

28) K.M. Crowe, H.W. Baer, Proc. Int. Conf. on Photonuclear Reactions and Applications, Asilomar (1973)

NUCLEI			EXPERIMENT[a]			SHELL MODEL		OTHER MODELS
$T_z=0\rangle \rightarrow \vert T_z=1\rangle$	J_i^π	J_f^π	$E_x(T_z=1)$ [MeV]	$E_x(T_z=0)$ [MeV]	R_γ [%]	R_γ [%]	Valence Orbitals	R_γ [%]
$^6Li \rightarrow {}^6He$	1^+	0^+	0.0	3.56	.306±.035	.36[b]	1p	.41±.11[c]
		2^+	1.8	5.36	.148±.025	.08[b]	1p	
$^{12}C \rightarrow {}^{12}B$	0^+	$(1^+,2^+,2^-)$	.35	15.45	.091±.009	.07[d]	1p,2s,1d	.105±.035[c]
		2^-	4.75	19.85	.185±.019(.30)[g]	.28[e]	1p,2s,1d	
		1^-	8.10	23.20	.159±.016(.42)[g]	.19[f]	1p,2s,1d	
$^{14}N \rightarrow {}^{14}C$	1^+	0^+	0.0	2.31	<.008	.008[h]	1p	
		2^+	7.01	9.17	.094±.024	.12[h]	1p	
		2^-	7.34	9.51		.009[h]	1p,2s,1d	
		Giant Res.	20.5	22.8				
$^{16}O \rightarrow {}^{16}N$	0^+	$(2^-,0^-,3^-,1^-)$	0.0	13.0	.15±.03	.168[k]	1p,2s,1d 2p,1f	
		2^-	7.70	20.7	.22±.05(.58)[g]			.43[i]
		GD + GQ	5.6-15.6	18.6-28.6	.25±.06(.97)[g]			1.65[j]

a) Berkeley group. (ref. 9) b) Vergados, Baer (ref. 16) c) Maguire, Werntz (ref. 16)
d) Skupsky (ref. 24) renormalized to correspond to X-ray data employed in a); include 1^+ and 2^+ states
e) Skupsky includes only 2^- state at Ex = 5.1 MeV; f) Skupsky 1^- states at Ex = 7.0, 7.5, 10.5 MeV
g) assume pole model contribution = 0. h) Vergados (ref. 25)
i) Murphy et al. (ref. 26) transition to 2^- state predicted at 17.5 MeV in ^{16}O.
j) Murphy et al. sum of contributions to GD states $(0^-,1^-,2^-)$ and GQ states $(1^+,2^+,3^+)$ between 17.5 and 29.1 MeV in ^{16}O.
k) Werntz (ref. 27)

Table I Comparison of experimental and theoretical radiative π-capture ratios in lp-shell nuclei.

Table II Comparison of experimental and theoretical capture rates for $^{6}Li(\pi^{-},\gamma)^{6}He$ (0^{+}, g.s.)

$\lambda_\gamma(1s)$ ($*10^{15}sec^{-1}$)	$\frac{\lambda_\gamma(1s)}{\lambda_a(1s)}$ (%)	$\lambda_\gamma(2p)$ ($*10^{10}sec^{-1}$)	$\frac{\lambda_\gamma(2p)}{\lambda_a(2p)}$ (%)	$R(\pi^{-},\gamma)$ [a] (%)	References
1.46 ± .22	.50 ± .08	4.12 ± .62	.18 ± .06	.31 ± .07	Roig, Pascual IA
1.51 ± .15	.51 ± .06	5.26 ± .06	.23 ± .06	.34 ± .07	McGuire, Werntz IA
2.08	.70 ± .05	4.32	.19 ± .05	.39 ± .08	Vergados, Baer IA
1.40	.47 ± .03	4.44	.52 ± .14	.30 ± .05	Vergados, Baer IA
2.3 ± .5	.78 ± .18			.62 ± .11	Delorme EP
1.86 ± .18	.63 ± .08			(.25 ± .07) [b]	Pascual, Fujii EP
1.9 + .4, -.2	.64 +.14, -.08			(.26 +.08, -.07) [b]	Fulcher, Eisen. EP
1.65	.56 ± .04			(.23 ± .06) [b]	Griffiths, Kim EP
				.306 ± .035	This Experiment

a) $R(\pi^{-},\gamma) = \frac{\lambda_\gamma(1s)}{\lambda_a(1s)} \times \Sigma\omega_s + \frac{\lambda_\gamma(2p)}{\lambda_a(2p)} \times \Sigma\omega_p$

where $\Sigma\omega_s = .40 \pm .09$, $\Sigma\omega_p = .60 \pm .09$

$\lambda_a(1s) = 2.95 \pm .20 \times 10^{17}\ sec^{-1}$, $\lambda_a(2p) = 2.28 \pm .61 \times 10^{13}\ sec^{-1}$

b) 1s-capture only

List of Figures

Figure 1 Photon spectra for nuclei with $1 \leq A \leq 4$. (b) Spectrum for deuterium from Ryan[19]. The curve is calculated for a 2-neutron ^1S-state scattering length $a_{nn} = -16.4$ fm. (c) Spectrum for ^{3}He. The solid curve is a pole model model calculation. (d) Spectrum for ^{4}He by Bistirlich et al.. The solid curve is an R-matrix calculation assuming excitation of three states as indicated.

Figure 2 Photon spectra for 1-p shell nuclei. Solid curves are pole-model calculations. The phase space curve (P.S.) in (a) is seen not to describe well the continuum.

Figure 3 Pole graph for radiative π-capture.

Figure 4 Photon spectra for medium mass and heavy nuclei. The curves are pole model calculations. Evidence for excitation of the bound states of ^{24}Na and ^{40}K can be seen clearly.

Figure 5 Photon energy spectrum from π-capture in ^{12}C. (a) spectrum with fitted function using three Breit-Wigner forms plus the pole model for the continuum. (b) Photon spectrum for pions with a mean energy of 40 MeV used for in-flight background subtraction. (c) Spectrum with the pole model subtracted. The solid curve is the best fit; the dashed curve is the prediction of Kelly and Ueberall for excitation of giant dipole states.

Figure 6 Photon spectrum for ^{3}He in region where the breakup channels pnn and dn dominate. The solid line is a pole model calculation as discussed in the text.

Figure 7 The electron-positron pair spectrometer and range-telescope geometry. The trigger for an event was $\pi 1 \times \pi 2 \times \pi 3 \times \overline{\pi S} \times (AxB)_i \times (AxB)_K$, $i \neq K, K \pm 1$

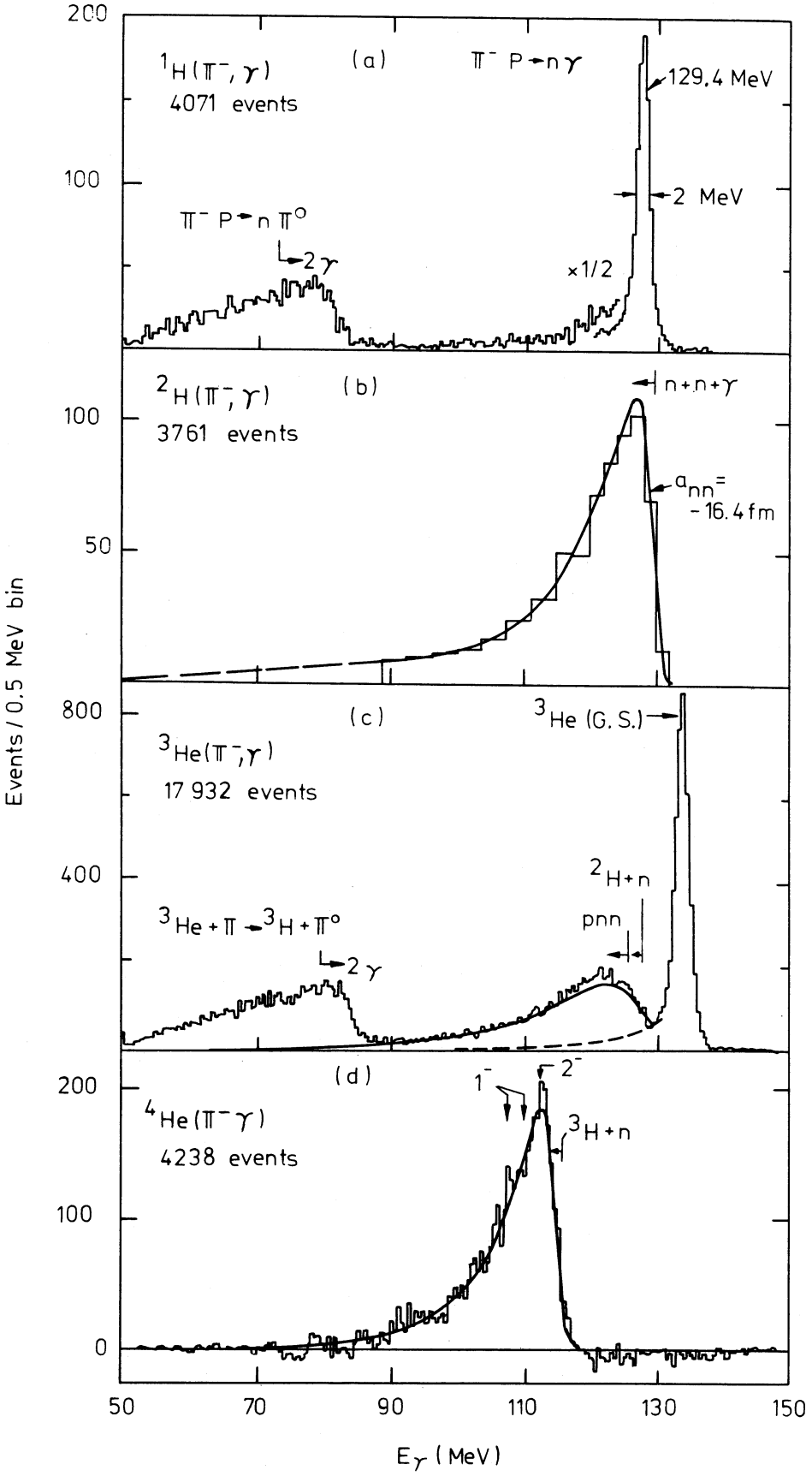
200
100
^{1}H(π^-, γ)
4071 events
(a)
π^- P → n γ
129.4 MeV
2 MeV
π^- P → n π^0
→2 γ
×1/2
100
50
^{2}H(π^-, γ)
3761 events
(b)
n+n+γ
a_{nn} = - 16.4 fm
800
400
^{3}He(π^-, γ)
17 932 events
(c)
^{3}He (G. S.)
^{2}H+n
pnn
^{3}He + π → ^{3}H + π^0
→2 γ
200
100
0
^{4}He($\pi^-\gamma$)
4238 events
(d)
1$^-$
2$^-$
^{3}H+n
Events / 0.5 MeV bin
50
70
90
110
130
150
E_γ (MeV)

Fig. 1

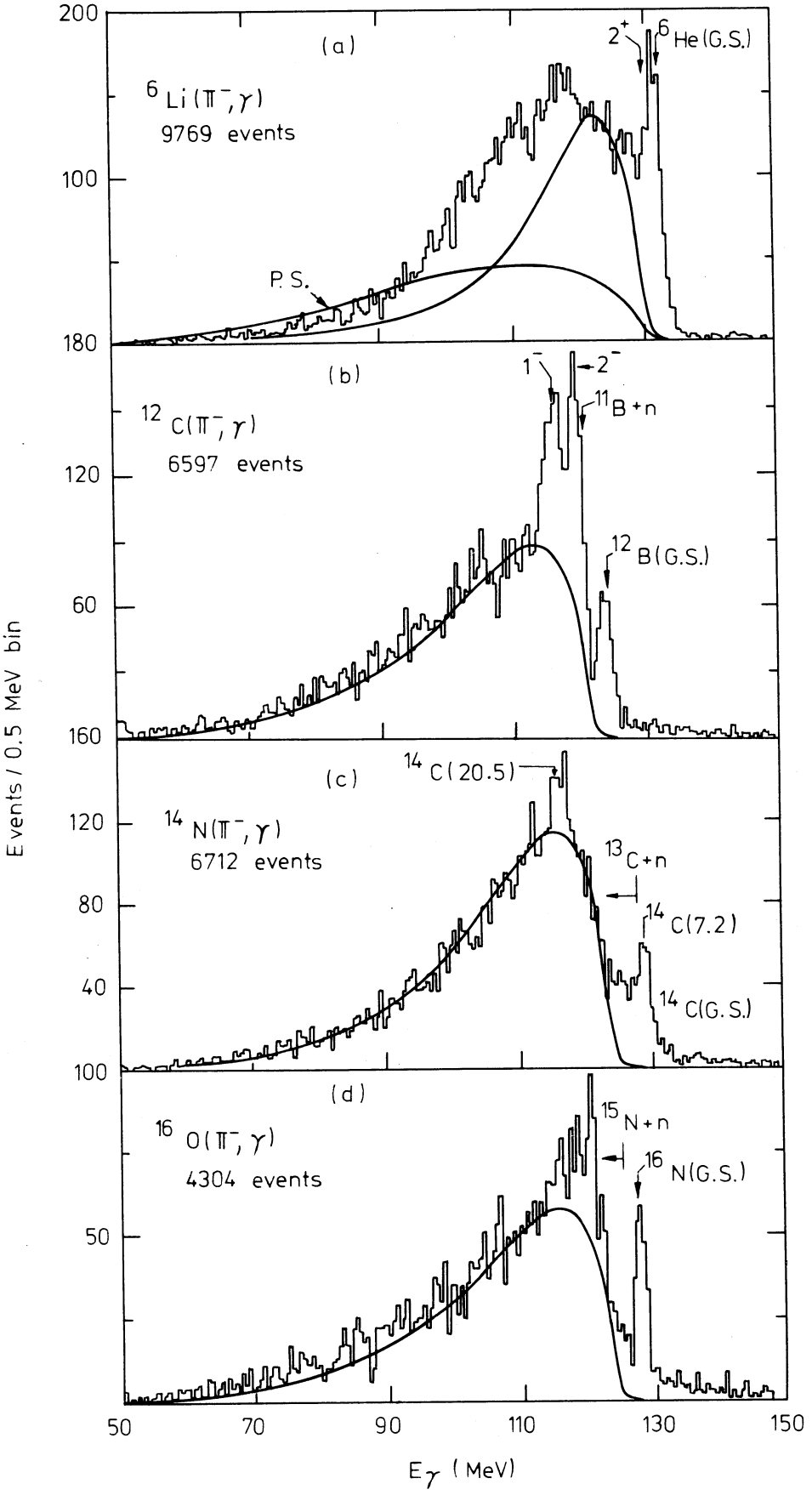
(a)
^{6}Li(π⁻,γ)
9769 events
P.S.
2⁺
^{6}He(G.S.)
(b)
^{12}C(π⁻,γ)
6597 events
1⁻
2⁻
^{11}B+n
^{12}B(G.S.)
(c)
^{14}N(π⁻,γ)
6712 events
^{14}C(20.5)
^{13}C+n
^{14}C(7.2)
^{14}C(G.S.)
(d)
^{16}O(π⁻,γ)
4304 events
^{15}N+n
^{16}N(G.S.)
Events / 0.5 MeV bin
Eγ (MeV)

Fig. 2

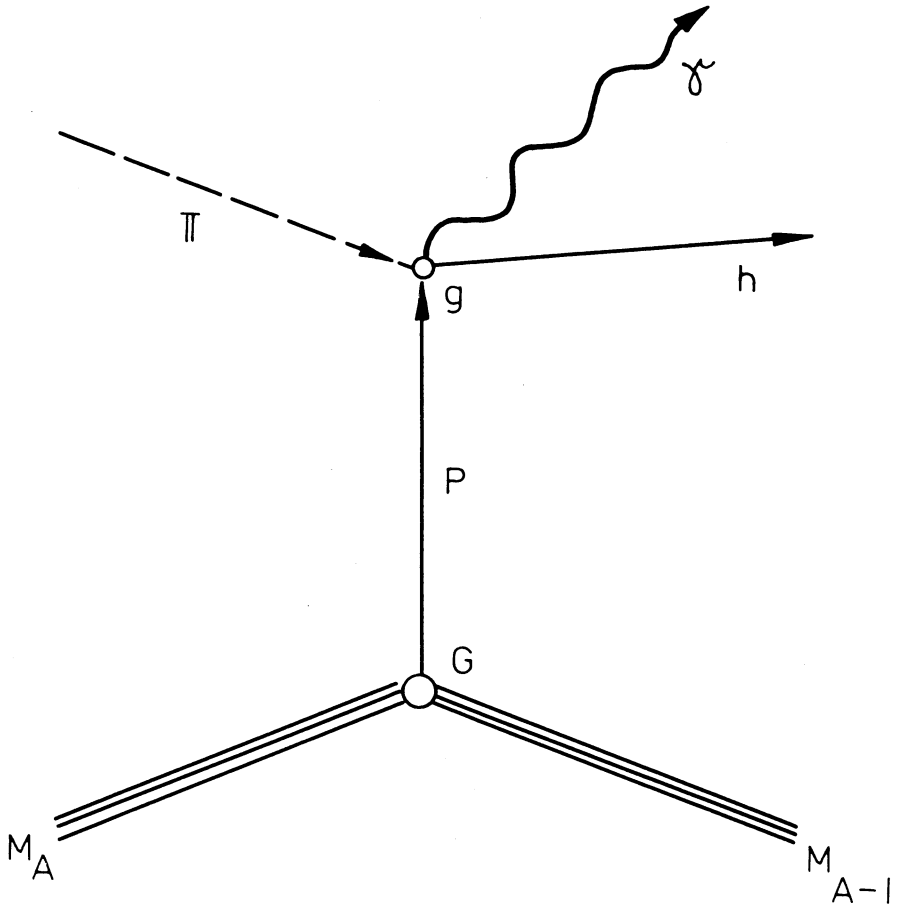

Fig. 3

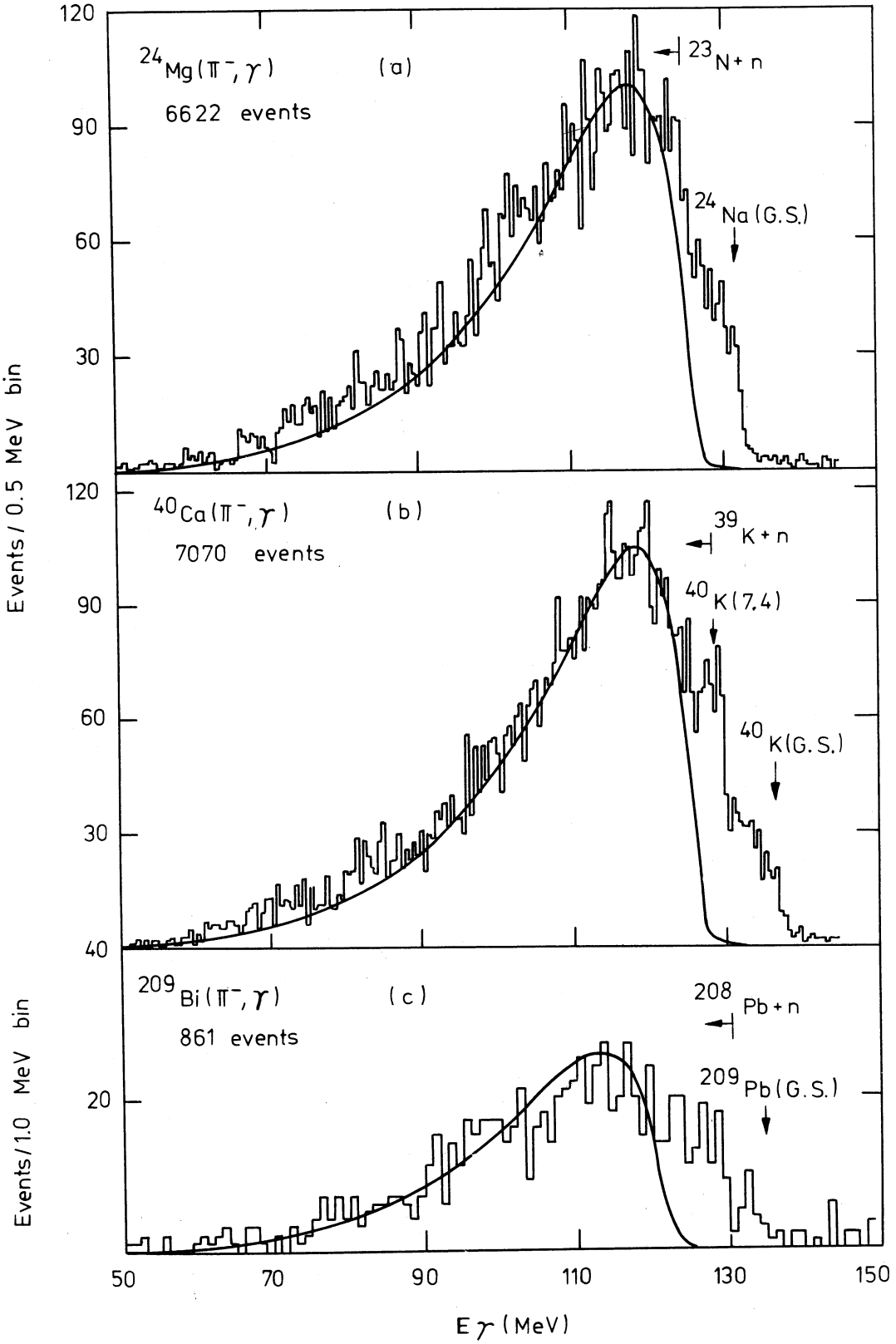
^{24}Mg(π^-,γ) (a)
6622 events
^{23}N + n
^{24}Na (G.S.)
^{40}Ca(π^-,γ) (b)
7070 events
^{39}K + n
^{40}K (7.4)
^{40}K (G.S.)
^{209}Bi(π^-,γ) (c)
861 events
^{208}Pb + n
^{209}Pb (G.S.)
Events / 0.5 MeV bin
Events / 1.0 MeV bin
Eγ (MeV)

Fig. 4

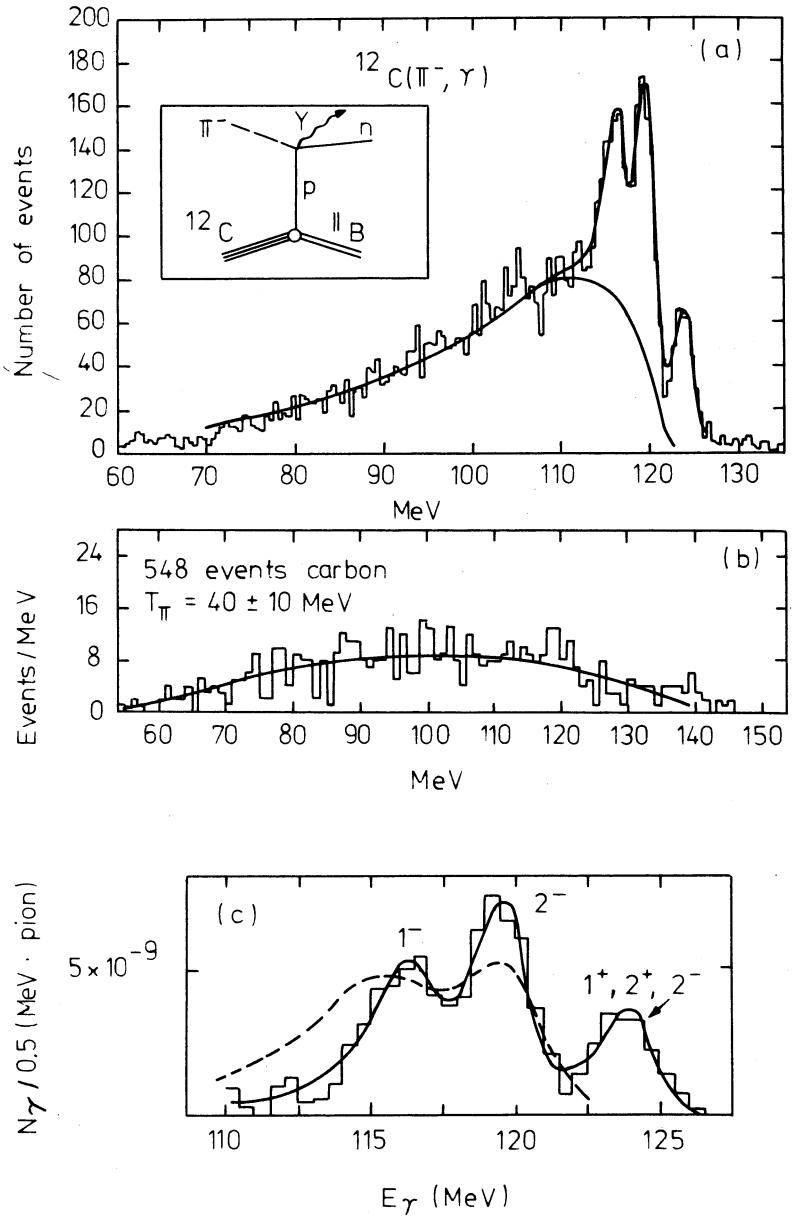
(a)
$^{12}C(\pi^-, \gamma)$
π^-
Y
n
p
^{12}C
^{11}B
Number of events
MeV
(b)
548 events carbon
$T_\pi = 40 \pm 10$ MeV
Events / MeV
MeV
(c)
5×10^{-9}
1^-
2^-
$1^+, 2^+, 2^-$
N_γ / 0.5 (MeV · pion)
E_γ (MeV)

Fig. 5

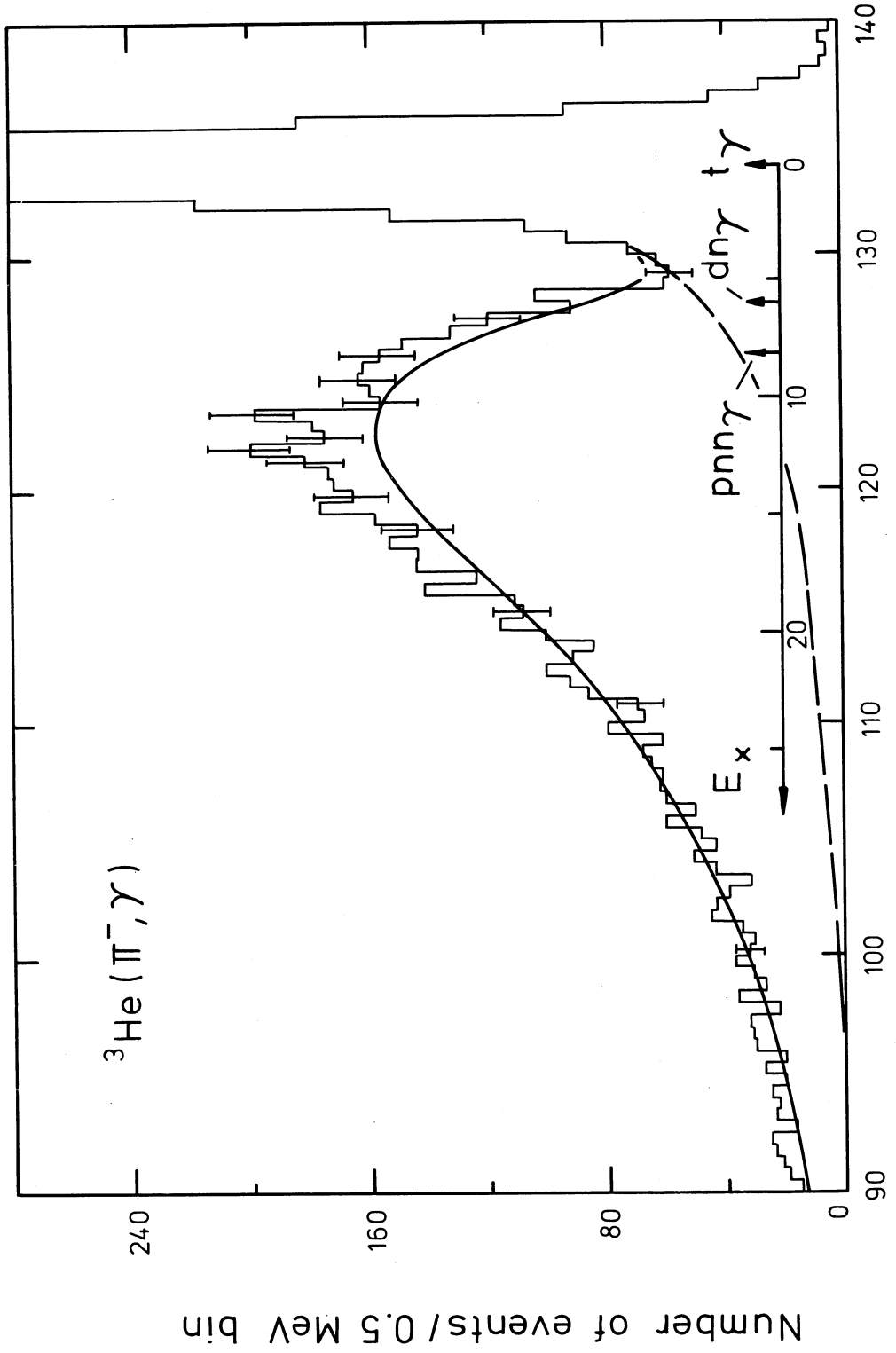
Number of events/0.5 MeV bin
240
160
80
0
90
100
110
120
130
140
E_γ (MeV)
$^3He(\pi^-,\gamma)$
E_x
0
10
20
$pnn\gamma$
$dn\gamma$
$t\gamma$

Fig. 6

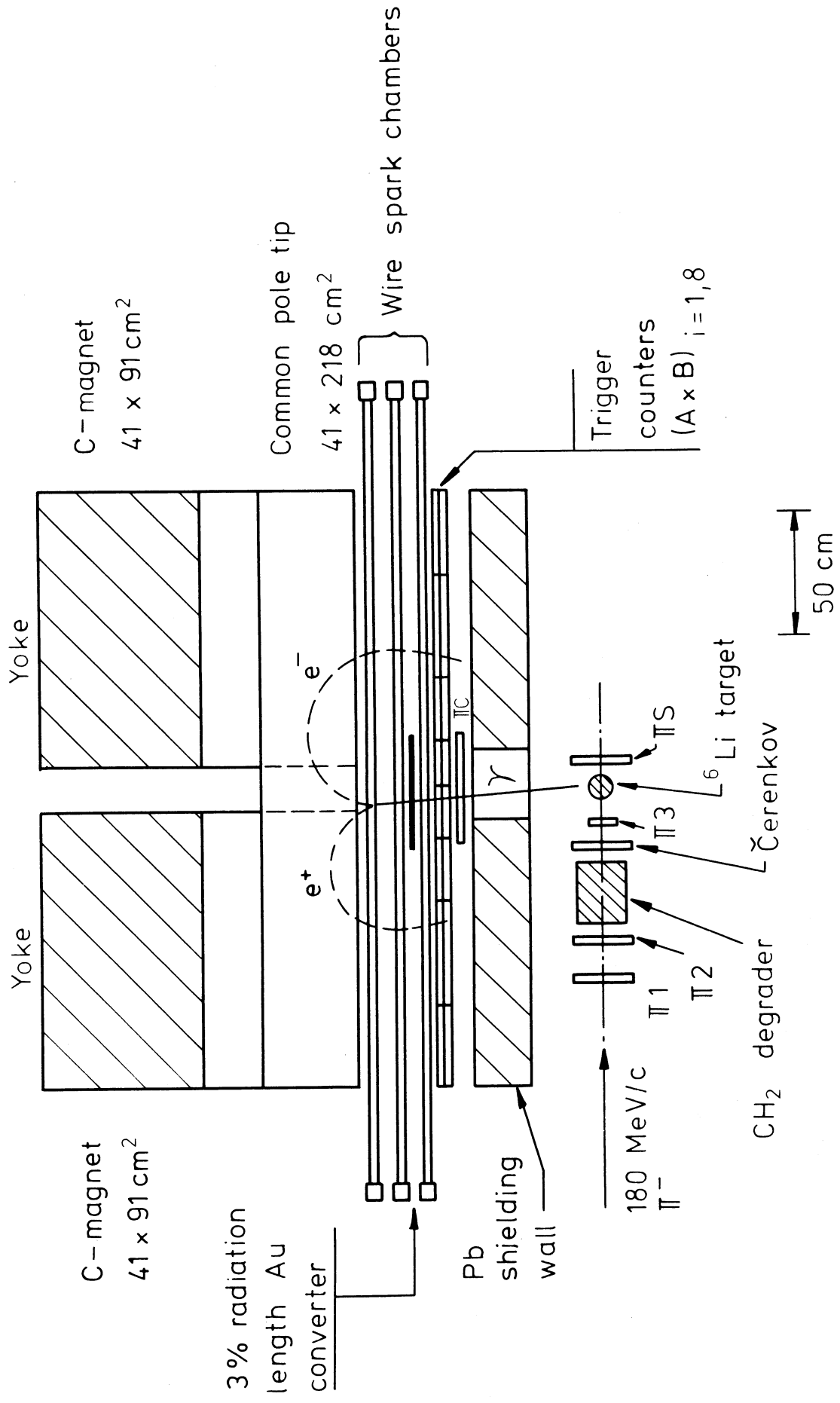
C-magnet
41 x 91 cm²
Common pole tip
41 x 218 cm²
Wire spark chambers
Trigger
counters
(A x B) i=1,8
Yoke
Yoke
C-magnet
41 x 91 cm²
e⁻
e⁺
γ
πC
πS
Li target
Čerenkov
π3
π2
π1
CH₂ degrader
180 MeV/c
π⁻
Pb
shielding
wall
3% radiation
length Au
converter
50 cm

Fig. 7

POSITIVE MUONS IN CONDENSED MEDIA

Alexander Schenck*) and Kenneth M. Crowe

Lawrence Berkeley Laboratory,
University of California,
Berkeley, California, USA.

1. INTRODUCTION

These lectures will be concerned with the application of positive muons as probes in condensed media physics and chemistry*). In each experiment muons are brought to rest in a target containing solid or liquid substances. Positive muons are implanted in this way in whatever substance one likes. Due to the finite momentum distribution of a muon beam and to range straggling, muons will stop almost homogeneously over the target volume, even if the volume is as large as 1000 cm^3. Therefore the muons will be exposed to the real bulk properties of the target material.

By implanting muons we have joined the growing community of ion implanters; in fact, through muon implantation, one is very often studying the same properties that others study with heavier ions. We will see later what the muons can achieve compared with heavier ions, and what its shortcomings are. For future complementary research with both muons and heavier ions, it may be a lucky circumstances that meson factories and the new generation of heavy-ion accelerators are coming into operation almost at the same time.

In contrast to negative muons, the implanted positive muons are not captured into atomic or molecular orbits, and neither interact with nor are captured by nuclei. We may

---

*) Present address: SIN, Villigen, Switzerland

consider an implanted positive muon to be a light isotope of hydrogen; very often it sufficies to think of the muon as a proton. When we ask ourselves "What happens to an implanted positive muon?" the first thing to do is find out what one knows about the fate of protons under the same conditions. Interestingly, as we will find out, knowledge concerning the proton under these conditions is generally scarce and hard to obtain. It is fortunate, therefore, that one can use the muon as a proton substitute to learn more about the proton's role in a condensed media environment.

The point of interest, of course, is the magnetic interactions of the muon within the medium of the target. The muon sees with its magnetic moment all the internal magnetic field components that are present at the site of the implanted muon. These local fields may be created by nuclei, electrons, paramagnetic ions, and all kinds of hyperfine interactions. By measuring the interaction energy, one may expect to learn something about these internal fields and their origin. However, it is not only possible to study the static features of local fields, it is also possible to obtain information regarding the dynamic properties of internal fields. This is accomplished by studying the spin depolarization of muons which originally were implanted more or less polarized.

The causes of depolarization processes can be quite different in origin; and we may expect to encounter all the spin relaxation mechanisms that are dealt with in NMR and ESR studies, as well as in others. It will become evident that chemical kinetics, for instance, play an important role in depolarization phenomena.

2. BASIC MUON PROPERTIES

How do we measure magnetic interaction energies? How do we observe spin relaxation? Let us first deal with these questions by summarizing some of the muon properties that are important to us. Table I contains some basic information about the muon[1] which will be adequate for our purposes in the context of this chapter. Except for its mass and its finite lifetime, the muon is in nearly every respect like an electron or positron.

In a magnetic field $\vec{H}$ the Zeeman splitting frequency is given as follows:

$$\omega = \frac{2\vec{\mu}_\mu \cdot \vec{H}}{\hbar} = \frac{eH}{m_\mu c} \approx 2\pi \frac{2.8}{207} H \left[\frac{\text{rad}}{\text{sec}}\right]$$

or (1)

$$\frac{\nu}{H} = \frac{\omega}{2\pi} \cdot \frac{1}{H} \approx 13.6 \frac{\text{kHz}}{\text{gauss}}$$

ω is also the Larmor precession frequency a muon would have in a transverse magnetic field of the same strength ($\vec{H} \perp \vec{S}_\mu$).

The positive muon decays with the emission of an energetic electron:

$$\mu^+ \longrightarrow e^+ + \nu_e + \bar{\nu}_\mu$$

As will be shown in Section 4, the decay positron shows an asymmetric distribution with respect to the spin of the muon due to the violation of parity in weak interactions. This distribution is given by the expression:

$$P(\theta) \sim (1 - a(E_e)\cos\theta) \qquad (2)$$

or

$$dN(\theta) \sim (1 - a(E_e)\cos\theta)\, d\Omega \qquad (3)$$

where $dN(\theta)$ is the decay rate into the solid angle $d\Omega$, and θ us the angle between μ^+-spin and e^+-trajectory. The asymmetry parameter $a(E_e)$ is a function of the positron energy E_e. Figure 1 shows roughly the dependence of a on the positron energy. If positrons of all energies are observed, one obtains an average asymmetry of $\bar{a} = 1/3$. By observing only the higher energy positrons, one can increase somewhat the average experimentally observed asymmetry.

Figure 2 displays the energy spectrum of the decay positrons. It is cut off at about 52.8 MeV. The average energy of the positrons is roughly 35 MeV. This is rather large compared with the energy of electrons emitted in β-decay of nuclei; therefore it is relatively easy to observe most of the electrons, even if the decaying muons are placed deep inside a target of convenient size.

In order to observe experimentally the asymmetric decay pattern, it is, of course, necessary that the spins of all mucns be more or less parallel, or in other words, that the implanted muons be polarized. Once this is accomplished, the effective asymmetry of the positron distribution, including the muon polarization, can easily be measured. As a matter of fact, highly polarized muon beams can be readily obtained from pions decaying in flight by means of a proper momentum selection. This is, again, a consequence of parity violation in the weak decay of pions, which leads to a complete polarization of the decay muons in the rest frame of the pion.[1] The achieved beam polarization is generally of the order of 80%. Taking the polarization into account

we rewrite Eq. (3) as follows

$$dN(\theta) \sim (1 - P\bar{a}(\overline{E_e})\cos\theta)\, d\Omega \qquad (4)$$

3. EXPERIMENTAL METHODS

Now, what are the experimental methods for measuring $P\bar{a}$? It is obvious that a separate measurement of P and $\bar{a}$ is possible only if one of the two quantities is known beforehand. This is generally not the case (for exceptions, see later).

It is convenient to distinguish between two experimental arrangements:

1) The target in which the muons are to be stopped is placed in zero magnetic field or in a longitudinal field with respect to the spin-polarization vector $\vec{P}$. The arrangement is indicated in Fig. 3. By observing the positron rates in the two counter telescopes, we are measuring the forward decay rate and the backward decay rate, respectively, with respect to the polarization vector. Calling the forward rate N^+ and the backward rate N^-, one can form the ratio (from Eq. 4):

$$\frac{N^- - N^+}{N^- + N^+} = P\bar{a}\,\overline{\cos(\theta = 0^\circ, 180^\circ)} \qquad (5)$$

This ratio is seen to be proportional to $P\bar{a}$ with a proportionality factor given by the average of $\cos\theta$ over the solid angle covered by the counters. This factor is of course < 1. (It is hereby assumed that $\overline{\cos(\theta=0^0)} = \overline{\cos(\theta=180^0)}$.) The experimentally observed asymmetry is thus smaller than $P\bar{a}$ due to finite solid-angle resolution. To

give a number: in many experiments $P\,\bar{a}\cos\theta$ is of the order of about 20%, if no other effects are present. Equation 5 is also correct if a time differential measurement is performed. P may then display a time dependence (see below).

2) The target is placed in a magnetic field whose direction is perpendicular to the muon polarization. The spinning muons will then start to precess with a frequency given by Eq. 1, the Larmor frequency; thus the asymmetric decay pattern will rotate. The situation is shown in Fig. 4. In order to make the precession visible, a time differential measurement has to be performed. The angle between muon spin and observable positron trajectory (fixed by the geometry of the counter telescope) will vary in time as

$$\theta = \omega t$$

The positron rate in the counter telescope as a function of muon lifetime in the target is then described by the following formula, starting from Eq. 4 and taking the experimental decay law into account:

$$dN(\theta,t) \sim \frac{1}{\tau_\mu} \exp(-t/\tau_\mu)\left[1 - P\bar{a}\cos(\omega t + \Phi)\right] d\Omega\, dt \qquad (6)$$

For an actual experimental set-up, taking finite time and solid angle resolution into account, which we shall describe by a factor $f<1$, Eq. 6 becomes:

$$\Delta N(\theta,t) \sim \frac{1}{\tau_\mu} \exp(-t/\tau_\mu)\left[1 - P\bar{a}f\cos(\omega t + \Phi)\right] \qquad (7)$$

ϕ is the phase of the polarization for t = 0, and depends on the actual e^+ counter alignment with respect to the polarization vector of the μ^+ beam. As will be discussed later, ϕ may also depend on the early fate of the muon in the target. P $\bar{a}$ f is the effective experimentally observable decay asymmetry; hence forth we will set A = P $\bar{a}$ f.

The physical interpretation of Eq. 7 is as follows: When a muon decays, the probability of observing a decay positron will be a maximum at the moment when the muon spin points into the positron telescope, and a minimum for the antiparallel case. The exponential decay curve, visible in a time differential measurement, will thus be cosine-modulated, as indicated in Fig. 5.

We have spoken about time differential measurements. How is this actually done and what is the experimental arrangement in practice? Schematic diagrams of an actual experimental arrangement are shown in Fig. 6. These diagrams are valid for the longitudinal field as well as the transverse field arrangement. The principal components of the necessary electronics are shown in the same figure.

A stopped muon is signaled by the logic combination $(B1 \cdot B2) \cdot (M1 \cdot M2) \cdot \bar{M}$. Likewise, a decay positron will be identified by the signal $(E1 \cdot E2) \cdot \bar{M}\bar{2}$. The μ-stop signal will be used to start a clock and to create a gate signal of about 10 μsec length. The positron signal in coincidence with the gate signal will stop the clock. The gate signal thus defines the time interval after the muon stop during which one waits for the decay electron. In this way, for each observed muon decay, one measures the individual lifetime of the decayed muon. From these data one can form a

histogram: positron rate versus elapsed lifetime, which should be described by one of the distribution formulas, Eq. 5 or Eq. 7, depending on the field arrangement. These formulas will then be fitted to the histograms, yielding the interesting parameters.

It is demanded, of course, that no second muon stops during the time one is waiting for the decay positron; otherwise, it becomes unclear from which muon the positron originated. This limits the actual stopping rate to about $10^4 \mu^+$/sec, a rate much less than it will be possible to achieve at SIN, for instance. Although this limitation is a very unfortunate feature of the time differential method, it is nevertheless the most versatile method and has to be used for most of the problems to be studied. However, the high muon fluxes at meson factories will be a great advantage because with them one can use extremely small targets. At SIN, an experimental set-up uses 0.5-cm^3 targets with a density of about 0.5 g/cm^2. (Conventional targets are much larger with densities of 8 to 20 g/cm^2 and cross sections adapted to the μ-beam cross sections.) This will allow one to investigate particularly small single crystals and other rare substances.

4. EXPERIMENTAL TYPES OF MUON DEPOLARIZATION PHENOMENA AND COMPLETE PHENOMENOLOGICAL RATE DISTRIBUTION FORMULAS

The first experimenters to check on parity invariance in muon decay were Garwin, Ledermann, and Weinrich.[2] Using a transverse field arrangement, they did indeed detect an asymmetry which in graphite, calcium, and polyethylene was close to the theoretically expected value of $\bar{a} = 1/3$. In nuclear emulsion, however, the asymmetry detected amounted to only about 1/6. This suggests the pre-

sence of some depolarization mechanism in nuclear emulsion that leads to a partial depolarization. Further, this partial depolarization must have happened in a very short time after the muon stopped because the residual polarization did not exhibit any time dependence; that is, $A(t) = A$. This kind of depolarization can be described as being fast but incomplete; we will call this process a "fast" depolarization.

A different kind of depolarization process was detected by Swanson[3] in 1958 in boron carbide (B_4C), studying also muon precession. The result is shown in Fig. 7. Plotted is the positron rate versus elapsed lifetime. The distribution shows the expected cosine modulation; but the amplitude exhibits a decrease in time, which can be described with an exponential decay law. The time constant for this damping is about 6.5 μsec. We will call a depolarization with a directly observable time dependence a "slow" depolarization.

Taking these two phenomena into account, we will rewrite Eq. 3 and Eq. 7 as follows:

Longitudinal field

$$\Delta N(t) \sim \frac{1}{\tau_\mu} \exp(-t/\tau_\mu) \left[1 - \xi_{\parallel} F_{\parallel}(t) A\right] \qquad (8)$$

Transverse field

$$\Delta N(t) \sim \frac{1}{\tau_\mu} \exp(-t/\tau_\mu) \left[1 - \xi_{\perp} F_{\perp}(t) A \cos(\omega t + \Phi)\right] \qquad (9)$$

$\xi_{\parallel}, \xi_{\perp}$ (≤ 1) = "fast" depolarization factors

$\xi_{\parallel}A, \xi_{\perp}A$ = effective residual asymmetry

$F_{\parallel}(t), F_{\perp}(t)$ = "slow" depolarization functions

ω = precession frequency of muon

Φ = phase of residual polarization for t extrapolated to zero.

In many cases F(t) is given by an exponential decay law (see Swanson[3]). More on F(t) later.

We are now in the midst of our subject matter. We are talking about destruction of muon polarization, which means either that the spins of individual muons must flip over or that the coherence of the precession phases of a muon ensemble is somehow destroyed. No doubt this must be related to the magnetic interactions of the muon within the target environment.

As far as the fast depolarization is concerned, very strong internal magnetic fields must be present in which the muon spin can turn over in a very short time. In view of this, Friedman and Telegdi[4] in 1957 proposed to explain the fast depolarization as a consequence of the formation of the system $(\mu^+ e^-)$, which they called muonium.

5. MUONIUM (Mu)

Muonium is formed when a positive muon captures an electron and thus becomes neutralized[5]. It is like atomic hydrogen except that its mass is about 1/10 of the hydrogen mass. The smaller mass of the muon, however, has only a little effect on the reduced mass of the complete system which is very close to the reduced mass of hydrogen:

Therefore, the binding energy and the size of this atom are practically the same as for atomic hydrogen.

$$m^*_{Mu} \simeq 0.995\, m^*_H$$

Muon spin and electron spin are coupled strongly by a hyperfine interaction of the Fermi contact type in the muonium ground state (refer to the lecture presented by V.L. Telegdi at this Conference). The Hamiltonian for the hyperfine interaction in an external magnetic field is given by the following well-known expression:[5]

$$H = A\vec{S}_\mu \vec{J}_e + g_J \mu_0^e \vec{J}_e \cdot \vec{H} + g_\mu \mu_0^\mu \vec{S}_\mu \vec{H} \qquad (10)$$

with

$$A = \hbar\omega_0 = \frac{8\pi}{3} g_J \mu_0^e g_\mu \mu_0^\mu |\Psi_S(0)|^2 \qquad (11)$$

where $\hbar\omega_0$ = hyperfine splitting energy in zero field, $\vec{S}_\mu$ = muon spin. $\vec{J}_e$ = electron spin, g_J and g_μ are electron and muon g-values, μ_0^e and μ_0^μ are electron and muon Bohr magnetons, and $|\Psi_S(0)|^2$ = electron density at the muon site. Energy eigenvalues can be calculated with the Breit-Rabi formula. Plotting the energy eigenvalues as a function of magnetic field strength, we obtain the Breit-Rabi diagram shown in Fig. 8.

At low fields, the total spin F is a good quantum number and the levels are labeled in terms of m_F. In a strong field the muon and electron spin are more or less decoupled; and we have to label separately by the electron and muon magnetic quantum numbers. There is a crossover of the two upper states at about 160 kilogauss; at this point

the external field is equal to the field produced by the electron at the muon site.

Zeeman eigenstates can easily be constructed as follows:

$$\psi_1 = |+\tfrac{1}{2}\rangle_e \, |+\tfrac{1}{2}\rangle_\mu \qquad (11a)$$

$$\psi_2 = \alpha \, |+\tfrac{1}{2}\rangle_\mu \, |-\tfrac{1}{2}\rangle_e + \beta \, |-\tfrac{1}{2}\rangle_\mu \, |+\tfrac{1}{2}\rangle_e \qquad (11b)$$

$$\psi_3 = |-\tfrac{1}{2}\rangle_e \, |-\tfrac{1}{2}\rangle_\mu \qquad (11c)$$

$$\psi_4 = \beta \, |+\tfrac{1}{2}\rangle_\mu \, |-\tfrac{1}{2}\rangle_e - \alpha \, |-\tfrac{1}{2}\rangle_\mu \, |+\tfrac{1}{2}\rangle_e \qquad (11d)$$

with

$$\alpha^2 + \beta^2 = 1$$

$$\alpha = \frac{1}{\sqrt{2}} \left(1 - \frac{X}{\sqrt{1+X^2}} \right)^{1/2}$$

$$\beta = \frac{1}{\sqrt{2}} \left(1 + \frac{X}{\sqrt{1+X^2}} \right)^{1/2}$$

$$X = \frac{(g_J \mu_0^e - g_\mu \mu_0^\mu) H}{\hbar \omega_0} \cong \frac{H}{1550}$$

where H is the external field in gauss. For large H, $\alpha \to 0$ and $\beta \to 1$, reflecting the decoupling of muon and electron spin.

When the muon captures an electron, the initial state may have either parallel spins or antiparallel spins; that is, $|+1/2\rangle_\mu \, |+1/2\rangle_e$ or $|+1/2\rangle_\mu \, |-1/2\rangle_e$, assuming that $|+1/2\rangle_\mu$ is the polarization of the stopped muons. Each initial state will be equally populated because there is normally an equal number of electrons with spin up and spin down in the target. An exception is to be expected in a ferromagnetic substance (see below).

The state with parallel spins, as is evident, is already an eigenstate of the Hamiltonian. This is not true for the antiparallel state, which will develop in time to a mixed state consisting of a time-dependent superposition of Ψ_1 and ψ_2, the two states with $m_F = 0$. That is, the mixed state is one in which the muon and the electron each precess-opposite to each other and with equal frequency-in the magnetic field set up by the other particle. The plane of precession contains the external magnetic field vector. We write:

$$|+\tfrac{1}{2}\rangle_\mu |-\tfrac{1}{2}\rangle_e \longrightarrow$$

$$\psi(t) = A \exp\left(\frac{-iE_2 t}{\hbar}\right)\psi_2 + B \exp\left(\frac{-iE_4 t}{\hbar}\right)\psi_4 \qquad (12)$$

with $A^2+B^2 = 1$.

Substituting Ψ_2 and Ψ_4 in this equation (using Eqs. 11b and 11d) we may rewrite Eq. 12 as follows

$$\psi(t) = P_+(t)|+\tfrac{1}{2}\rangle_\mu |-\tfrac{1}{2}\rangle_e + P_-(t)|-\tfrac{1}{2}\rangle_\mu |+\tfrac{1}{2}\rangle_e \qquad (13)$$

with

$$P_+(t) = \alpha A \exp\left(\frac{-iE_2 t}{\hbar}\right) + \beta B \exp\left(\frac{-iE_4 t}{\hbar}\right)$$

$$P_-(t) = \beta A \exp\left(\frac{-iE_2 t}{\hbar}\right) - \alpha B \exp\left(\frac{-iE_4 t}{\hbar}\right)$$

$|P_+(t)|^2$ is then the probability of finding the muon in the state $|+ 1/2\rangle_\mu$; $|P_-(t)|^2$ is the probability of finding the muon in the $|-1/2\rangle_\mu$ state, respectively: the time dependent polarization of the muon in the mixed state is then: $|P_+(t)|^2 - |P_-(t)|^2$. After some arithmetic, taking

into account that

$$\psi(t=0) = |+\tfrac{1}{2}\rangle_\mu |-\tfrac{1}{2}\rangle_e$$

we obtain

$$P(t) = |P_+(t)|^2 = 1 - 4\alpha^2\beta^2 + 4\alpha^2\beta^2 \cos\left(\frac{E_2 - E_4}{\hbar} t\right) \qquad (14)$$

As can be seen, the dependence of the polarization is represented by a very fast modulation with frequency with ω_0, the hyperfine splitting

$$\frac{1}{\hbar}(E_2 - E_4) \geq \omega_0$$

frequency $\{\omega_0 \tilde{=} 2\pi(4.46\times10^9)\frac{\text{rad}}{\text{sec}}\}$. As this modulation is very fast, it cannot be resolved experimentally and appears to be averaged out to zero. Hence, in a longitudinal field the net polarization in the mixed state, which can be measured, is given as follows:

$$\bar{P} = 1 - 4\alpha^2\beta^2 = \frac{x^2}{1+x^2} \qquad (15)$$

and the total polarization, adding the polarization in the triplet state, is then:

$$\bar{P}_{tot} = \frac{1}{2} + \frac{1}{2}\frac{x^2}{1+x^2} \qquad (16)$$

Equation 16 is plotted in Fig. 9. The quenching of depolarization at high fields (Paschen-Back region) reflects again the decoupling of muon and electron spin at high

fields. Depolarization of muons in the free muonium state is thus a consequence of the limited time resolution of the experimental apparatus. In principle, no polarization is lost in an irreversible thermodynamic manner.

6. EXPERIMENTAL OBSERVATIONS AND SPECULATIONS UP TO 1966

Many experiments in early times tried to observe the quenching of the fast depolarization by strong longitudinal magnetic fields. In fact, up to 1966 most experiments were concerned with this aspect.[6-12] One common observation was that apparently no depolarization occurred in metals. In all other cases depolarization of various degrees was visible. Some kind of quenching of the depolarization in the Paschen-Back region was generally observed; however, in most cases Eq. 16 did not represent the data. In the following, some of the findings will be presented.

Figure 10 shows quenching curves for various temperatures, obtained by stopping muons in sulphur. This figure is taken from Eisenstein et al.[12] At room temperature even high magnetic fields (4 kilogauss) cannot restore the polarization to better than 50% of the initial polarization. At liquid helium temperatures, complete quenching is already achieved at about 400 gauss.

Figure 11, taken from the work of the same authors, shows quenching curves at room temperature in LiF, MgO, and red phosphorous. Again the data do not follow the predicted behavior.

Figure 12 is taken from the work of Buhler et al.[11] Shown are experimentally observed quenching curves in various materials. Again there is no agreement with the

curve given by Eq. 16.

The above figures reveal a very small polarization in zero magnetic field. By increasing the field a little, a sharp increase in residual polarization occurs which quickly levels off to a much slower increase. This is one of the puzzles that has not yet been explained satisfactorily. (This effect may be due to randomly oriented magnetic fields from impurities).

In view of these disagreements, it was repeatedly proposed that multiple muonium formation may be made responsible for the observed behavior. Multiple muonium formation was thought to happen during the slowing down process. Several authors designed formulas to take this into account.[7,11,13] In some cases[12] the new formulas lead to improved fits. In view of the addition of two or more additional parameters, this is not too surprising and it may not mean very much (see also Ref. 11). The principal question we have to ask ourselves is whether multiple muonium formation during the slowing down process has the power to produce any depolarization. Obviously this is a question of timescale, which we will treat in the next chapter.

Up to 1966, very few experiments had been performed in a transverse field arrangement.[3,14,15] The most relevant one is the already mentioned one by Swanson.[3] The results are collected in a rough manner in Table II. Metals and semimetals show no depolarization, such as in the longitudinal field case. Other inorganic and organic substances show a fast depolarization of varying degree; but contradictory to the longitudinal field case, the residual

polarization appeared to be independent of applied transverse field strength. No reasonable explanation of these findings was offered in Ref. 3.

The general absence of depolarization in metals was originally thought of as resulting from a very fast electron exchange process:

$$\mu^+e^-\uparrow + e^-\downarrow \longrightarrow \mu^+e^-\downarrow + e^-\uparrow$$

resulting in a decoupling of muon and electron spin (see Yakovleva[16]). The muon would thus precess as if free but would still be bound to an electron. This view was later replaced by what is still believed to be the case: that Coulomb screening of the muons by conduction electrons will prevent muonium formation; if muonium is ever formed, it will donate its electron to the conduction band.

Finally, a measurement by Feher et al.,[17] who used silicon targets with different impurity concentration, should be mentioned. The results obtained in zero magnetic field are shown in Fig. 13. At high n-type impurity concentration (the sample being effectively a conductor) no depolarization occurred; neither did it occur in a sample with high p-type impurity concentration. However, almost complete depolarization was achieved at a n-type impurity concentration corresponding to about 10^{14} free electrons/cm^3. The free electron concentration thus has a very important influence on depolarization in semiconductors. In a later paper,[12] quenching curves obtained in doped silicon were interpreted in terms of the formation of shallow donor muonium, which is much less strongly bound muonium with a consequently smaller hyperfine interaction.

7. THE SLOWING DOWN PROCESS AND THE STATUS OF THE MUON AFTERWARDS

The most important gross features of the slowing down process are displayed in the flow diagram shown in Fig. 14. The boxes contain information on the mechanisms involved and give relevant references. On the left side, time estimates for the different sections of the slowing down process are given, making use of Refs. 18-21. The right side gives a list of depolarization processes (and estimates of their magnitude) that are supposed to occur during the different parts of the slowing down process. As can be seen, the time that passes between "stable" muonium formation and complete thermalization is too short to cause any appreciable rotation of the muon spin in the hyperfine field in the mixed singlet-triplet state of muonium. The depolarization effect will be even smaller if less strongly bound muonium is formed. Also in the electron capture and loss region only a little depolarization can be expected to occur. Thus, the total depolarization during slowing down may safely be estimated to be $< 0.1\%$. From proton neutralization measurements (see Fig. 15), it can be inferred that the neutralization of muons (that is, muonium formation) will occur with effectively 100% yield.[22]

Near the end of the energy range, say at about 20 eV, muonium is likely to participate in hot-atom reactions[18] by which it may be bound diamagnetically into a molecule, or it may become part of a chemical radical with an unpaired electron. As there is a lot of energy available in epithermal (hot) reactions, many reactions will become possible that are forbidden in the thermal region for lack of energy to overcome potential barriers (high activation energies).

The situation after slowing down is summarized as follows:

i) No appreciable depolarization has occurred;

ii) Muons are in the state of thermalized muonium, or

iii) Muons are part of hot-atom reaction products:

a) Molecules with saturated bonds (μ^+ in a diamagnetic environment)

b) Chemical radicals (μ^+ and unpaired electron are coupled by hyperfine interaction-similar system to Mu, but with smaller ω_0).

What is to be expected then?

i) Chemical reactions of thermalized muonium (= hydrogen) and of muon radicals.

ii) Interactions of the (paramagnetic) impurity with its environement: $\mu^+ e^-$ (in solids) $\rightarrow U_2$ center.

iii) Modifications of the electronic structure of $\mu^+ e^-$; that is, muonium forms an impurity state in the host lattice.

iiii) Direct interactions of the muon with its environment, diffusion etc.

8. MUON PRECESSION AT THE QUASI-FREE LARMOR FREQUENCY AND SLOW DEPOLARIZATION IN SOLIDS

In this and the following section we want to discuss phenomena that can be observed by looking at the fraction of muons that proceeded through the hot-atom channel and ended up in a molecule with saturated chemical bonds; that is, muons with no hyperfine interaction acting on them. We will consider only the transverse field case, by studying muon precession at the quasi-free Larmor frequency. This section will be devoted to precession phenomena in solids.

For a given field H the precession frequency is given by

$$\omega = \frac{e}{m_\mu c} H = \gamma_\mu H \qquad (17)$$

We will now consider the case in which H is a function of position.

1.a) Assume that H has only a limited number of discrete values over the target volume. We then have to replace the cosine in the rate distribution formula by a sum over cosines with different discrete frequencies ω_i:

$$\cos(\omega t + \Phi) \longrightarrow \sum_i P_i \cos(\omega_i t + \Phi) \qquad (18)$$

where P_i is the fraction of muons that precess with ω_i. It is clear that this will result in a more or less complicated beat phenomenon in the precession pattern.

b) Next let us assume that there is a continuous distribution of field values over the target volume,

$$H = H(x,y,z)$$

We then have to replace the cosine in Eq. 7 by an integral:

$$\cos(\omega t + \Phi) \longrightarrow \int \cos[\omega(x,y,z) + \Phi]\, dx\, dy\, dz \qquad (18')$$

It is assumed also that the muon stopping rate is constant over the target volume. This integral can be rewritten as follows

$$\int_{\text{target volume}} \longrightarrow \int_0^\infty e^{i(\omega t + \Phi)} f(\omega)\, d\omega$$

which now implies only an integration over ω. $f(\omega)$ is a distribution function of the probability density for finding muons precessing with frequency ω; that is, it is the frequency spectrum.

The frequency spectrum $f(\omega)$ can be observed directly in NMR experiments in solids, and is nothing more than the NMR line shape. Thus, the muon precession pattern is the Fourier transform of the corresponding NMR line shape that would be measured in a NMR experiment with stopped muons.[23] Such an experiment is possible, and has been performed for a magnetic moment determination.[24]

The above integral can often be expressed as:

$$\int_0^\infty e^{-i(\omega t + \Phi)} f(\omega)\, d\omega \cong F(t) \cos(\omega^* t + \Phi) \qquad (19)$$

where ω^* is the average frequency and $F(t)$ can be approximated by a Gaussian or exponential decay function with relaxation time T_2. $F(t)$ thus describes a slow relaxation and can be identified with the $F(t)$ introduced into Eq. 9.

For complicated field distributions, such as in a supercondictor of Type II, the precession pattern will,

of course, be much more complex. It may however, be used to determine such field distributions, being the spatial Fourier transform thereof (see for example, Ref. 25).

c) Suppose now that the muon could diffuse easily in the crystal. Then the internal field distribution would appear somewhat washed out, and we would have a condition which in NMR is known as motional narrowing.[23] The NMR line will become smaller, a splitting will disappear, and the Fourier transform will show a damping with a much longer relaxation time T_2. This effect should be visible, particularly in metals, with T_2 displaying a marked temperature dependence. The diffusion of μ^+ in copper has been studied in this way by Gurevich et al.[76]

2. What magnetic field is really determined by measuring the precession frequency ω, assuming now a constant ω over the target volume? Of course, it is the local field seen by the muon at its site. This local field is not necessarily identical with the applied external field. Generally, the local field at some position in a crystal will be given by[20]

$$\vec{H}_{loc} = \vec{H}_{ext} + \vec{H}_{dm} - \vec{H}_{L} + \vec{H}_{int} \qquad (20)$$

$\vec{H}_{ext}$ = external field

$\vec{H}_{dm}$ = demagnetization field, depending on the geometry of the sample

$\vec{H}_L$ = Lorentz cavity field, the field at the center (probe site) of a spherical cavity cut (as a mathematical fiction) out of the specimen. The field is produced by the magnetization density on the surface of the cavity.

$\vec{H}_{int}$ = internal magnetic field produced by magnetic sources inside the cavity ($=\Sigma h_i$).

By expression the local field according to Eq. 20 one has taken into account the discontinuous structure of a crystal.

a) In a diamagnetic crystal $\vec{H}_{dm} + \vec{H}_L$ are vanishingly small. In an insulator, contributions to $\vec{H}_{int}$ arise only from nuclear moments (see the example below). In a paramagnetic crystal $\vec{H}_{dm} + \vec{H}_L$ are still very small and may in many cases just be neglected. $\vec{H}_{int}$ will consist of contributions from the various paramagnetic ions inside the cavity. For a crystal with cubic symmetry or for isotropic media $\vec{H}_{int}$ will be zero. For more details see Ref. 27.

b) In a metal there will be a very special internal field originating from the polarization of conduction electrons in an external magnetic field. In NMR experiments this field causes the famous Knight shift.[23,27] The field is given by the expression

$$\vec{H}_{int} = \frac{8\pi}{3} |u(0)|^2 \chi_s \vec{H}_{ext} \qquad (21)$$

with χ_s = Pauli spin susceptibility

$= \frac{1}{2}\chi_e \hbar^2 N(\varepsilon_F)$

$|u(0)|^2$ = density of conduction electrons at the muon site

$N(\varepsilon_F)$ = density of states at the Fermi level

$= \frac{2\pi m^*}{\hbar^2}\left(\frac{3nV}{\pi m'}\right)^{2/3}$

m^* = effective mass of conduction electrons, depends on the actual band structure.

Conventional measurements of the Knight shift require the performance of NMR with a metal probe. Due to the skin effect, the hf-field will penetrate only into a thin surface region, and it may sometimes be questionable whether one measures the bulk Knight shift of the probe material or some surface properties. With the help of the muon one would measure <u>real</u> bulk Knight shifts.[14]

c) In ferromagnetic and antiferromagnetic substances the measurement of H_{int} may shed light on some of the properties of these magnetic materials which are still not understood and which are still the subject of a lively controversy. A first example of a measurement in Ni (M, L.G. Foy et al.)[28] has been described by Kossler at this conference.

3. Examples. We will now describe a measurement which provides a good illustration of the possible phenomena discussed in paragraphs 1a, 1b and 2a of this section. This experiment was performed with a single crystal of gypsum ($CaSO_4 \cdot 2H_2O$).[29] The basic assumption is that

muons are placed by hot reactions of muonium into the site of a proton in one of the two water molecules that are present in the unit cell of this crystal. The next neighbor proton will create a magnetic dipole field at the site of the muon, given by this expression

$$\delta H_\mu = \pm \frac{\mu_p}{r^3}(3\cos^2\theta - 1) \qquad (22)$$

where μ_p=magnetic moment of proton, θ= angle between the magnetic moment vector of the proton and the muon-proton radius vector, and r=the muon-proton distance.

Depending on whether the proton spin is parallel or antiparallel to an external field, the dipole field will either add to or subtract from the external field. As we have two differently oriented H_2O molecules in the unit cell we will expect up to four different muon precession frequencies, as is evident from Fig. 16. ω_2 and ω_3 belong to the first pair; ω_1 and ω_2 belong to the second pair. In addition, the muon will feel the field components due to protons (and perhaps to magnetic impurities) farther away, which will lead to a frequency distribution around each ω_1. From NMR measurement one can infer that the distribution is of Gaussian shape.

Taking the Fourier transform of this complete pattern, one obtains for F(t) the following expression:

$$F(t) = \exp\left(\frac{-t^2}{T_2^2}\right)\cos\left(\frac{\Delta\omega_1}{2}t\right)\cos\left(\frac{\Delta\omega_2}{2}t\right) \qquad (23)$$

with

$$\Delta\omega_1 = \omega_2 - \omega_1 = \omega_4 - \omega_3$$

$$\Delta\omega_2 = \tfrac{1}{2}(\omega_4 - \omega_1) + \tfrac{1}{2}(\omega_3 - \omega_2)$$

$$T_2 = 4/\Delta\omega$$

There are actually two beat frequencies, $\Delta\omega_1$ and $\Delta\omega_2$, and a damping function of Gaussian form with a relaxation time T_2 related to the field distribution width $\Delta\omega$. The actual numbers for the beat frequencies $\Delta\omega_1$ and $\Delta\omega_2$ depend on the crystal orientation in the external field and can be calculated without difficulty.

Figure 17 shows data for F(t) for two different crystal orientations. The solid lines are calculated ones, not fits. Clearly visible is the beat behavior as well as the damping. The agreement between data and calculated curve in the second case does not look too good; however, in this case the crystal orientation in the external field was not accurately known.

9. SLOW DEPOLARIZATION IN PARAMAGNETIC LIQUIDS

The NMR line shape in liquids is generally described by a Lorentzian curve. The Fourier transform of this is an exponential decay function describing the relaxation of the transverse (with respect to the external magnetic field) spin components. Slow muon depolarization in transverse fields is thus expected to obey an exponential decay law:

$$F_\perp(t) = e^{-t/T_2} \qquad (24)$$

where T_2 is the transverse or spin-spin relaxation time. Relaxation in this case means the loss of phase coherence among the spins of the precessing muons. Slow depolarization in a longitudinal field arrangement is also described by an exponential decay law:

$$F_{\perp}(t) = e^{-t/T_2} \qquad (25)$$

with T_1 = the longitudinal or spin-lattice relaxation time. Relaxation in this case consists of transitions between the Zeeman states of the muons caused by interactions with the lattice, the lattice providing or absorbing the energy quanta involved. No longitudinal slow depolarization has yet been measured in paramagnetic solutions.

The muons that are observed at the free muon Larmor precession frequency must be, as emphasized before, in a diamagnetic position, either placed there by hot-atom reactions or by thermal reactions of muonium. From results on hot-tritium chemistry in aqueous solutions one knows that preferentially the molecule THO is formed.[30] It can be assumed that the same will happen in hot-atom reactions of muonium, yielding the molecule MuHO. As the residual polarization in pure water is about 0.5, we conclude that about 50% of all muons go through the hot-atom channel, by replacing a proton in a water molecule.

The muon now has the same place as a proton, and it can be assumed that the muon spin will be subject to relaxation processes in the same way as the proton spin. Proton spin relaxation phenomena in aqueous solutions have been investigated quite intensively by the method of NMR.[23]

Particularly suitable for studying slow relaxation phenomena with muons are paramagnetic aqueous solutions, where T_2 can be expected to be small enough to be detected over the muon lifetime.[31] From the theory of relaxation[23] it follows that

$$\frac{1}{T_2} \sim (\mu)^2 \qquad (26)$$

where μ= magnetic moment of the particle involved. By comparing proton and muon relaxation times in the same solution under the same conditions, one thus expects the ratio:

$$\frac{T_2(p)}{T_2(\mu)} = \frac{\mu_\mu^2}{\mu_p^2} \sim 10 \qquad (27)$$

Figure 18 shows T_2 data for muons obtained in paramagnetic Fe^{3+} solutions.[32] Plotted is T_2 versus paramagnetic ion concentration. The lower data points, connected by a solid straight line, were obtained from a solution of $Fe(NO_3)_3$. The upper solid line represents proton NMR results in the same solution. The ratio between the muon and proton data is indeed about 10. For lack of NMR data, the results obtained in $FeCl_3$ and $Fe(Cl O_4)_3$ could not be analyzed in the same way. The deviation between the data from $Fe(NO_3)_3$ solutions and data from $Fe(Cl O_4)_3$ and $FeCl_3$ solutions is not fully understood and needs further investigation.

There is one important point. NMR measurements were generally done in solutions with concentration not exceeding 10^{21} paramagnetic ions/cm^3, for reasons related to problems regarding line width, signal strength, rf power, and others. This limits proton-NMR measurements to cases

with relaxation times above microseconds. It is, however, easy to measure much shorter relaxation times with muons in much stronger concentrated solutions. In principle, transverse and also longitudinal relaxation times can be measured down to, say, 10^{-8} sec.

In strongly concentrated solutions, not suitable for study by NMR, new effects may show up. This is demonstrated by measurements performed with $MnCl_2$ solutions of up to 5 moles/l Mn^{2+} concentration (3×10^{21} ions/cm^3).[33] The analysis also gives a good example of what kind of effects are involved and what information may be extracted from experimental results. At lower concentration, $MnCl_2$ solutions have been extensively studied with proton-NMR by many authors, particularly by Bloembergen et al.[34]

The model used in the analysis is that the paramagnetic Mn^{2+} ions are surrounded by six water molecules forming a hydration sphere. Protons (or muons) in this hydration sphere are subject to two time-dependent magnetic interactions: dipole-dipole interaction between paramagnetic ion and proton (or muon), and a scalar coupling or spin-exchange interaction caused by the nonvanishing wave-function of the ion at the site of the proton (or muon) in the hydration sphere. These interactions lead to the following expressions for the transverse relaxation time T_2:[34,35]

$$\frac{1}{T_2} = \frac{4}{60}\frac{1}{r^6} S(S+1)\gamma_{p(\mu)}^2 \gamma_{ion}^2 \hbar^2 \left[7\tau_c + 13\tau_c (1+\omega_S^2\tau_c^2)^{-1}\right]$$

$$+ \frac{1}{3} S(S+1) A_{p(\mu)}^2 \hbar^{-2} \left[\tau_e + \tau_e (1+\omega_S^2\tau_e^2)^{-1}\right] P \qquad (28)$$

The first term on the right-hand side od Eq. 28 is due to the dipole-dipole interaction, and the second term is caused by the spin-exchange interaction. The symbols are defined as follows: S=ion spin (5/2); r=internuclear distance between ion and proton (muon); γ_p or γ_μ and γ_{ion}= the respective gyromagnetic ratios; $A_\mu = 3.18\ A_p$, the coupling constant for exchange interaction; ω_s=Larmor precession frequency of the ion; P=probability of finding a proton (or a muon) in the hydration sphere; and τ_c and τ_e are the respective correlation times, which are a measure of the time dependence of the involved interactions.

The time dependence of the dipole-dipole interaction may be caused by rotational diffusion of the Mn^{2+} complex, by chemical exchange of the H_2O (MuHO) molecules, and by spin relaxation of the paramagnetic ion, each measured by correlation times τ_r, τ_h, and τ_s. Thus

$$\frac{1}{\tau_c} = \frac{1}{\tau_r} + \frac{1}{\tau_h} + \frac{1}{\tau_s} \qquad (29)$$

and correspondingly,

$$\frac{1}{\tau_e} = \frac{1}{\tau_h} + \frac{1}{\tau_s} \qquad (30)$$

(The scalar coupling is not influenced by rotational diffusion).

The temperature dependence of the correlation times τ_r, τ_h is described by a type of Arrhenius law

$$\tau = \tau_0 e^{V/RT} \qquad (31)$$

where V is the activation energy for rotational diffusion or chemical exchange. The temperature dependence of τ_s is more complicated and involves the mechanisms leading to the electronic relaxation.[34]

Equations 28, 29, 30 and 31 represent in a typical way the amount of information obtainable from relaxation studies in paramagnetic solutions. Fig. 19a shows in a double logarithmic plot the dependence of T_2 on ion-concentration according to Eq. 28, 29, 30using the magnetic moment at the muon (solid line). The dashed curves show the dipole-dipole and spin exchange induced dependences separately. All parameters were taken from Ref.[34] For concentrations below 10^{20} $MnCl_2^{++}/cm^3$ there is a good agreement between the scaled predictions for muons. Note that the data break sharply and there seems to be a quenching of the relaxation mechanism. A reasonable approach toward understanding these deviations from Eq. 28 is to assume that some of the correlation times become concentration-dependent at higher concentrations due to intermolecular interactions of Mn^{2+} complexes. In particular, spin-spin interactions among Mn^{2+} ions might lead to concentration-dependent correlation times. Indeed, ESR measurements by Garstens and Liebson and Hinckley and Morgan[36] show a concentration-dependent line width in concentrated Mn^{2+} solutions. The data can be approximated by

$$\tau_s^* = \frac{1.24 \cdot 10^{-9}}{N^2} + 1.27 \cdot 10^{-11} \text{ sec}$$

where τ_s^* is now used as an additional effective correlation time in the proton(muon)-ion interactions.[37] N=ion concentration in moles/liter. The temperature dependence of τ_s^*

can also be obtained from Ref. 36. For a 3 M solution, one finds

$$\frac{1}{\tau_s^*} = 1.76 \cdot 10^7 \left[710 - 2.8 \cdot 10^3 \exp\left(-\frac{1.26 \cdot 10^3}{RT}\right)\right] \qquad (32)$$

The total correlation time τ_e for the spin-exchange interaction is now given by

$$\frac{1}{\tau_e} = \frac{1}{\tau_s} + \frac{1}{\tau_s^*} + \frac{1}{\tau_h} \qquad (33)$$

where τ_s is the usual electron spin relaxation time and τ_h is the mean time for the muon to remain in the hydration sphere. The total correlation time τ_c for the dipole-dipole interaction is given by

$$\frac{1}{\tau_c} = \frac{1}{\tau_r} + \frac{1}{\tau_h} + \frac{1}{\tau_s} + \frac{1}{\tau_s^*} \qquad (34)$$

where τ_r is the rotational correlation time. At room temperature $\tau_s \sim 3 \times 10^{-9}$, $\tau_h \sim 2 \times 10^{-8}$, $\tau_r \sim 3 \times 10^{-11}$ sec.[34]

In Fig. 20 we again present our data from Fig. 19, however, the concentration (P) dependence is now divided out. If the correlation times were concentration-independent, $1/T_2P$ would be constant. If we insert the total correlation times τ_e and τ_c (Eqs. 33 and 34) into the general expression Eq. 28 with the other parameters taken from Ref. 35, we get the solid line in Fig. 20, which fits our data excellently. The dashed lines in Fig. 20 represent spin-exchange and dipole-dipole contributions separately.

If we use, however, Eq. 28 together with Eqs. 32 and 33 and the temperature dependence for τ_r and τ_h from Ref. 34, we obtain the dotted curve in Fig. 20 for 11 kG, which-as is clearly evident-does not adequately describe the measured T_2-versus-temperature data in a 3 M solution.

By assuming that Eq. 33 correctly describes the temperature dependence of τ_s^* and by not considering an abnormal τ_h behavior, we are forced to adopt parameters different from the ones in Ref. 34 in the expression

$$\tau_h = \tau_h^0 \exp(V_h/RT) \qquad (35)$$

where V_r is the activation energy of the rotational motion of the Mn^{2+} complex. Using V_r=8.5kcal/mole-liter and τ_r^0=1.73x10^{-17}sec, we obtain for $1/T_2P$ versus temperature the lower solid curve at 11 kG and the upper one at 4.5 kG external field strength.[38]

The large value for the activation energy at 3 M concentration as compared with V_r=4.5 kcal/mole-liter at low concentration seems to be reasonable in view of the strongly increased viscosity of a 3 M $MnCl_2$ solution [η(3 M)≈3.2 centipoises]. It would be of great interest to establish some firm experimental relationships here with respect to the dynamics of this liquid.[38]

We now discuss some questionable assumptions in our analysis.

1) The results of Ref. 36 for ESR line width were obtained in an external field of 3 kG. In our analysis we

neglected possible field dependence of the ESR line widths and assumed the same values in fields of 4.5 and 11 kG. This is justified only if the relevant correlation time τ obeys the inequality $\tau\omega_s(11\ \text{kG})<1$ or $\tau<5\times10^{-12}$ sec.

2) The results of Ref. 36 were obtained in $Mn(ClO_4)_2$ solutions, whereas we used $MnCl_2$ solutions.

3) Although we had to change V_r and τ_r^0 in order to fit the temperature dependence of a 3 M solution, we had to assume that τ_r remains relatively independent of concentration at 295°K in order to obtain the fit in Fig. 19a.

4) In view of the quality of the fit, as shown in Fig. 19a, τ_h has been assumed to be concentration-independent. This assumption needs, of course, further justification. In particular, a concentration-dependent activation energy for chemical exchange might reduce the value of V_r to less than 8.5 kcal/mole-liter.

5) The whole analysis was performed on the basic assumption that $Mn(H_2O)_6^{2+}$ formation continues almost unchanged up to the strongest concentrations.

These assumptions emphasize how further use of muon-depolarization studies might also contribute to our knowledge about structure and dynamics of fluids. In order to accomplish this program in Mn^{2+} solutions, measurements of relaxation times have to be performed in transverse as well as in longitudinal fields, as a function of varying field strengths, as a function of temperature in various concentrations, and finally in solution with different anions.

10. QUASI-FREE MUONIUM EVOLUTION

In view of the possibility that muonium reacts chemically and that the muonium-electron spin may relax, a more refined treatment of muon depolarization becomes necessary. Such a refined treatment was given by the Russian physicists Ivanter and Smilga[39,40] starting from some older work by Yakovleva and Nosov.[41] In the following two sections we will try to give a brief description of their treatment and the results.

We begin with the usual muonium Hamiltonian but introduce, in addition, a term $\hat{F}$ representing the electron-lattice interaction and a term $\hat{W}$ representing a lattice-lattice interaction; both terms are time dependent.[42] The latter makes sure that polarization transferred from the electron to the muonium lattice environment is dissipated throughout the lattice.

$$H = A\vec{S}_\mu \cdot \vec{J}_e + g_J \mu_c^e \vec{J}_e \cdot \vec{H} + g_\mu \mu_c^n \vec{S}_\mu \cdot \vec{H} + \hat{F} + \hat{W} \qquad (36)$$

We define a spin density matrix for muonium in terms of the Pauli spin matrices σ_i:

$$\rho = \frac{1}{4}\left[1 + \vec{P}_\mu \vec{\sigma}_\mu + \vec{P}_e \cdot \vec{\sigma}_e + \sum_{i,j=1} \rho_{ij}\, \sigma_\mu^i \sigma_e^j\right] \qquad (37)$$

$\vec{P}_\mu$ is the muon polarization vector with components ρ_{10}, ρ_{20}, ρ_{30} (x,y,z); and P_e is the electron polarization vector components ρ_{01}, ρ_{02}, ρ_{03}. We are interested in the time evolution of $\vec{P}_\mu$. The time derivative of ρ is given by the usual formula

$$\frac{d\rho}{dt} = -\frac{i}{\hbar}[H,\rho] \qquad (38)$$

Generally this will lead to equations known as the Wangsness-Bloch equations.

Let us first neglect $\hat{F} + \hat{W}$; that is, we are interested only in the free evolution of the muon polarization in the muonium state. Inserting Eqs. 36 and 37 into Eq.38 and using the commutator relations of the σ, we obtain the following system of differential equations:

$$\frac{d\rho_{il}}{dt} = \frac{\omega_0}{2}(\rho_{j0}\varepsilon_{iej} - \rho_{ok}\varepsilon_{iek}) + \omega_j^e \rho_{ik}\varepsilon_{ejk} + \omega_j^\mu \rho_{ke}\varepsilon_{ijk}$$

$$\frac{d\rho_{e0}}{dt} = -\frac{\omega_0}{2}\rho_{jk}\varepsilon_{ejk} - \omega_i^\mu \rho_{k0}\varepsilon_{eik} \qquad (39)$$

$$\frac{d\rho_{oe}}{dt} = \frac{\omega_0}{2}\rho_{jk}\varepsilon_{ejk} + \omega_i^e \rho_{ok}\varepsilon_{eik}$$

Without specifiying the time-dependent terms $\hat{F}$ and $\hat{W}$, we know from the very beginning that the effect of $\hat{F} + \hat{W}$ must result in a damping of the pure and mixed electron components because of the random time structure of $\hat{F}$ and $\hat{W}$. Introducting a common relaxation rate 2ν for all pure and mixed electron components, we simply have to complete the system (Eqs. 39) as follows:

$$\dot{\rho}_{ie} = \frac{\omega_0}{2}(\rho_{j0}\varepsilon_{iej} - \rho_{ok}\varepsilon_{iek}) + \omega_j^e \rho_{ik}\varepsilon_{ejk} - \omega_j^\mu \rho_{ke}\varepsilon_{ijk} - 2\nu\rho_{ie}$$

$$\dot{\rho}_{e0} = -\frac{\omega_0}{2}\rho_{ik}\varepsilon_{ejk} - \omega_i^\mu \rho_{k0}\varepsilon_{eik} \qquad (40)$$

$$\dot{\rho}_{oe} = \frac{\omega_0}{2}\rho_{jk}\varepsilon_{ejk} + \omega_i^e \rho_{ok}\varepsilon_{eik} - 2\nu\rho_{oe}$$

It now turns out that this system splits naturally into two irreducible parts, one involving only the longitudinal components of $\vec{P}_\mu$ and $\vec{P}_e$, the other only the transverse components with respect to $\vec{H}$. Schematically we write:

$$\dot{\rho} = \left(\begin{array}{c|c} \text{long} & \\ \hline & \text{trans} \end{array} \right) \rho$$

with ρ expressed as a column matrix. The matrix is then a 16x16 matrix. We now want to treat the subsystem referring to the transverse components in somewhat more detail. The magnetic field is directed along Z, and the initial polarization along X. Following Ref. 39 we introduce the following complex combinations

$$\begin{aligned} \rho_\mu &= \rho_{10} + i\rho_{20} \quad , \quad \rho_e = \rho_{01} + i\rho_{02} \\ \rho_\mu' &= \rho_{31} + i\rho_{32} \quad , \quad \rho_e' = \rho_{13} + i\rho_{23} \end{aligned} \tag{41}$$

ρ_μ, for instance, represents the muon polarization projected on the (x,y) plane ($\perp \vec{H}$). We further introduce

$$\tilde{\rho} = \begin{pmatrix} \rho_\mu \\ \rho_e \\ \rho_\mu' \\ \rho_e' \end{pmatrix} \tag{42}$$

The subsystem under consideration can then be written as

$$\frac{d\tilde{\rho}}{dt} = A\tilde{\rho} \tag{43}$$

with

$$A = \frac{\omega_0}{2}\begin{pmatrix} 2i\mathfrak{J}x & 0 & -i & i \\ 0 & -\left(\frac{4\nu}{\omega_c}+2ix\right) & i & -i \\ -i & i & -\left(\frac{4\nu}{\omega_c}-2i\mathfrak{J}x\right) & 0 \\ i & -i & 0 & -\left(\frac{4\nu}{\omega_c}+2ix\right) \end{pmatrix} \tag{44}$$

Solutions

a) We first set $\nu = 0$ (no electron relaxation). We ask for the time dependence of the muon polarization in, e.g. the x-direction, the direction of the positron telescope. As a solution of Eq. 43 we obtain[43]

$$P_x(t) = \frac{1}{4}\left\{\left(1+\frac{\omega_+}{Q}\right)\cos(\omega_{12}t) + \left(1-\frac{\omega_+}{Q}\right)\cos(\omega_{23}t)\right.$$

$$\left. + \left(1-\frac{\omega_+}{Q}\right)\cos(\omega_{14}t) + \left(1+\frac{\omega_+}{Q}\right)\cos(\omega_{34}t)\right. \tag{45}$$

with

$$\omega_\pm = \frac{eH}{m_e c}(1 \pm \mathfrak{J}) \tag{46}$$

$$Q = \left(\tfrac{1}{4}\omega_0^2 + \omega_+^2\right)^{1/2} \tag{47}$$

$$\mathfrak{J} = m_e/m_\mu$$

The ω_{ij} are Zeeman transition frequencies (see Fig. 8) with the following selection criteria (weak field notation):

$$\omega_{12} : \quad \Delta F = 0 \;, \; \Delta m_F = 1$$

$$\omega_{23} : \quad \Delta F = 0 \;, \; \Delta m_F = -1$$

$$\omega_{14} : \quad \Delta F = 1 \;, \; \Delta m_F = 1$$

$$\omega_{34} : \quad \Delta F = 1 \;, \; \Delta m_F = -1$$

For $H \to \infty$ the components with ω_{23} and ω_{14} will disappear, which again is a result of the decoupling of the muon and electron spins in the Paschen-Back region.

For very small magnetic fields, the above formula simplifies to the following expression

$$P_x(t) = \cos \frac{\omega_{14}-\omega_{34}}{2} t \left(1 + \cos \frac{\omega_{14}+\omega_{34}}{2} t \right) \qquad (48)$$

Figure 21 shows a plot of $P_x(t)$ versus t. Because $\frac{\omega_{14} + \omega_{34}}{2} = \omega_0$ the experimentally observable polarization will be only

$$P_{x(exp)}(t) = \cos \frac{\omega_{14}-\omega_{34}}{2} t = \cos \omega_{12} t$$

Thus, one can observe the precession of the muon with the triplet Larmor frequency of muonium, which is 1/2 the free electron precession rate.

Either Fig. 21 or Eq. 48 can be constructed by direct physical consideration for the very weak field condition:

muons in the triplet state will precess relatively slowly, while muons in the mixed state will precess relatively fast in the (x,y) plane. The evolution in time of the total polarization is shown in Fig. 22. Projection of the time evolution of the rosette in this figure on the x-axis will result in the curve shown in Fig. 21.

For somewhat larger fields (~100 gauss) one obtains an expression for $P_x(t)$ as follows:

$$P_x(t) = \cos\left(\frac{\omega_{12}-\omega_{23}}{2}t\right)\cos\left(\frac{\omega_{12}+\omega_{23}}{2}t\right)\left(1+\cos\omega_e t\right) \qquad (49)$$

$$\Omega = \frac{\omega_{12}-\omega_{23}}{2} \quad , \quad \omega_e = \frac{\omega_{12}+\omega_{23}}{2}$$

There appears a beating factor with a frequency Ω which is just half of the difference between ω_{12} and ω_{23}. The beat frequency thus occurs in a region where the $|F=1, m_F=0\rangle$ term starts to be field dependent.

Figure 23 shows the result of a measurement by Gurevich et al.,[43] who observed muonium precession at 95 gauss in quartz. And indeed, as can be seen, the precession pattern shows a very nice beating behavior. From the beat frequency and the precession frequency ω_e one can calculate the hyperfine frequency ω_0:

$$\omega_0 = \frac{\omega_e^2}{\Omega} \qquad (50)$$

b) Now assume that $\nu \neq 0$. For completeness we shall also list the observable part of the solution of Eq. 43 in the case, that beats are visible.[43] The latter implies:

$$\omega_e^2 \gg \nu^2$$

$$P_x(t) = \tfrac{1}{2} e^{-t/\tau_1}\left[\left(\cos\Omega^* t + \frac{\sin\Omega^* t}{3\tau_1\Omega\left[1-(3\tau_1\Omega)^{-2}\right]}\right)\cos\omega_- t\right.$$

$$\left. + \frac{2\omega_+}{\omega_c\left[1-(3\tau_1\Omega)^{-2}\right]}\sin\Omega^* t \sin\omega_- t\right] \qquad (51)$$

There appears an exponential damping factor, with a time constant τ_1 related to ν:

$$\tau_1 = \frac{2}{3\nu} \qquad (52)$$

There is also a beat frequency Ω^*, which turns out to be also dependent on τ_1

$$\Omega^* = \Omega\left[1-(3\tau_1\Omega)^{-2}\right]^{1/2} \qquad (53)$$

$\omega_\pm$ and Ω are defined as before. Thus, the electronic relaxation will lead to a damping of muon polarization as well as to a shift in the beat frequency. If chemical reactions of muonium were to occur, there would also be a damping, but no shift in the beat frequency. In principle, a shift in the beat frequency could be used to distinguish between these two possibilities, although in practice the shifts are very small and are mostly beyond experimental determination.

Anyhow, electronic relaxation may play an important role in muon depolarization in the muonium state. Figure 24 shows the results of a measurement by Myasishcheva et al.[44] They observed muonium precession at very small fields in fused quartz. As can be seen, the precession pattern displays a marked damping, depending on temperature. Interestingly, the damping is faster at lower temperature than at higher temperature. Future measurements will show whether we observe muonium chemistry in solids or are dealing with real relaxation phenomena. Both aspects are very interesting.

11. CHEMICAL REACTIONS OF MUONIUM

Following the treatment of Ivanter and Smilga,[39] we assume that chemical reactions of muonium will lead to compounds in which the muon is in a diamagnetic position. That is, the muon spin is no longer subject to a hyperfine interaction and the muon will precess in a transverse magnetic field as though free. The above assumption does not necessarily reflect the spectrum of the chemical reaction channels that may be present, as will be discussed later.[45] We are asking: What is the remaining polarization of these muons which have evolved from muonium?

The disappearance of muonium by chemical reactions can be described by an exponential decay law:

$$[Mu] = [Mu]_0 e^{-t/\tau_{ch}} \qquad (54)$$

with τ_{ch} = average chemical lifetime and $[Mu]_0 = 1$. The fractions of Mu's that react and disappear at time t in

an interval dt is then given by

$$dn_\mu = -\frac{1}{\tau_{ch}} e^{-t/\tau_{ch}} dt$$

This fraction of the quasi-free muons will start to precess with the muon Larmor frequency ω_μ and will possess a polarization as in the muonium state at time t:

$$\rho_\mu(t) = \rho_x^\mu(t) + i\rho_y^\mu(t) \qquad (55)$$

using the complex notation as in Eqs. 39-43.

The total polarization at time t_0 is then given by a superposition of all these fractions precessing with frequency ω_μ up to the time t_0, plus a term describing the polarization of the muons still in the muonium state:

$$\tilde{P}_\perp(t_0) = \int_0^{t_0} \rho_\mu(t) e^{i\omega_\mu(t-t_0)} e^{-t/\tau_{ch}} \frac{dt}{\tau_{ch}} + \rho_\mu(t_0) e^{-t/\tau_{ch}} \qquad (56)$$

For t_0 going to infinity or, in practice, to values much larger than τ_{ch}, we will obtain the residual polarization, that is left over after muonium has long ceased to exist.

Fortunately, $\tilde{P}_\perp(t_0 \to \infty)$ can be identified with the Laplace transform of the system

$$\dot{\tilde{\rho}} = A\tilde{\rho}$$

It is then possible to obtain an algebraic expression for $\tilde{P}_\perp(\infty)$ by standard methods without the need to solve the system of differential equations explicitly. Similarly, the residual polarization in a longitudinal field can be derived. Table III contains the explicit expressions for the residual polarizations. Note that $P_\perp(\infty)$ is a complex expression with

$$P_x = Re\left[\tilde{P}_\perp(\infty)\right] \qquad P_y = Im\left[\tilde{P}_\perp(\infty)\right] \tag{57}$$

The phase ϕ of the residual polarization is then obtained from

$$\tan\phi = \frac{P_y}{P_x} \tag{58}$$

In the presence of a hot-reaction channel, the formulas will have to be supplemented. If h is the fraction of muons that proceeded through the hot-atom channel, the total residual polarization may be expressed as follows:

Transverse component

$$\vec{P}_{tot\perp} = h\vec{x} + (1-h)(P_x\vec{x} + P_y\vec{y}) \tag{59}$$

Longitudinal component

$$P_{\parallel tot} = h + (1-h)P_\parallel \tag{60}$$

As stated earlier, the fraction h of muons has conserved its full polarization; and the phase of this polarization is identical to that of the μ-beam polarization, which is $\phi_h = 0$ for the experimental set up shown in Fig. 3.

From Eq. 57 or Eq. 59 we calculate a $P_{x,tot}$ and a phase which are to be identified with $\xi_\perp$ and ϕ of the positron distribution ($\phi_0 = \phi_h = 0$); see Eq. 9. Likewise $\xi_\parallel = P_{z,tot}$. Equation 59 and Eq. 60 will be referred to as the Ivanter and Smilga equations.

Figure 25 shows schematically the dependence of $P_x = \xi_\perp$ and ϕ on the average chemical lifetime in a small field as given by the Ivanter and Smilga equations, assuming $\nu=0$ and $\phi_0=0$. The dashed curves refer to the case with no hot-atom reactions, the solid ones to the case including these. At very short chemical lifetimes ($<1/\omega_0$) all muons will evolve from muonium with effectively the same spin phase. Consequently the superposition will lead to no depolarization, and the phase of the residual polarization is given by the phase of the initial polarization. With increasing chemical lifetime, an increasingly random distribution of muon spin phases will be established, resulting in a decreasing residual polarization. From Fig. 22 it is evident that the phase of the residual polarization will first get slightly positive and then negative due to the different signs of the magnetic moment of the electron and the muons.

An irreversible depolarization in a transverse field is thus brought about by the more or less partial randomization of the phases of the free muon precession, which is caused by chemical reactions of muonium at random times. Let us turn now to the question of how one can verify these mechanisms of muon depolarization by muonium formation and subsequent chemical reactions. Concerning chemical reactions, it would be desirable to change the muonium lifetime in some systematic way. This can be done

in a solution, where it is possible to dissolve a substance with which muonium can react in any range of concentrations that one likes. Let us call the substance X. The solute is assumed to be chemically inert. We may have a reaction equation of the form

$$Mu + X \longrightarrow MuX$$

The equation governing the reaction rate for such a simple reactions is

$$\frac{d[Mu]}{dt} = -k[Mu][X] \qquad (61)$$

with the already introduced solution

$$[Mu] = [Mu]_0 e^{-t/\tau_{ch}}$$

where k is the specific reaction constant and

$$\tau_{ch} = \frac{1}{k[N]} \qquad (62)$$

Thus, there is a simple relation between the chemical lifetime and the concentration of some substance with which muonium can react.

Example

It is well known that iodine molecules dissolved, for instance, in methyl alcohol will rapidly capture atomic hydrogen. The same may be expected for muonium. An experiment designed to measure the residual polarization of muons in this solution as a function of I_2 concentration was carried out by the Berkeley group.[46,47] Figure 26 shows the results obtained in a transverse field of about 100 gauss.

At zero iodine concentration, the residual polarization is about 50% of the initial polarization. This residual polarization is explained as due to muons which proceeded through the hot channel. At medium I_2 concentration, we recognize the predicted saddle point; and at high concentrations, depolarization seems to disappear altogether. We also see that the phase behaves in just the predicted manner. Figures 27 and 28 show data from the same solution obtained, however, in fields of 1 kG and 4.5 kG. As expected for strong fields, the saddle point has disappeared and the curve is much steeper due to a speed-up of the muonium precession. We now can fit the Ivanter and Smilga formulas for the residual polarization and the phase to these data, from which fit we obtain the absolute value for the specific reaction constant*; in this case it turned out to be

$$k = 1.4 \pm 0.2 \cdot 10^{11}\ \ell/\mathrm{sec \cdot mol}$$

The reaction that takes place is

$$\underline{I}_2 + Mu \longrightarrow Mu\underline{I} + \underline{I}$$

This is a very large specific reaction constant, which is typical for a region where only diffusion limits the speed of reaction events. Each collision between two reaction partners leads to a reaction.

The activation energy for such processes must consequently be zero or negative. Absolute reaction constants may be measured in this way down to about 5×10^8 l/mole·sec. Smaller reaction constants may be measured from direct observation of muonium precession damping.

It is now of interest to compare muonium reaction rates with those for atomic hydrogen, provided atomic hydrogen reaction rates are known. From gas kinetic considerations, the absolute reaction constant is given by the following expression[48]

$$k = \frac{Z}{[X][Mu]} = (r_X + r_{Mu})^2 \left[8\pi kT \left(\frac{1}{m_{Mu}} + \frac{1}{m_X}\right)\right]^{1/2} \qquad (63)$$

where Z is the collision number, [X] and [Mu] the relevant concentrations, r_X and r_{Mu} are the atomic radii, and m_{Mu} and m_X are the masses of the atoms. For atomic hydrogen, we would have to insert an r_H and an m_H. In general, the mass of muonium and of hydrogen is much smaller than the mass of the substance X; so we may neglect $1/m_X$, beside $1/m_{Mu}$ or $1/m_H$. The ratio of k_{Mu}/k_H is then

$$\frac{k_{Mu}}{k_H} \cong \left(\frac{m_H}{m_{Mu}}\right)^{1/2} \simeq 3 \qquad (64)$$

If we adopt a more realistic approach to reaction kinetics in solutions, we will think in terms of diffusion. The specific reaction constant is then given by[48]

$$k = \frac{kT}{\eta_{Mu}} \frac{(r_X + r_{Mu})^2}{r_X r_{Mu}} \qquad (65)$$

with η the viscosity,

$$\eta \sim \sqrt{m_{Mu}}\, e^{E/kT} \qquad (66)$$

where E is a diffusional activation energy. Assuming the same activation energy for the diffusion of atomic hydrogen and muonium, we find for the ratio k_{Mu}/k_H the same value as above.

The reaction constant for the reaction

$$H + I_2 \longrightarrow HI + I$$

has been measured.[49] Adopting this value, we obtain

$$\left(\frac{k_{Mu}}{k_H}\right)_{exp} \cong 3.2$$

which is in close agreement with the predicted value.

The assumption of equal diffusion activation energy for Mu and H is questionable. Due to the lighter mass of the Mu, muonium will also have a larger zero point vibration energy, which may lead to a smaller activation energy for jumping from one site to the other. In addition, tunneling may become possible for muonium, also because of its lighter mass. The same considerations are, of course, applicable with respect to chemical activation energies. Thus, a muonium reaction may proceed much faster than just by a factor of three (for examples, see below).

So far, we have assumed that chemical reactions of muonium will place the muon into a diagmagnetic environment. But it may also happen that the result is a chemical radical with an unpaired electron. The muon is then still subject to a hyperfine interaction, although a weaker one. The radical itself may subsequently react. Thus, there will be an ongoing depolarization until the muon

finally ends up in some diamagnetic environment. Phenomenological formalisms treating this more complicated situation have been worked out by Brewer et al.[50] and by W. Fischer.[51] For details see these references.

We want to mention one interesting difference in the approaches of Brewer et al. and Fischer. The formalism of Brewer assumes tacitly that the muon-electron spin correlation will not change during the transition from muonium to radical. This may be explained by assuming that the muonium electron becomes the unpaired electron. The formalism of Fischer assumes that the unpaired electron spin has no correlation with the muon spin at the instant the radical is formed. This may be explained by assuming that the unpaired electron is one belonging to the original molecule with which muonium reacted. Actually, both formalisms have the power to describe both cases. Only future measurements will show how it really is. Anyhow,there is the possibility of learning something about the rate of certain electrons in chemical reactions. It should also be mentioned that by fitting the Brewer formulas to data points, one can crudely determine the hyperfine frequency in the radicals. As the hyperfine frequency is related to the spin density of the unpaired electron at the muon site, this will give important information on the electronic structure of the radical.

So far, we have shown the results for iodine dissolved in methyl alcohol as the typical example. However, there are a number of more complicated cases which have recently been studied experimentally. The general mechanism is summarized by Fig. 29. The case of I_2 in methyl alcohol is represented by a combination of the left-hand path for the hot reaction (50%) and the extreme right-

hand path for the remaining thermalized portion.

Figure 30 shows the case where Br_2 is dissolved in benzene at 200 gauss. The dotted lines are the fit obtained with the same model as used for iodine (Fig. 26), with an obviously poor fit. To correct this discrepancy the inner paths in Fig. 29 are introduced, and the parameters are varied for a good fit. The solid line is the best fit obtained. Similarly, H_2O_2 in water was studied (Fig. 31). Results for HNO_3 in water are shown in Fig. 31; and finally, Fig. 33 shows results for $Fe(ClO_4)_3$ in water. In comparing these rate constants with the corresponding rates for analogous radicals in which the muon is replaced by a proton, the difference in masses of Mu and H should affect only the "dynamics" of the processes. Even MuO$^\bullet$, the lightest muonic radical envisioned, should diffuse through liquids at the same rate as its protonic analog, HO$^\bullet$; the "kinetics" are virtually indistinguish able. Comparisons of reaction rates of muonic and protonic versions of these radicals should therefore admit of straight-forward interpretation in terms of the dynamics of the activated complex.

The most serious difficulty with this interpretation is the uncertainty as to which radical is actually being produced. In the cases of HNO_3 and $FE(ClO_4)_3$ solutions, for instance, we do not attempt to identify the radical species. The fitted value for ω_r/ω_0, while imprecise, does provide a hint as to likely candidates, suggesting MuO$^\bullet$ in the case of $Fe(ClO_4)_3$. However, this cannot be regarded as conclusive evidence, and the products of the reactions

$$Mu + NO_3^- \xrightarrow{K_{mxr}} R \text{ (unidentified)}$$

$$Mu + ClO_4^- \xrightarrow{K_{mxn}} \text{(Muonium containing radical)}$$

must be regarded as unknown. It would be possible to determine the hyperfine coupling in the radicals to higher precision using a longitudinal field technique, but this has not yet been undertaken.

In some cases it is possible to deduce the identity of the radical, if there is only one species of "reagent" and the products of its reaction with H are well known. In hydrogen peroxide solutions, for instance, there seems little doubt that reactions

$$Mu + H_2O_2 \xrightarrow{k_{mxd}} HO^{\bullet} + MuHO$$

$$Mu + H_2O_2 \xrightarrow{k_{mxr}} MuO^{\bullet} + H_2O$$

must dominate.[52] Therefore the radical species is most probably $MuO^{\bullet}$. Our value for the rate constant for reaction of $MuO^{\bullet}$ with H_2O_2 is $k_{rxd}=(1.4\pm0.2)\times10^{9}$ liter/mole sec. The corresponding rate for $HO^{\bullet}+H_2O_2$ is about $(3\pm2)\times10^{7}$ liter/mole sec, a factor of 50 slower.[49] This difference is almost certainly due to dynamic isotope effects, and deserves serious theoretical consideration.

The addition of H to benzene to form cyclohexadienyl is also a well-established reaction,[53] a fact which lends credence to the assumption that $C_6H_6Mu^{\bullet}$ is the radical involved in reactions

$$Mu + C_6H_6 \xrightarrow{k_{mcr}} C_6H_6Mu^{\bullet}$$

$$C_6H_6Mu^{\bullet} + Br_2 \xrightarrow{k_{rxd}} D \text{ (unidentified)}$$

We are unaware of any measurement of the reaction rates for $C_6H_7^{\bullet}$ with Br_2 or I_2; our measurements of $k(C_6H_7Mu^{\bullet} + Br_2) = (3.6\pm1.0)\times10^9$ liter/mole sec and $k(C_6H_6Mu^{\bullet}+I_2) = (2\pm1)\times10^9$ liter/mole sec may represent the only information available on these reactions. In view of the large size of the $C_6H_6Mu^{\bullet}$ molecule and the similarity of the rates with Br_2 and I_2, the reaction is probably diffusion controlled in liquids.

In summary, one sees that there is much more to be learned by extending this type of measurement; we are seeing only the beginning of an extensive program of interesting chemical studies.

12. MUONIUM IN SOLID INSULATORS

The evolution of muonium in an insulator is basically described by the formalism in section 10. If muonium has a sufficiently long lifetime (no chemical reactions), direct muonium precession should be observable-as has been seen in ice, quartz,[44,51,54] and frozen CO_2.[44] The observed damping, as already mentioned, is probably the result of relaxation of the muonium electron spin. If chemical reactions between muonium and the solid take place rapidly, the Ivanter and Smilga equations may be applicable in describing the residual polarization.

As conjectured in section 7, muonium in a solid will form an impurity state. This may lower the electronic wavefunction density at the muon site; consequently, the hyperfine interaction energy

$$A = \hbar\omega_0 = \frac{8\pi}{3} g_J \mu_0^e g_\mu \mu_0^\mu |\psi_s(0)|^2$$

is expected to be lower than in free muonium. Because $|\psi_S(0)|^2 = \frac{1}{\pi r_0^3}$, one may speak of an increase of the size of muonium in the crystal lattice.

Although muonium in ice, quartz, and solid CO_2 is well represented within the experimental accuracy by the Hamiltonian of Eq. 10, with ω_0 equal to the ω_0 of free muonium, results obtained in semiconductors (see next section) do indicate a change of size.

If we view muonium in a crystal as a paramagnetic impurity, by analyogy with ESR results on paramagnetic impurities it is no longer obvious that the Hamiltonian of Eq. 10 provides a good description of a muonium center in a crystal under all circumstances. Instead, one is led to a Hamiltonian which is common in ESR work on paramagnetic impurities and which is known as the effective spin Hamiltonian:[55]

$$H = \vec{J}_e \cdot \hat{A} \vec{S}_\mu + \mu_0^e \vec{H} \hat{g}_e \vec{J}_e + \mu_0^\mu \vec{H} \hat{g}_\mu \vec{S}_\mu \qquad (67)$$

where $\hat{A}$, $\hat{g}_e$ and $\hat{g}_\mu$ are now tensors and $\vec{J}$, $\vec{S}$ are effective spins, not real spins. This phenomenological Hamiltonian thus becomes anisotropic. Values of J, S, $\hat{g}$, and $\hat{A}$ may be quite different from the true ones; and the relation between the effective entities and the real ones is often quite complicated. Anyway, by adopting such an effective spin Hamiltonian, one is able to describe quite complicated ESR patterns and their dependence on spatial orientation of the ESR probe. The next section will give an example in which this Hamiltonian is also appropriate for muonium in a semiconductor.

We now want to discuss a measurement of the longitudinal residual polarization in a single crystal of KCl by Ivanter et al.[56] Figure 34 shows the results in dependence on the magnetic field strength. The Ivanter and Smilga formula Eq. 60 was fitted to these data, yielding

$$H_0 = \frac{H}{X} = \frac{\hbar\omega_e}{g_J\mu_0^e - g_n\mu_0^\mu} = 1540 \pm 60 \text{ G}$$

and the product $\nu\tau_{ch}$=1.81±0.10. The fit is indicated by the solid line in Fig. 34. As can be seen, the low-field data are by no means reproduced by the fit. Apparently there are different mechanisms governing the low-field behavior. ω_0 appears to coincide within its error bars, which are quite large, with the vacuum value. Unfortunately, it is not possible to obtain separate values for ν and from the fit. This would be possible, however, if one could somehow fix the value for ω_0.

From ESR measurments on U_2 centers in KCl, the hydrogen analogue to muonium in a crystal, one obtains a hyperfine splitting frequency for the hydrogen ground state which is 3% smaller than the vacuum value.[57] Using for muonium in this crystal a 3% smaller value of ω_0, one arrives at the following numbers for ν and τ:

$$\nu = 3.5 \cdot 10^9 \text{ sec}^{-1}$$

$$\tau = 6.4 \cdot 10^{-10} \text{ sec}$$

The lifetime appears rather short, which may be reasonable as the measurements were performed at room temperature. However, ν, which is the inverse of the spin-lattice relaxation time of the muonium electron, appears to be surprisingly large. If muonium were in a pure s-state no

coupling of the electron spin to the diamagnetic lattice should occur; that is, there would be no coupling to phonons and, consequently, no relaxation should be visible, A spin-lattice interaction becomes possible if the spin is coupled to some orbital angular momentum (LS coupling), which in turn is sensitive to the electric crystal field. The crystal field is time modulated by phonon modes. Hence, the ground state of muonium in this crystal must contain some admixtures of excited muonium states, for instance, the 2p state. This admixture hat to be facilitated by the static part of the electric crystal field. An indication for this mechanism in the case of KCl is the 3% smaller hyperfine frequency of U_2 centers.

It is evident that a careful analysis of muon depolarization data involves a lot of crystal properties, and one might even hope to learn something about crystal properties by this procedure.

In the original work of Ivanter and Smilga, ν is always tacitly assumed to be field independent. This assumption is by no means obvious. Table IV lists formulas for the relaxation times of paramagnetic impurities in ionic crystals[58] as derived for different phonon processes: 1) the direct process, a one-phonon process; 2) the Raman process, involving two phonons; and 3) the Orbach process, which involves an excited electronic level. Only the Orbach process is field independent. Future muon depolarization measurements promise to shed some light on the phenomena actually ocurring. These processes are not, as is evident, a particular feature of the muon, but are of relevance in many other solid state phenomena.

So far, we have only considered muonium in a non-magnetic insulator. Some particularly nice effects may be expected for muonium in a ferromagnetic insulator.[59] The muonium electron will be coupled by an exchange interaction to the ferromagnetically ordered spins of the sample-not so, however, the muon. The relevant Hamiltonian would thus be of the form:

$$H = A\vec{S}_\mu \cdot \vec{S}_e + \left(g_e \mu_e^e \vec{H}_{loc} + \sum_i J_i \vec{S}_i\right)\vec{S}_e + g_\mu \mu_e^\mu \vec{H}_{loc} \cdot \vec{S}_\mu \qquad (68)$$

with J_i being an exchange integral of the muonium electron with a neighbor electron, labeled i, whose spin is S_i. Thus, the electron will see an effective magnetic field which may be different by many orders of magnitude from the field that acts on the muon. There will also be an interesting possibility for the muonium electron relaxation in ferromagnetic insulators, namely, the absorption or emission of magnons, the quanta of ferromagnetic spin waves. The measurement of relaxation times in these substances may lead, for instance, to a determination of magnon scattering cross sections with muonium.[59] Further, the presence of a majority spin on a ferromagnet leads to an unequal population of the $^1S_0$ and $^3S_1$ states of muonium.

13. MUONIUM IN SEMICONDUCTORS

The behavior of muons in semiconductors which form muonium can be studied by using the beating technique described in Section 10. Gurevich et al.[43] observed that the hyperfine splitting deviated from the vacuum value

$$\frac{\nu_{Ge}}{\nu_0} = 0.56 \pm 0.01$$

Brewer et al.[60] have repeated these measurements in silicon and germanium using a slightly more sensitive technique. The extraction of frequencies in the muon polarization spectra is made by using Fourier analysis of the entire elapsed time distribution; the computer program subtracts the background, corrects for natural decay, and obtains the frequency distribution over a wide range. For each strong component one can obtain a rough mean life for the damping. Figure 35 shows the results of such an analysis for p-type silicon at 70°K. Quartz is shown for comparison; the line separation varies with $1/\omega$:

$$\frac{\nu_{\omega}}{\nu_0} = 0.45 \pm 0.02$$

This result would seem to contradict the earlier study of Feher et al.[17] where the "shallow donor" proposal was put forth; apparently, a large change in the electron wave-function is not occurring. Wang and Kittel[61] have shown that a "deep donor" model, in which the muonium is trapped within an interstitial site leading to a slight swelling of the wave function, must be responsible for this reduction in ν_0.

In their study, Wang and Kittel looked at several models. Briefly, the potential function for the bound electron is cut off at large radii due to screening by the valence band electrons of the neighboring silicon atoms. By invoking other data on the properties of the semiconductors, they are able to explain the magnitude of the reduction of ν_0, as well as the small difference between silicon and germanium. Other searches for atomic hydrogen in semiconductors have never yielded any results although it is well known that hydrogen diffuses freely in Ge and Si.

Their conclusion is that we know more about muonium in Ge and Si than about H or H_2 in these crystals upon which rests most of modern solid state electronics technology.

In our cold p-type silicon spectra, we see not only the two familiar muonium peaks but also two others of similar amplitude, which we have called "anomalous muon precession" for lack of a positive identification of their source. Figure 35 shows a comparison between Fourier spectra for silicon and fused quartz in the same field, demonstrating the absence of anomalous precession in quartz. Whereas the muonium frequencies rise approximately linearly with field up to a few hundred gauss, and are independent of the orientation of the crystal in the field, the anomalous frequencies have the field dependence shown in Fig. 36, and are slightly anisotropic, as indicated. Both anomalous precession and muonium precession have a lifetime on the order of 300 nsec. Neither of these signals has been detected in n-type Si at 77^0K or in any silicon sample at room temperature.

The anomalous frequencies are much higher than the free muon precession frequencies in weak magnetic fields. The muon must therefore be coupled to a particle or system with a larger magnetic moment than its own, as in muonium, where it is coupled to an electron by the contact interaction. The field dependence of the data can in fact be fitted to frequences ν_{12} and ν_{34} of a modified Breit-Rabi formula (see Fig. 7), if the different crystal orientations are treated as separate cases. However, it is necessary to allow both the hyperfine coupling strength and the g-factor of the electron to vary in order to obtain a fit. For the case of the 111 crystal axis parallel to the field, the best value for ν_0/ν_0 (vac) is

0.0198±0.0002; for 100 parallel to the field, the best value is $\nu_0/\nu_0(\text{vac})=0.0205\pm0.0003$. In both cases the best value for g_J is 13±3. Clearly, the spin g-factor of an electron cannot be much different from 2, nor can a pure contact interaction be anisotropic; this modified Breit-Rabi description is meant only as a phenomenological characterization of the data.

These results can be interpreted in terms of a number of physical models. Perhaps the simples is shallow-donor muonium. Here the electron wavefunction is spread over many lattice sites, whereas the entire deep-donor muonium atom fits into one interstitial site. An s-state cannot produce the observed behavior, due to the relatively invariable spin g-factor of the electron. However, in the 2p state the orbital g-factor can be large and anisotropic: the electron wavefunction for a shallow donor must be a superposition of conduction band states, which may have small anisotropic effective masses. If the spin-orbit coupling for the electron is large, j_e becomes a good quantum number, and $\vec{J}_e'$ formally replaces $\vec{J}_e=\vec{S}_e$ in the Breit-Rabi Hamiltonian. A possible objection to this model is the requirement of a minimum lifetime of $\sim$300 nsec for the 2p excited state. Hindrance of the normally fast radiative E1 transition 2p → 1s can be explained by the small overlap between electron wavefunction in the shallow-donor 2p state and the deep-donor 1s state.

A second physical model is suggested by the large variety of ESR centers which have been observed in radiation-damaged silicon.[62] The muon may create a paramagnetic lattice defect (e.g., a broken bond) at the end of its

range, combining with it to form a muon -defect bound state. Such a center can also be described by a modified Breit-Rabi Hamiltonian.

The possibility that the anomalous precession is due to formation of a bound state of a muon with an impurity atom is considered remote. The fractional concentration of impurity atoms in our sample is 10^{-8} or less; muons can be expected to slow from 100 eV to thermal velocities within 10^3 collisions.[63] Thus the probability of a muon passing within several lattice sites of an impurity atom at subionizing velocity is negligible. Furthermore, the time for deep-donor muonium atoms to diffuse to impurity atoms with muon affinities must be longer than $\sim$300nsec, the observed relaxation time for muonium precession.

However, in stopping, the muon must generate a high density of free electrons and holes, with which it may subsequently combine. If we regard the μ^+as a positive impurity ion in an interstitial position, observations of impurity-exciton bound states in silicon[64] provide a precedent for two models involving excitons. The first model is the neutral muonium-exciton molecule ($\mu^+e^-e^-h^+$), in which the two electrons are assumed to have paired spins, in analogy with ground-state H_2.The μ^+ is thus coupled to the hole by a dipole-dipole interaction. Orientational effects are predicted by this model if the molecule is "pinned" by being wedged into an oblong interstitial site in the unit cell.[65] A second model of this type is the ionized muonium-exciton molecule ($\mu^+e^-g^+$), in which all three particles are coupled via contact interactions. These models draw support from the fact that measured free exciton lifetimes in silicon at 80^0K are about 400 nsec.[66]

None of the above physical models for anomalous muon precession can be eliminated on the basis of existing data; however, we feel that shallow-donor 2p muonium is the most probable explanation. In an earlier study at Columbia,[17,11] the "quenching" of μ^+ depolarization in silicon by a magnetic field applied parallel to the muon polarization was interpreted in terms of transitory muonium formation. Their results in p-type silicon at $< 77^0$K suggested the existence of two species of muonium with different hyperfine couplings. However, their prediction that muonium in silicon would only form a short-lived shallow-donor state is contradicted by our observation of long-lived deep-donor 1s muonium. If the anomalous precession is in fact due to shallow-donor 2p muonium (albeit long-lived), their conclusions will be at least partially vindicated. In any event, it is clear that positive muons can provide a great deal of new information about the behavior of hydrogen-like impurities in silicon.

14. COMPARISON WITH OTHER METHODS

It may be approrpiate to list some of the advantages and disadvantages in measuring certain parameters with the help of the muon as compared with other methods, e.g. to U_2 centers. With regard to relaxation times, Fig. 37 summarizes the situation. The figure has been taken from Ref. 67 and has been supplemented by the range of relaxation times measurable by the muon and muonium, respectively.

The electronic relaxation times are generally measured by the method of ESR (electron spin resonance). The shortest relaxation times that can be measured are of the order of 10^{-9} sec. At least 10^{12} electron spins are

needed to obtain a sufficient signal-to-noise ratio. ESR is normally not applicable in zero external field. With the help of the muon, electronic relaxation times can be measured down to 10^{-11}sec. Only about 10^{6} decay events need to be observed. The main disadvantage is that the longest relaxation times that can be measured are only of the order of several μsec. And, of course, implantation of muonium may not lead to the occupation of a site that is wanted for investigation.

The situation is similar with respect to nuclear T_1 and T_2 times. NMR, the most common method for measuring nuclear relaxation times, will not reach below 10^{-6}sec, whereas the muon can be used to measure relaxation times down to 10^{-8}sec. In zero local magnetic field, NMR becomes inapplicable; in metals, as argued before, NMR is a difficult-to-perform technique. However, with NMR one can measure very long relaxation times-minutes-whereas the upper limit in the muon technique is about 500 μsec. With respect to measurements of hyperfine frequencies, g_J factors, Zeeman splitting frequencies (Larmor Frequencies), etc., ESR and NMR have the huge advantage of being very accurate. Application of the muon resonance technique is limited because of the muon's finite lifetime, which introduces a minimum line width.

Finally, there are a number of methods for measuring local fields in, for instance, metals and ferromagnetics: e.g., γγ-PAC, Mössbauer effect, oriented nuclei, NMR, and others. Many of these apply also to implanted ions. Besides the fact that many of these methods are restricted to certain substances, the main trouble with these methods is that the electron core of the probes causes a number

of disturbing effects, such as core polarization, that mask or even change the weaker local fields to be measured. Also, many of the nuclei used as probes have a nuclear electric qudrupole moment which participates in all kinds of disturbing interactions, making it difficult to obtain the desired information on internal local magnetic fields. But the muon is, so to speak, a bare particle carrying only a magnetic moment. Its feedback effects on the local field properties may be small and calculable. This is just what one requires from an ideal probe for exploring bulk properties.

15. CONCLUDING REMARKS

We have mentioned some of the still persisting puzzles, and how their investigation may cast light on solid state properties, on diffusion mechanisms in a solution, on the chemical kinetics of the hydrogenlike muonium, and on interesting isotope effects. There are other puzzles that may have something to do with solid state chemistry or radical physics in a solid which have not been mentioned: such as, the very short T_2 times of about 30 to 50nsec which one has measured in sulphur[68] solid $Fe(NO_3)_3$, and $Gd(NO_3)_3$.[69]

As far as chemistry is concerned, the situation looks most promising as the Ivanter and Smilga formulas and the refined theories of Brewer and Fischer provide a sound basis on which to analyze data and to extract meaningful parameters. In many acid organic and inorganic solutions, atomic hydrogen reaction rates are known,[70] making it possible to study isotope effects. In neutral solutions many fewer studies have been performed; and in alkaline solutions practically nothing is known due to a

competitive interference from OH^- ions which prohibits use of conventional methods. Here, muonium would be the ideal substitute for atomic hydrogen. Interestingly, the temperature dependence of atomic hydrogen reaction rates, as well as the dependence on the kind of solvent, have practically never been explored.[71]

With regard to solid state physics, the application of muons has resulted in a number of interesting phenomena, and the future prospects are most encouraging. A meaningful application, however, requires that researchers continue with some effort to learn how to ask meaningful questions that can be ansered with the help of the muon, and that do not center on the muon's part of the problem under investigation.

REFERENCES

1) For more details see e.g., A.O. Weissenberg, Muons (North Holland, 1967).

2) R.L. Garwin, L.M. Ledermann, and M. Weinrich, Phys. Rev. 105, 1415 (1957).

3) R.A. Swanson, Phys. Rev. 112, 580 (1958)

4) J.I. Friedmann and V.L. Telegdi, Phys. Rev. 105, 1681 (1957); Phys. Rev. 106, (1957)

5) V.W. Hughes, Ann. Rev. Nucl. Sci. 16, 445 (1966).

6) J. Orear, G. Harris, and E. Bierman, Phys. Rev. 107, 322 (1957).

7) J.C. Sens, R.A. Swanson, V.L. Telegdi, D.D. Yovanovitch, Phys. Rev. 107, 1465 (1957).

8) A.O. Weisenberg and V.A. Smirnit-Skii, Sov. Phys. JETP 12, 175 (1960).

9) G. Charpak, F.J. M.Forley, R.L. Garwin, T. Muller, J.C. Sens, V.L. Telegdi, C.M. York, and A. Zichichi, Nuovo Cimento 22, 199 (1961).

10) S. Gorodetzky, Th. Muller, M. Port, A. Zichichi, Phys. Lett. 2, 133 (1962).

11) A. Buhler, T. Massam, Th. Muller, M. Schneegans, and A. Zichichi, Nuovo Cimento 29, 812 (1965).

12) B. Eisenstein, R. Prepost, and A.M. Sachs, Phys. Rev. 142, 217 (1966).

13) R.A. Ferrell, Y.C. Lee, and K.M. Pal, Phys. Rev. 118, 317 (1960).

14) D.P. Hutchinson, J. Menes, G. Shapiro, and A.M. Patlach, Phys. Rev. 131, 1351 (1963).

15) A. Buhler et al., Nuovo Cimento 29, 824 (1965).

16) L.V. Iakovleva, Sov. Phys. JETP 35, 676 (1959).

17) G. Feher, R. Prepost, and A.M. Sachs, Phys. Rev. Lett. 5, 515 (1960).

18) K.M. Crowe, J.F. Hague, J.E. Rothberg, A. Schenck, D.L. Williams, R.W. Williams, and K.K. Young, Phys. Rev. D5, 2145 (1972).

19) S.K. Allison, Rev. Mod. Phys. 30,1137 (1958).

20) E. Fermi and E.E. Teller, Phys. Rev. 72,399 (1947).

21) R.M. Mobley, thesis (Yale University, 1967), unpublished.

22) S.K. Allison and M. Garcia-Munoz, in Atomic and Molecular Processes, D.R. Bates, Ed. (Academic Press, New York, 1962), Ch. 19.

23) A. Abragam, The Principles of Nuclear Magnetism (Clarendon Press, Oxford, 1970).

24) T. Coffin, R.C. Garwin, S. Penman, L.M. Lederman, and A.M. Sachs, Phys. Rev. 109, 973 (1958)

25) J. Alonso and L. Grodzins, in Hyperfine Structure and Nuclear Radiations, E. Matthias and D.A. Shirley, Eds. (North Holland, Amsterdam, 1968), p. 549.

26) See e.g., K.H. Hellwege, Einführung in die Festkörperphysik II, (Springer Verlag, Berlin, 1970), Ch.22.1.

27) See e.g., A. Narath, in Hyperfine Interactions, A.J. Freeman, K.B. Frankel, Eds. (Academic Press, New York, 1967), p. 287.

28) M.L.G. Foy, N. Heiman, W.J. Kossler, and C.E. Stronach, Phys. Rev. Lett. 30, 1064 (1973).

29) A. Schenck and K.M. Crowe, Phys. Rev. Lett. 26, 57 (1971).

30) R. Wolfgang, Progr. Reaction Kinetics 3, 99 (1965).

31) For a compilation see e.q., N.J. Poulis and W.P.A. Hass, Landolt-Bornstein, Zahlenwerte und Funktionen, Vol. II, Part. 9, "Magnetic Properties I" (Springer Verlag, Berlin, 1962).

32) A. Schenck, Phys. Lett. 32A, 19 (1970) and unpublished results.

33) A. Schenck, D.L. Williams, J.H. Brewer, K.M. Crowe, and R.F. Johnson, Chem. Phys. Lett. 12, 544 (1972).

34) N. Bloembergen and L.O. Morgan, J. Chem. Phys. 34, 842 (1961).

35) R.A. Bernheim, T.H. Brown, H.S. Gutowsky, and D.E. Woessner, J. Chem. Phys. 30, 950 (1959),

36) C.C. Hinckley and L.O. Morgan, J. Chem. Phys. 44, 898 (1966).

37) A.W. Nolle and L.O. Morgan, J. Chem. Phys. 36, 378 (1962).

38) B.B. Garrett and L. Morgan, J. Chem. Phys. 44, 890 (1966).

39) I.G. Ivanter and V.P. Smilga, Sov. Phys. JETP 27, 301 (1968).

40) I.G. Ivanter and V.O. Smilga, Sov. Phys. JETP 28, 796 (1969).

41) V.G. Nosov and I.V. Iakovleva, Sov. Phys. JETP 16, 1236 (1963); and Nucl. Phys. 68, 609 (1965).

42) R.K. Wangsness and F. Bloch, Phys. Rev. 89, 728 (1953).

43) I.I. Gurevich, I.G. Ivanter, E.A. Meleshko, B.A. Nikal'skii, V.S. Roganov, V.I. Selivanov, V.P. Smilga, B.V. Sokolov, and V.D. Shestakov, Sov. Phys. JETP 33, 253 (1971).

44) G.G. Myasishcheva, Yu. V. Obukhov, V.S. Roganov, and V.G. Firsov, Sov. Phys. JETP 26, 298 (1968).

45) V.G. Forsov and V.M. Byakov, Sov. Phys. JETP 20, 719 (1965); A.I. Babaev, M. Ya. Balats, G.G. Myasishcheva, Yu. V. Obukhov, V.S. Roganov, and V.G. Firsov, Sov. Phys. JETP 23, 583 (1966).

46) J.H. Brewer, K.M. Crowe, R.F. Johnson, A. Schenck, and R.W. Williams, Phys. Rev. Lett. 27, 297 (1971).

47) J.H. Brewer, K.M. Crowe, F.N. Gygax, R.F. Johnson, D.G. Felming, and A. Schenck, to be published in Phys. Rev. A.

48) See e.g., E.A. Moelwyn-Hughes, Physical Chemistry, 2nd ed. (Pergamon Press 1965).

49) M. Anbar and P. Neta, Int. J. Appl. Rad. and Isotopes 18, 493 (1967).

50) J.H. Brewer, F.N. Gygax, and D.G. Fleming, Phys. Rev. A8, 77 (1973).

51) W.E. Fischer, SIN-preprint (1973).

52) J.P. Sweet and J.K. Thomas, J. Phys. Chem. 68, 1363 (1964).

53) B.D. Michael and J. Hart, J. Phys. Chem. 74, 2878(1970).

54) I.I. Gurevich et al., Phys. Lett. 29B, 387 (1969).

55) See e.g., B. Bleany, in Hyperfine Interactions, A.J. Freeman, R.B. Frankel, Eds. (Academic Press, New York, 1967), Ch. I.

56) I.G. Ivanter, E.V. Minaichev, G.G. Myasishcheva, Yu. V. Obukhov, V.S. Roganov, G.I. Savel'ev, V.P. Smilga, and V.G. Firsov, Sov. Phys. JETP 35, 9 (1972).

57) J.M. Spaeth, Z. Phys. 192, 107 (1966).

58) See e.g., A.A. Manenkov and R. Orbach, Eds. Spin-Lattice Relaxation in Ionic Solids (Harper and Row, New York, 1966).

59) H.C. Siegmann, S. Strässler, and P. Wachter, Proceedings of the Meeting on Muons in Solid State sics (Bürgenstock, Switzerland, 1971), 2. Teil, . 91.

60) J.H. Brewer, K.M. Crowe, F.N. Gygax, R.F. Johnson, B.D. Patterson, D.G. Fleming, and A. Schenck, Phys. Rev. Lett. 31, 143 (1973).

61) J. Shy-Yih Wang and C. Kittel, Phys. Rev. B7, 713 (1973).

62) G. Lancaster, ESR in Semiconductors (Plenum Press, New York, 1967).

63) This estimate is obtained by considering the mean energy loss in elastic collisions with stationary quasi-free silicon atoms.

64) J.R. Haymes, Phys. Rev. Lett. 4, 361 (1960).

65) V.M. Samoilov, Sov. Phys. JETP 31, 1189 (1970).

66) V.S. Vavilov and E.L. Nolle, Sov. Phys. Semicond. 2, 616 (1968).

67) H.H. Wickman, in Hyperfine Structure and Nuclear Radiations, E. Matthias and D.A. Shirley, Eds. (North Holland, Amsterdam, 1968).

68) I.I. Gurevich, L.A. Makr'ina, E.A. Meleshko, B.A. Nikol'skii, V.S. Roganov, V.I. Selivanov, and B.V. Sokolov, Sov. Phys. JETP 27, 235 (1968).

69) Unpublished data of Berkeley group.

70) P. Neta, Chemical Reviews 72, 533 (1972).

71) P. Neta, private communication (1973).

72) See e.g., E. Segre, Nuclei and Particles (Benjamin, New York, 1965), Ch. II.

73) G.W. Ford and C.J. Mullin, Phys. Rev. 108, 477 (1958).

74) G. Wentzel, Phys. Rev. 75, 1810 (1949).

75) H.S.W. Massey and E.H.S. Burhop, Electronic and Ionic Impact Phenomena (clarendon Press, Oxford, 1952), p. 441.

76) I.I. Gurevich et al. Phys. Lett. 40A, 143 (1972).

Table I

Muon properties

Spin ($\vec{S}_\mu$)	1/2
Mass (m_μ)	206.7 m_e=105.6 MeV
Magnetic moment ($\vec{\mu}_\mu$)	$\frac{g_\mu eh}{2m_\mu c}$ S ($3.18\mu_p$)
Lifetime (τ_μ)	2.2 µsec

g =anomalous Landé factor.

Table II

Results of the Swanson experiment.[3]

Target substance	Residual polarization
Metals (al, Be, Li, Mg)	No depolarization visible
Semimetals (Si, graphite)	No depolarization visible
SiC, B_4C	No depolarization visible
P, S	0.05 - 0.1%
CsI, NaCl	0.12 - 0.17%
H_2O	0.5%
Organic substances (liquid, solid)	0.2 - 0.8%

Table III

Expressions for residual polarizations

$$\tilde{P}_{\parallel}(\infty) = 1 - (\omega_0\tau)^2\left(\tfrac{1}{2} + \nu_\perp\tau\right)\Big\{ (1 + 2\nu_\perp\tau)^2 + (\omega_0\tau)^2\left[\frac{(1+2\nu_\perp\tau)(1+\nu_\parallel\tau)}{(1+2\nu_\parallel\tau)} + x^2(1+\zeta)^2\right]\Big\}^{-1}$$

where ω_0 is the hyperfine frequency

τ is the chemical lifetime

$\nu_\perp$ is the electron spin relaxation parameter perpendicular to the field

$\nu_\parallel$ is the electron spin relaxation parameter along the field

$X = H/H_0$, the dimensionless magnetic field

$\zeta = m_e/m_u$

$$P_\perp(\infty) = -\frac{1}{\tilde{\tau}}\left\{\gamma_\parallel + i\,\frac{A_0^2B_0^2 - (A_0+B_0)^2}{A_0B_0^2 - (A_0+B_0)}\right\}^{-1}$$

where $\gamma_\parallel = 4\nu_\parallel/\omega_0$

$$A_0 = i\left(\frac{1}{\tilde{\tau}} + \gamma_\parallel\right) + 2x\left(\zeta - \frac{\tilde{\omega}_\mu}{2x}\right)$$

$$B_0 = i\left(\frac{1}{\tilde{\tau}} + \gamma_\perp\right) - 2x\left(1 + \frac{\tilde{\omega}_\mu}{2x}\right)$$

$$\tilde{\tau} = \frac{\tau\omega_0}{2}$$

$$\tilde{\omega}_\mu = \frac{2\omega_\mu}{\omega_0}$$

Table IV

Formulas for relaxation of paramagnetic impurity spins in ionic crystals due to phonon process (H=magnetic field strength; T=temperature)

Process	Relaxation rate
Direct process:	
one-phonon exchange	$\frac{1}{T_1} \approx A\ H^4 T$
Raman process:	
two-phonon exchange	$\frac{1}{T_1} \approx B_1 T^9 + B_2 H^2 T^7$
Orbach process	$\frac{1}{T_1} \approx C \exp\left(-\frac{\Delta_c}{kT}\right)$

FIGURE CAPTIONS

Fig. 1 Asymmetry spectrum obtained with the magnetic spectrometers of Kruger and Crowe. The asymmetry coefficient (in%) is plotted as a function of positron energy.

Fig. 2 Positron energy spectrum from μ^+-decay.

Fig. 3 Schematic experimental arrangement in a longitudinal field. M1, M2, E1, E2 are counters.

Fig. 4 Schematic experimental arrangement in a transverse field. The asymmetric decay pattern in rotating past the counters.

Fig. 5 Experimental histogram of time from μ^+ stop until e^+ detection.

Fig. 6 Schematic plot of an actual experimental arrangement.

Fig. 7 Muon precession in boron carbide after decay and background correction.

Fig. 8 Breit-Rabi diagram of muonium hyperfine structure. (Not drawn to scale)

Fig. 9 Quenching of depolarization in muonium state in a longitudinal magnetic field.

Fig. 10 Quenching of the depolarization in sulfur at three temperatures.

Fig. 11 Quenching of the depolarization in LiF, MgO, and red P at room temperature.

Fig. 12 Summary of the experimental results for longitudinal fields up to 4 kG.

Fig. 13 Experimental values of the asymmetry parameter, a, for decay positrons from stopped muons (a) versus free electron concentration in n-type silicon and free hole concentration in p-type silicon; (b) in one sample of n-type germanium (phorphorus-doped) at room temperature and liquid nitrogen temperature; and (c) in a graphite sample for which the maximum value of $\alpha=0.33$ is assumed to correspond to full muon polarization. The abscissas for n-type and p-type silicon have been joined at the value of the intrinsic concentration for room temperature ($10^{10}cm^{-3}$). Since the product of the numbers of free holes and electrons in thermal equilibrium with the lattice is constant at a given temperature (i.e., 10^{20} for silicon at room temperature), the entire abscissa represents an increasing free electron concentration to the right (or an increasing hole concentration to the left).

Fig. 14 Flow diagram for slowing down process. It contains the time estimates for the different sections of the slowing down process. The boxes to the right side give a list of depolarization processes that are supposed to occur.

Fig. 15 Evidence that protons approach the end of their range as M atoms. The critical velocity is $\alpha_c = 2.2 \times 10^6$ m/sec.

Fig. 16 Illustration of the muon proton dipole-dipole interaction in a single crystal of gypsum.

Fig. 17 Plot of the experimental asymmetry A·F(t) versus muon life time for two different crystal orientations. (upper: magnetic field (100), (010); lower: $< \vec{H}$, (100)$\simeq 140^0$; $< \vec{H}$, (010) $\simeq 110^0$)
The asymmetry is calculated for 0.5-μsec intervals versus muon lifetime. The constant background is approximately 2% at t=o. The solid curve shows the theoretical AF(t) calculated from Eq. 23.

Fig. 18 Slow relaxation times versus Fe^{3+}-ion concentration (H=11 kG).

Fig. 19a Dependence of T_2 on Mu^{++}-ion concentration. Dasked curves show the dipole-dipole and spin exchange induced dependences seperatly.

Fig. 19b Concentration dependent effective correlation time in muon-ion interactions due to spin-spin interaction among Mu^{2+} ions. (From ESR-measurements of Ref. 36.)

Fig. 20a Data from Fig. 19a. The concentration dependence is divided out.

Fig. 20b Temperature dependence of the relaxation time T_2 (concentration dependence is divided out). for external transverse fields 4.5 and 11.0 kgauss.

Fig. 21 Evolution of muonium in 100 gauss (Brewer et al.[51].)

Fig. 22 Evolution of muonium in 100 gauss: Locus traced out by the tip of the muon polarization vectors in the plane perpendicular to the magnetic field (J.H. Brewer, thesis Berkeley 1972, unpublished.)

Fig. 23 Two-frequency precession (beats) of the muonium spin in fused quartz. The continuous curve represents the theoretical dependence.

Fig. 24 Muonium precession curves in fused quartz at different temperatures, with 18.5 nsec c channel width.

Fig. 25 Dependence of the residual polarization and phase on the average chemical lifetime. Dasked curves: no hot fraction present; solid curves: hot fraction (h=0.5) present.

Fig. 26 Dependence of the residual polarization and phase in a solution of I_2 in CH_3OH on I_2 concentration. External field H≅100 gauss. The solid line represents a fit of the Ivanter and Smilga expression Tab. III.

Fig. 27 Same as Fig. 26, but with an external field of H= 1 Kgauss.

Fig. 28 As Figs. 26, 27; external field H=4.5 kgauss.

Fig. 29 Flow chart of depolarization mechanisms.

Fig. 30 Polarization and phase of muons in a Br_2 solution in benzene at 200 gauss. Dotted line is a fit excluding radical formation. The solid line is a fit based on the phenomenological theory including the possibility of radical formation.

Fig. 31 Polarization and phase of muons in a H_2O_2-solution in water. The meaning of the lines are the same as in Fig. 30.

Fig. 32 The same results as in Figs. 30 and 31 for HNO_3 solved in water.

Fig. 33 The same results as in Figs. 30, 31 and 32 for $Fe(CLO_4)_3$ solved in water.

Fig. 34 $\mu\dot{\mu}$-polarization in a single crystal of potassium chloride as a function of a longitudinal magnetic field.

Fig. 35 Precession frequencies and amplitudes for muonium in quartz and silicon. (p-type at 70^0K).

Fig. 36 Field dependence of the anomalous precessions in silicon.

Fig. 37 Comparison of the possibilities of measuring relaxation parameters with the help of the muon with various other methods.

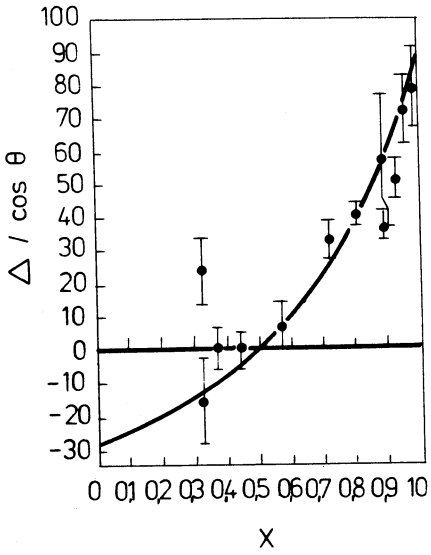
100
90
80
70
60
50
40
30
20
10
0
-10
-20
-30
Δ / cos θ
0 0,1 0,2 0,3 0,4 0,5 0,6 0,7 0,8 0,9 10
X

Fig. 1

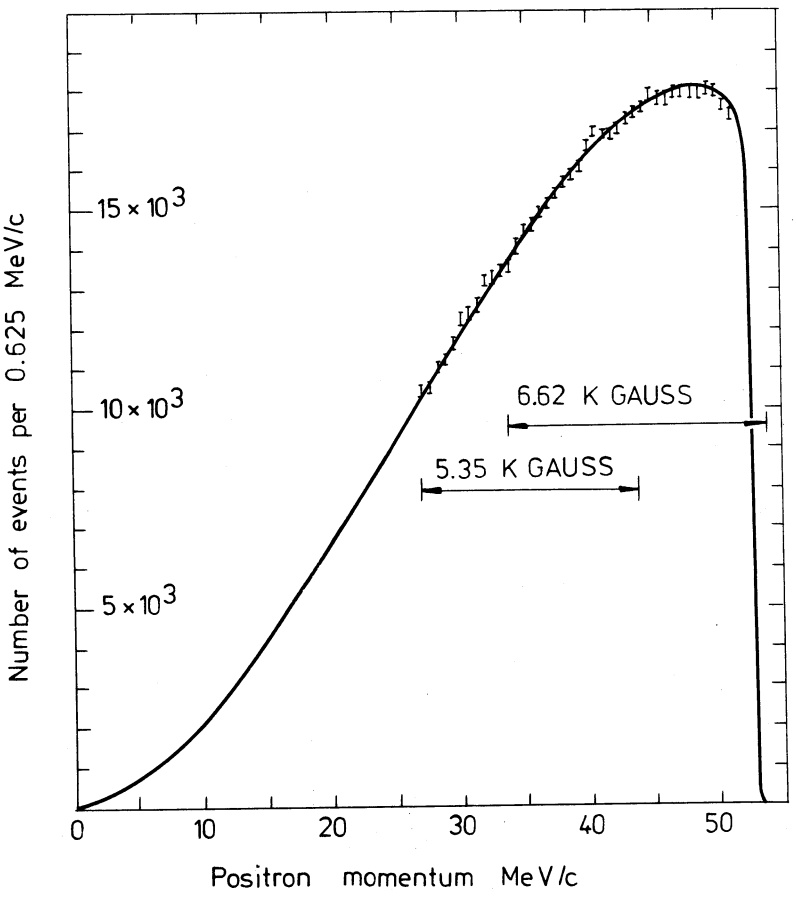
15 × 10³
10 × 10³
5 × 10³
Number of events per 0.625 MeV/c
6.62 K GAUSS
5.35 K GAUSS
0
10
20
30
40
50
Positron momentum MeV/c

Fig. 2

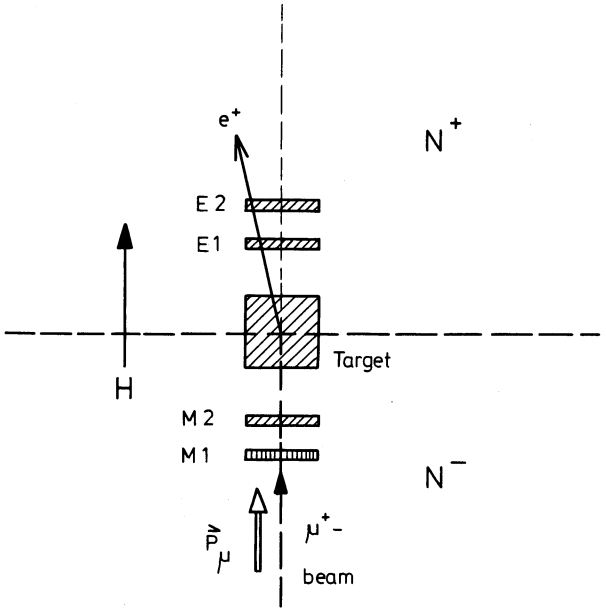

Fig. 3

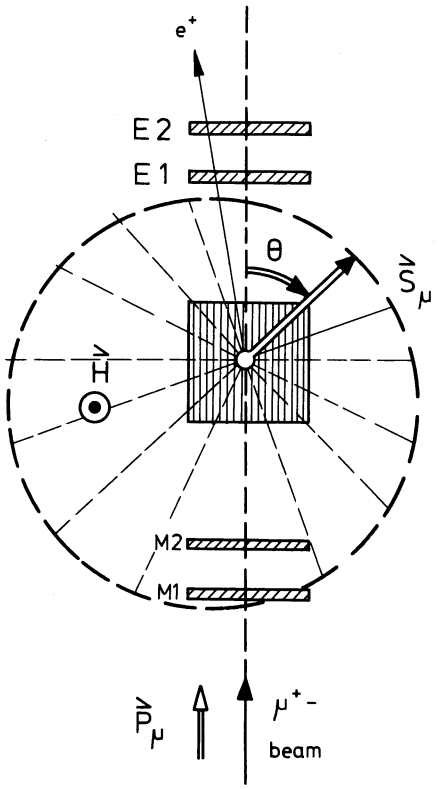

Fig. 4

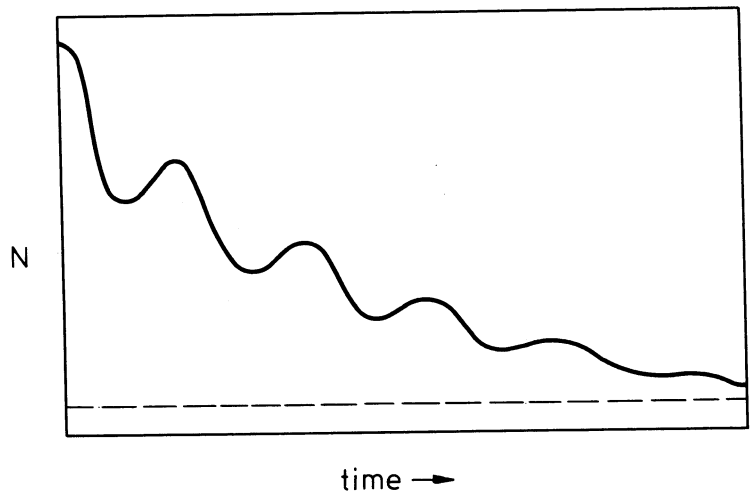
N
time

Fig. 5

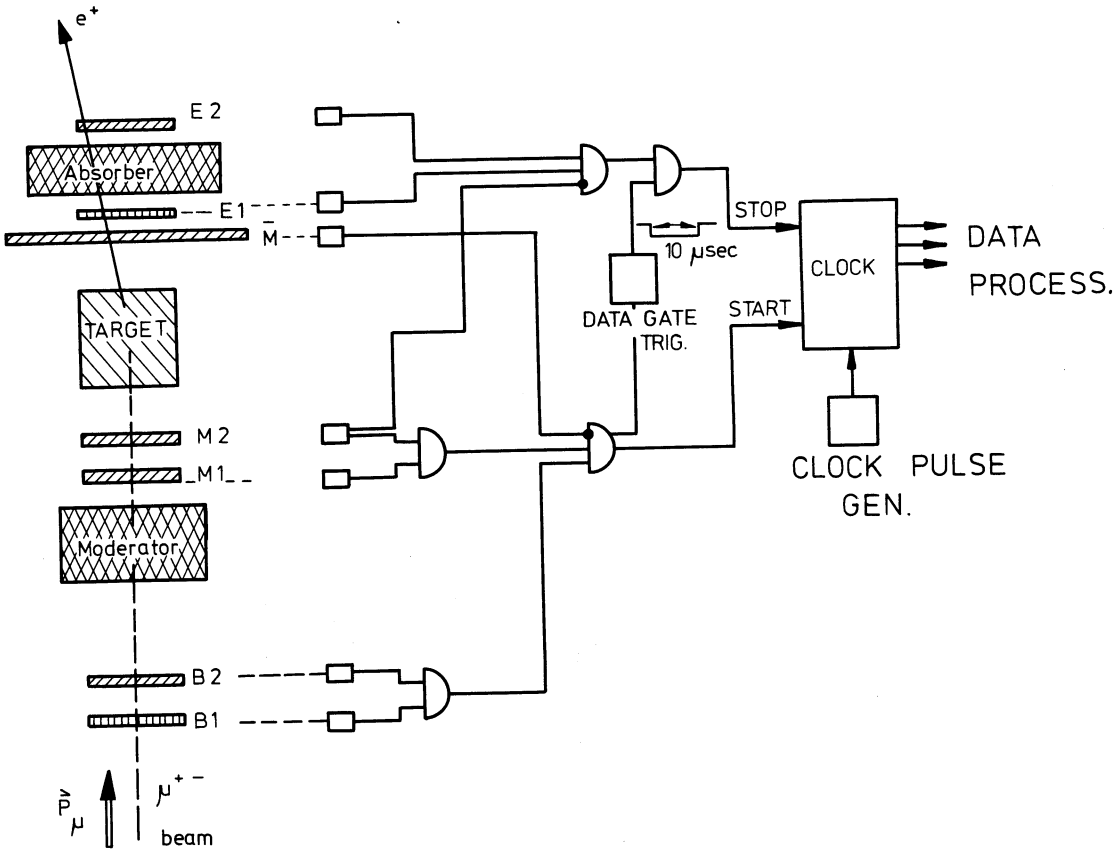
e+
E 2
Absorber
E1
M
TARGET
M 2
M1
Moderator
B 2
B1
μ+ −
beam
STOP
10 μsec
DATA GATE TRIG.
START
CLOCK
DATA PROCESS.
CLOCK PULSE GEN.

Fig. 6

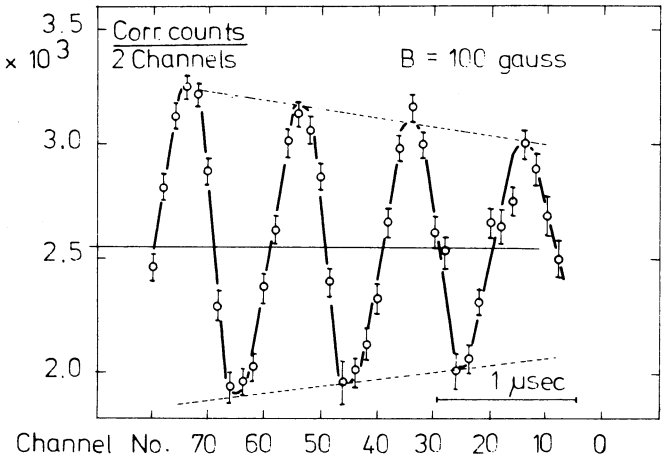
3.5
× 10 3
Corr. counts
2 Channels
B = 100 gauss
3.0
2.5
2.0
1 μsec
Channel No. 70 60 50 40 30 20 10 0

Fig. 7

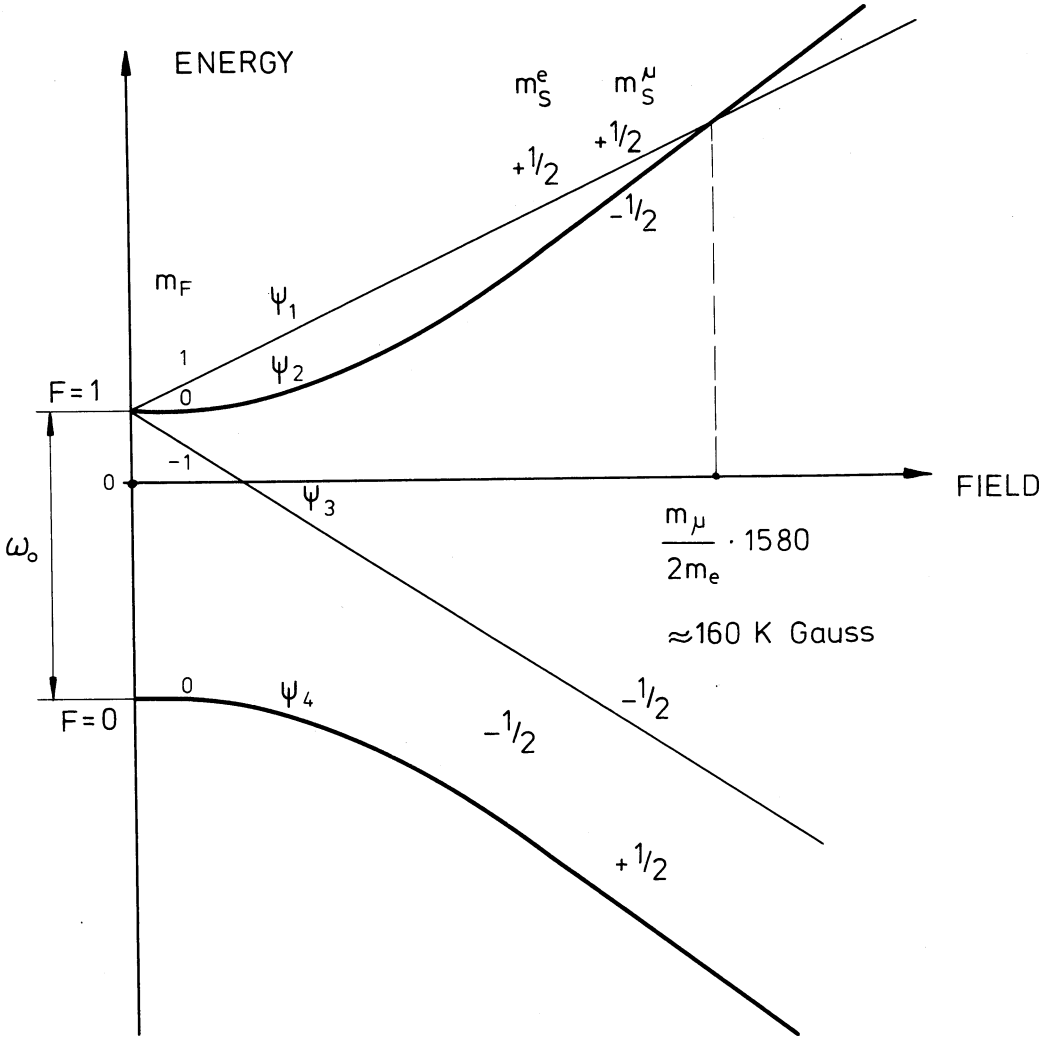
ENERGY
m_s^e
m_s^μ
$+1/2$
$+1/2$
$-1/2$
m_F
ψ_1
1
ψ_2
F=1
0
-1
0
FIELD
ψ_3
ω_o
$\frac{m_\mu}{2m_e} \cdot 1580$
$\approx$160 K Gauss
0
ψ_4
F=0
$-1/2$
$-1/2$
$+1/2$

Fig. 8

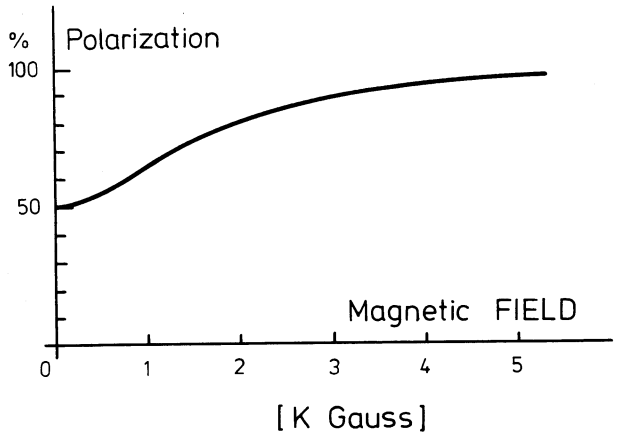
%
Polarization
100
50
Magnetic FIELD
0
1
2
3
4
5
[K Gauss]

Fig. 9

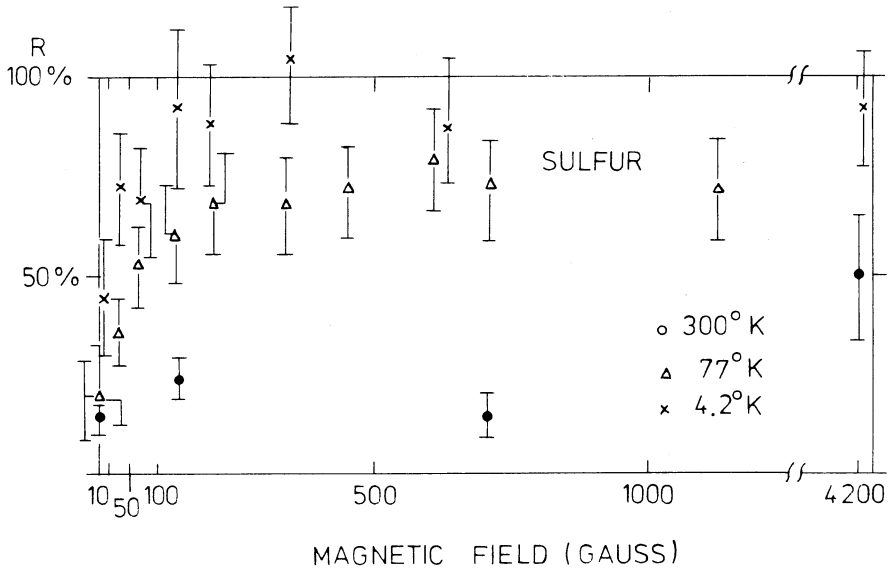
R
100 %
50 %
SULFUR
o 300° K
Δ 77° K
× 4.2° K
10
50
100
500
1000
4200
MAGNETIC FIELD (GAUSS)

Fig. 10

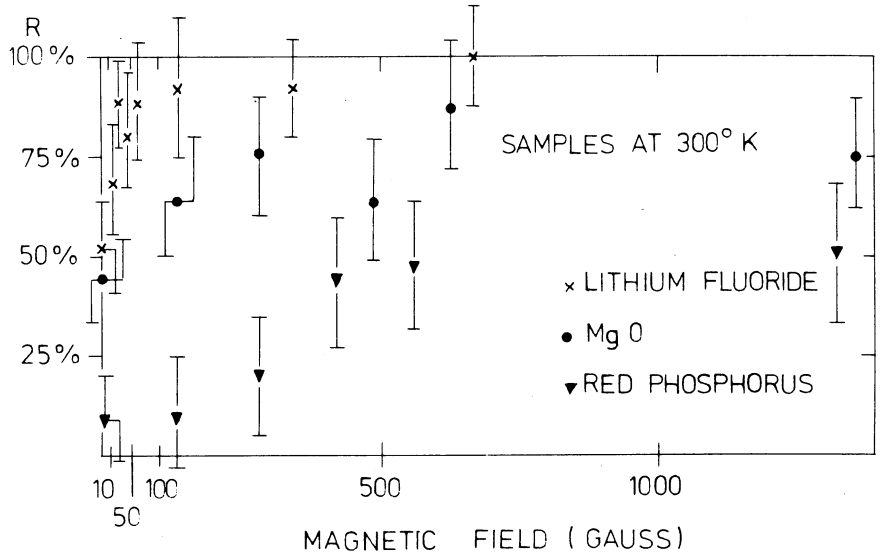
R
100 %
75 %
50 %
25 %
SAMPLES AT 300° K
× LITHIUM FLUORIDE
• Mg O
▼ RED PHOSPHORUS
10
50
100
500
1000
MAGNETIC FIELD (GAUSS)

Fig. 11

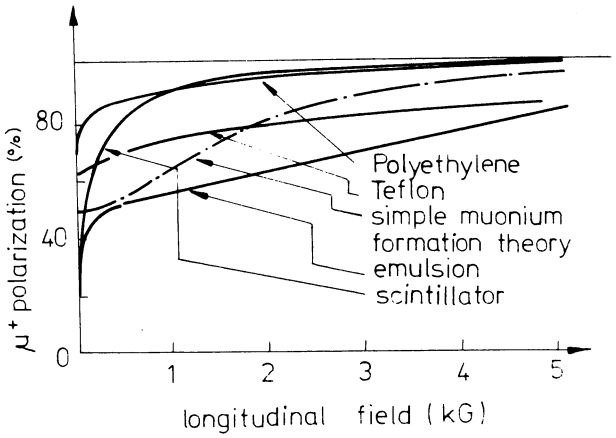
80
40
0
μ^+ polarization (%)
1
2
3
4
5
longitudinal field (kG)
Polyethylene
Teflon
simple muonium
formation theory
emulsion
scintillator

Fig. 12

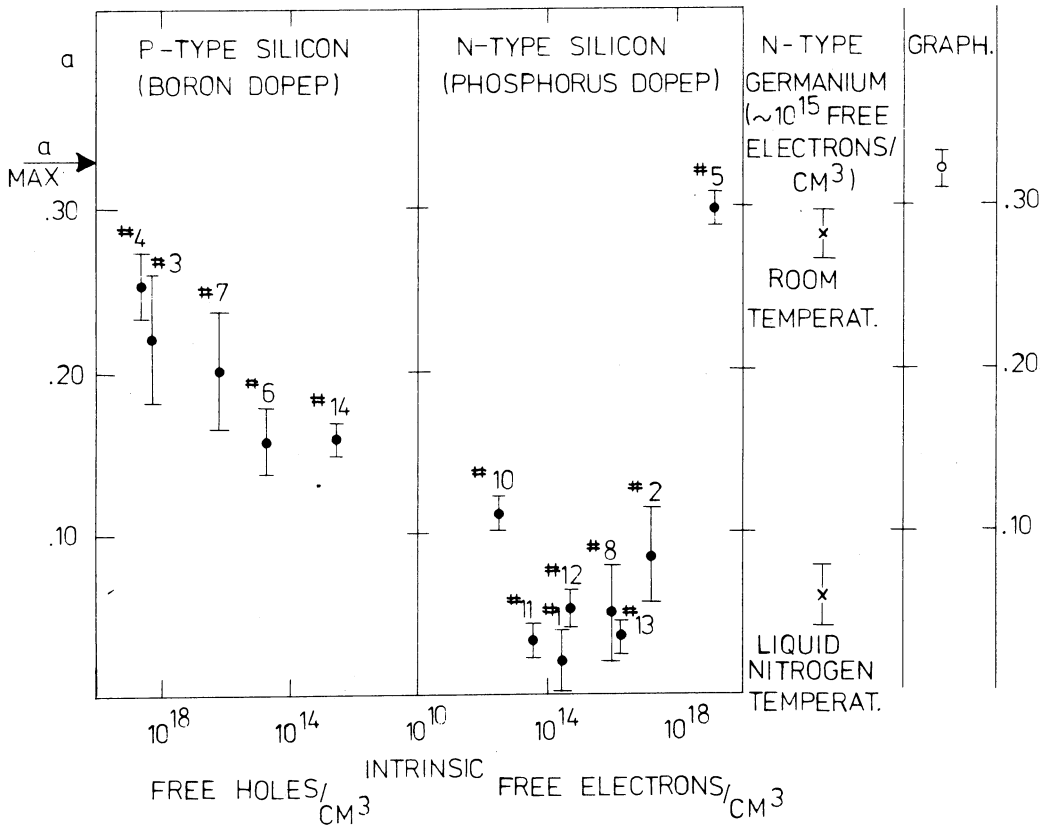
a
P-TYPE SILICON
(BORON DOPEP)
N-TYPE SILICON
(PHOSPHORUS DOPEP)
N-TYPE
GERMANIUM
(~10^15 FREE
ELECTRONS/
CM^3)
GRAPH.
a
MAX
.30
.20
.10
#4
#3
#7
#6
#14
#5
#10
#2
#8
#12
#11
#1
#13
ROOM
TEMPERAT.
LIQUID
NITROGEN
TEMPERAT.
10^18
10^14
10^10
10^14
10^18
INTRINSIC
FREE HOLES/CM^3
FREE ELECTRONS/CM^3

Fig. 13

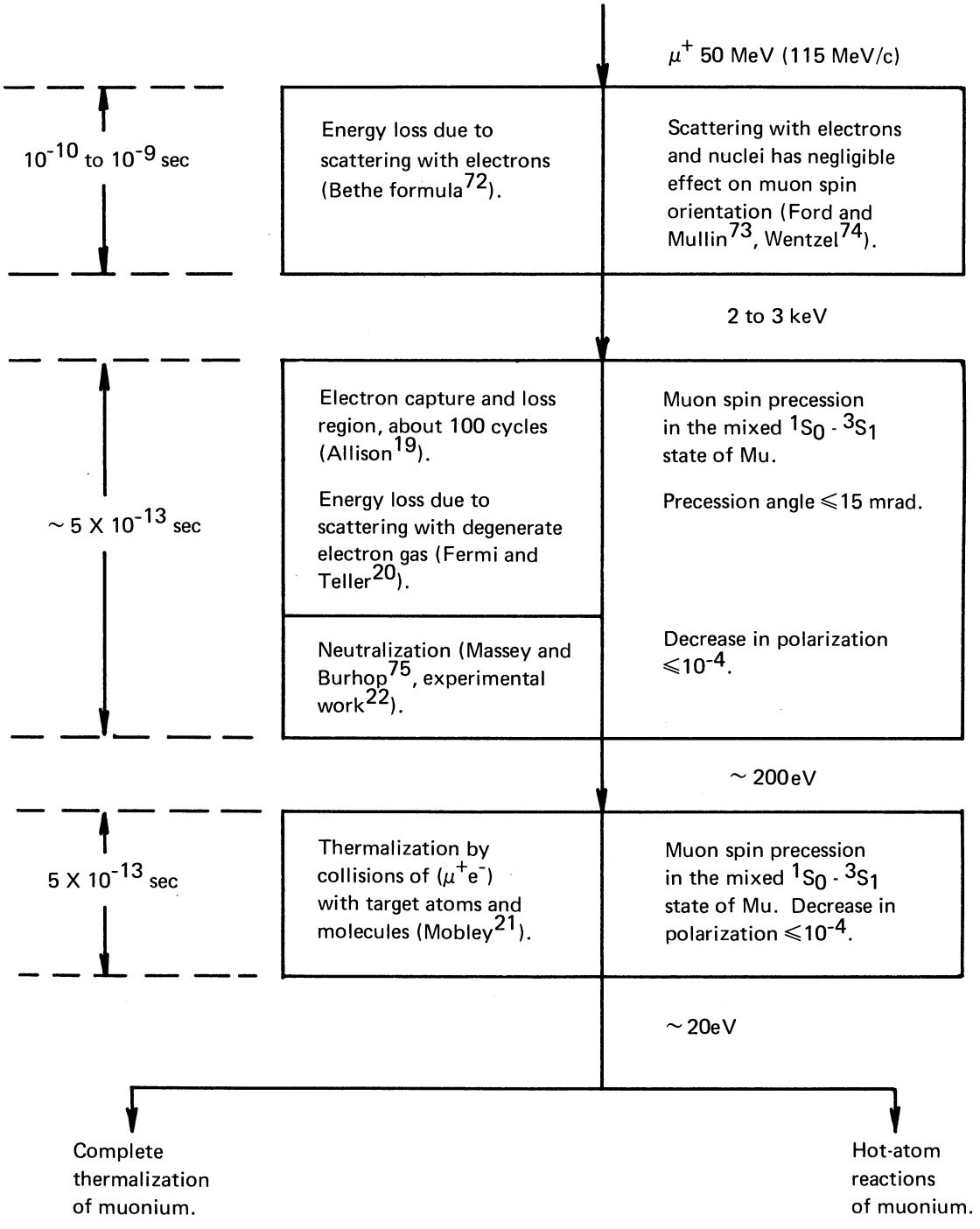

XBL7310-4280

Fig. 14

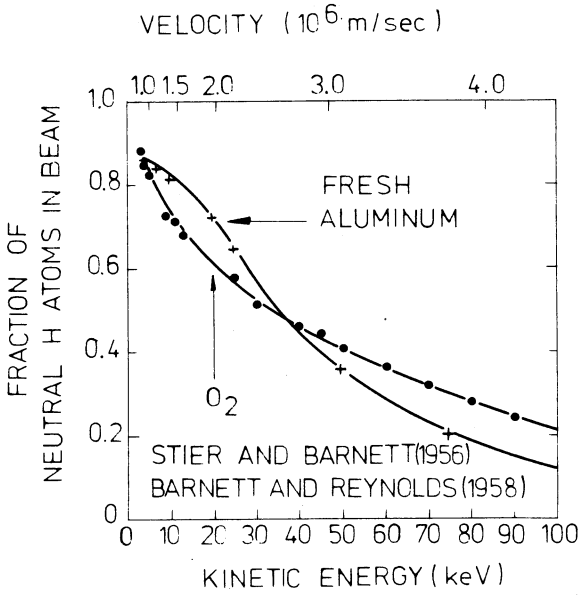
VELOCITY (10^6 m/sec)
1.0 1.5 2.0 3.0 4.0
FRACTION OF NEUTRAL H ATOMS IN BEAM
1.0
0.8
0.6
0.4
0.2
0
FRESH ALUMINUM
O_2
STIER AND BARNETT(1956)
BARNETT AND REYNOLDS(1958)
0 10 20 30 40 50 60 70 80 90 100
KINETIC ENERGY (keV)

Fig. 15

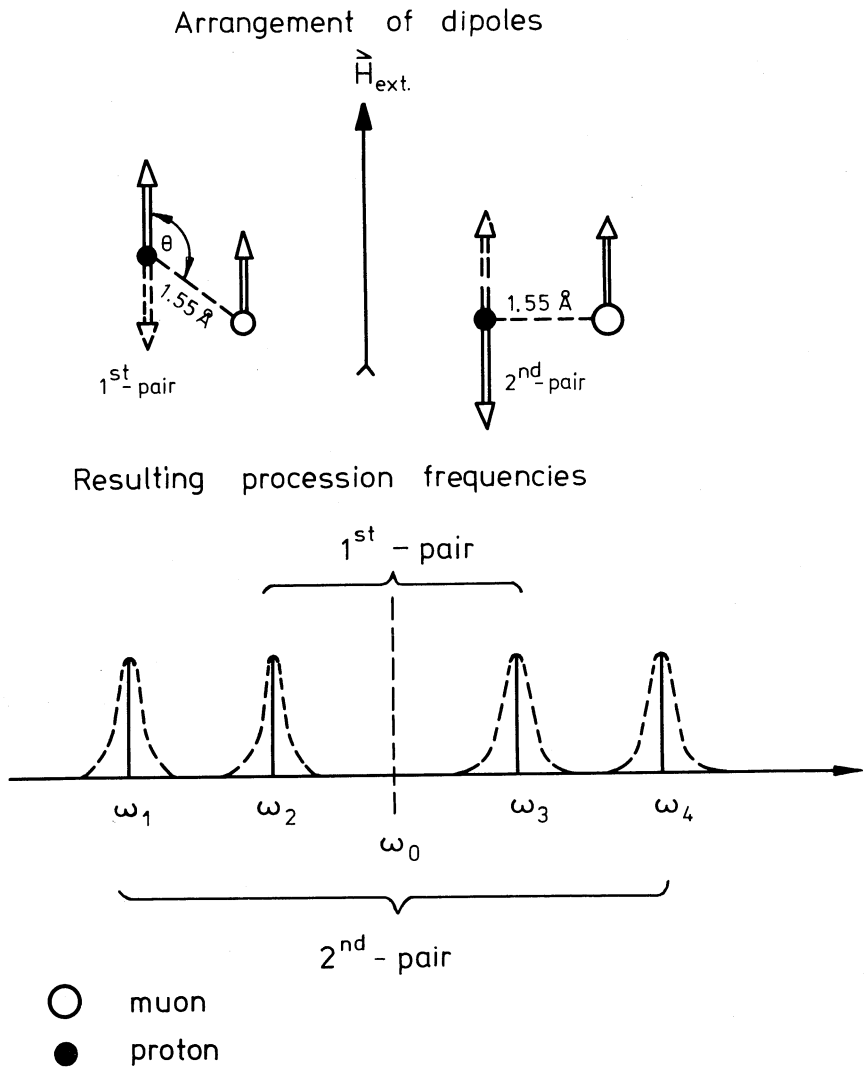
Arrangement of dipoles
$\vec{H}_{ext.}$
θ
1.55 Å
1st - pair
1.55 Å
2nd - pair
Resulting procession frequencies
1st - pair
ω_1
ω_2
ω_0
ω_3
ω_4
2nd - pair
muon
proton

Fig. 16

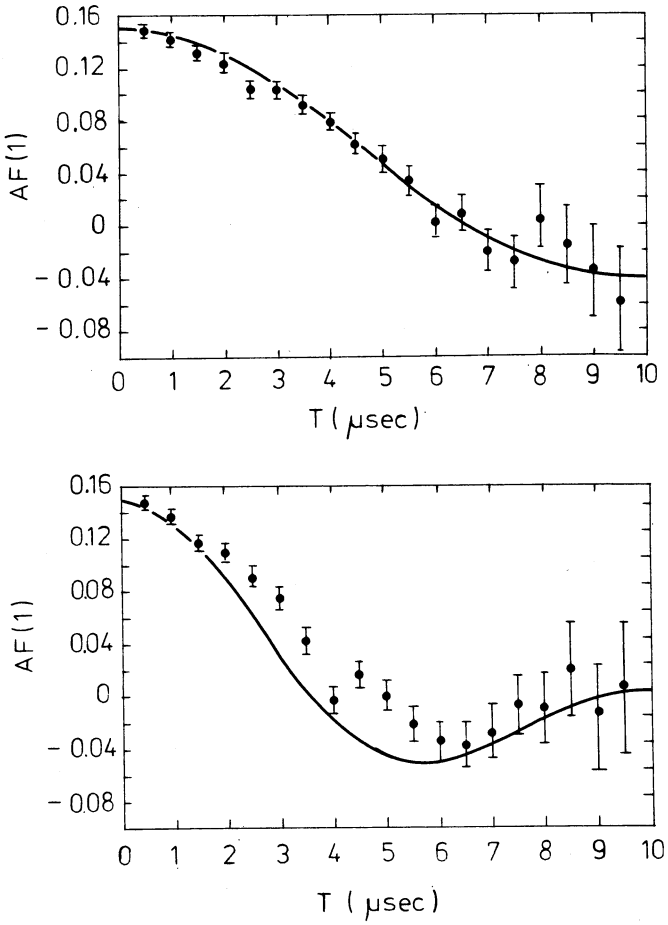
0.16
0.12
0.08
0.04
0
- 0.04
- 0.08
AF(1)
0 1 2 3 4 5 6 7 8 9 10
T (μsec)
0.16
0.12
0.08
0.04
0
- 0.04
- 0.08
AF(1)
0 1 2 3 4 5 6 7 8 9 10
T (μsec)

Fig. 17

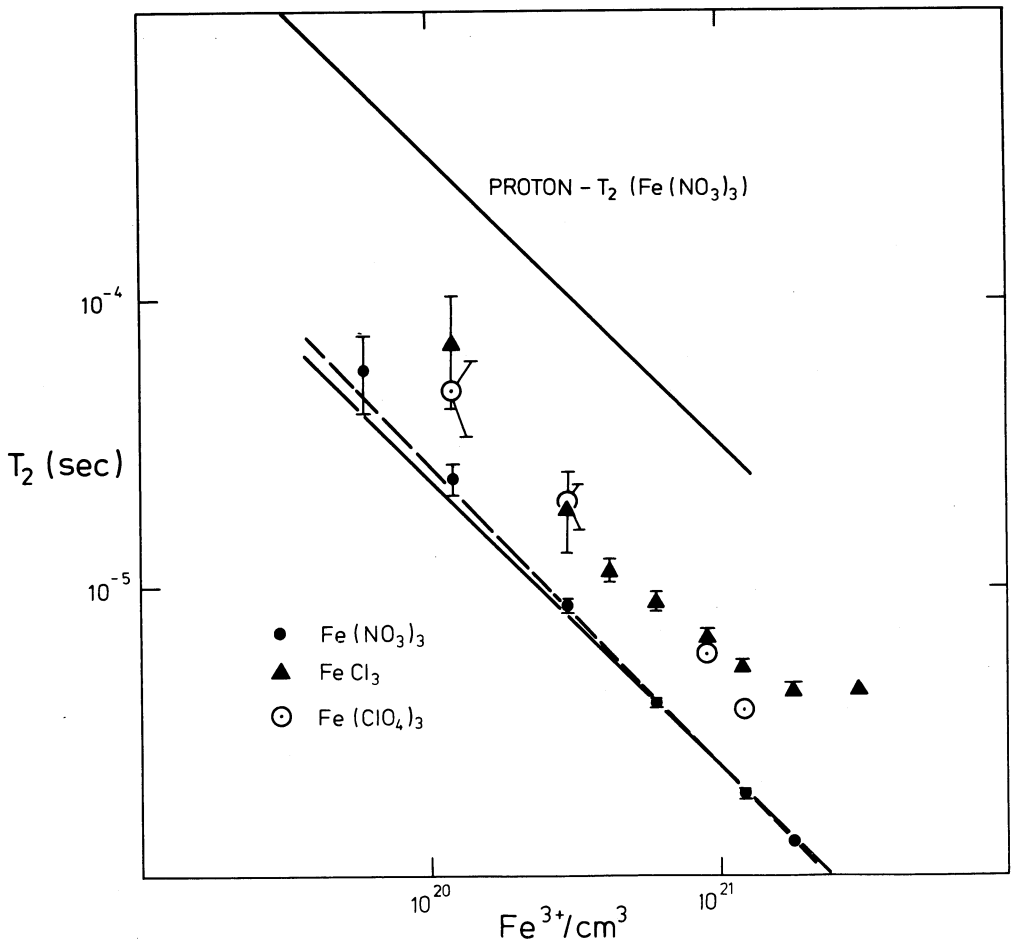
PROTON - T_2 ($Fe(NO_3)_3$)
T_2 (sec)
10^{-4}
10^{-5}
$Fe(NO_3)_3$
$FeCl_3$
$Fe(ClO_4)_3$
10^{20}
10^{21}
Fe^{3+}/cm^3

Fig. 18

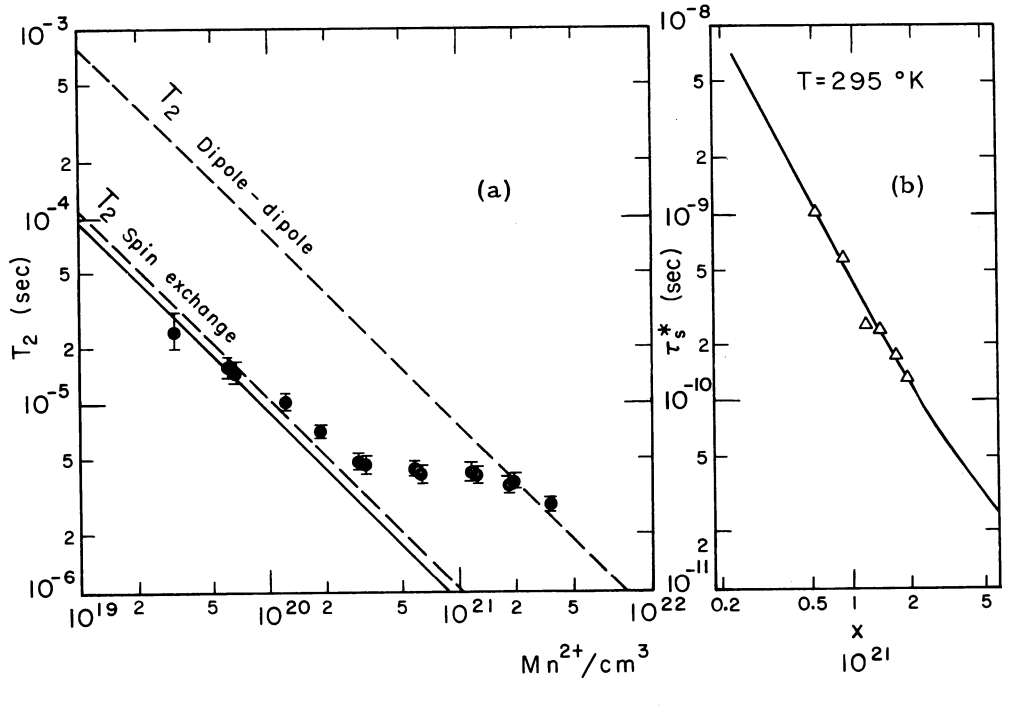
T_2 Dipole - dipole
T_2 Spin exchange
(a)
T_2 (sec)
Mn^{2+}/cm^3
T = 295 °K
(b)
τ_s^* (sec)
x
10^{21}
XBL718-4008

Fig. 19

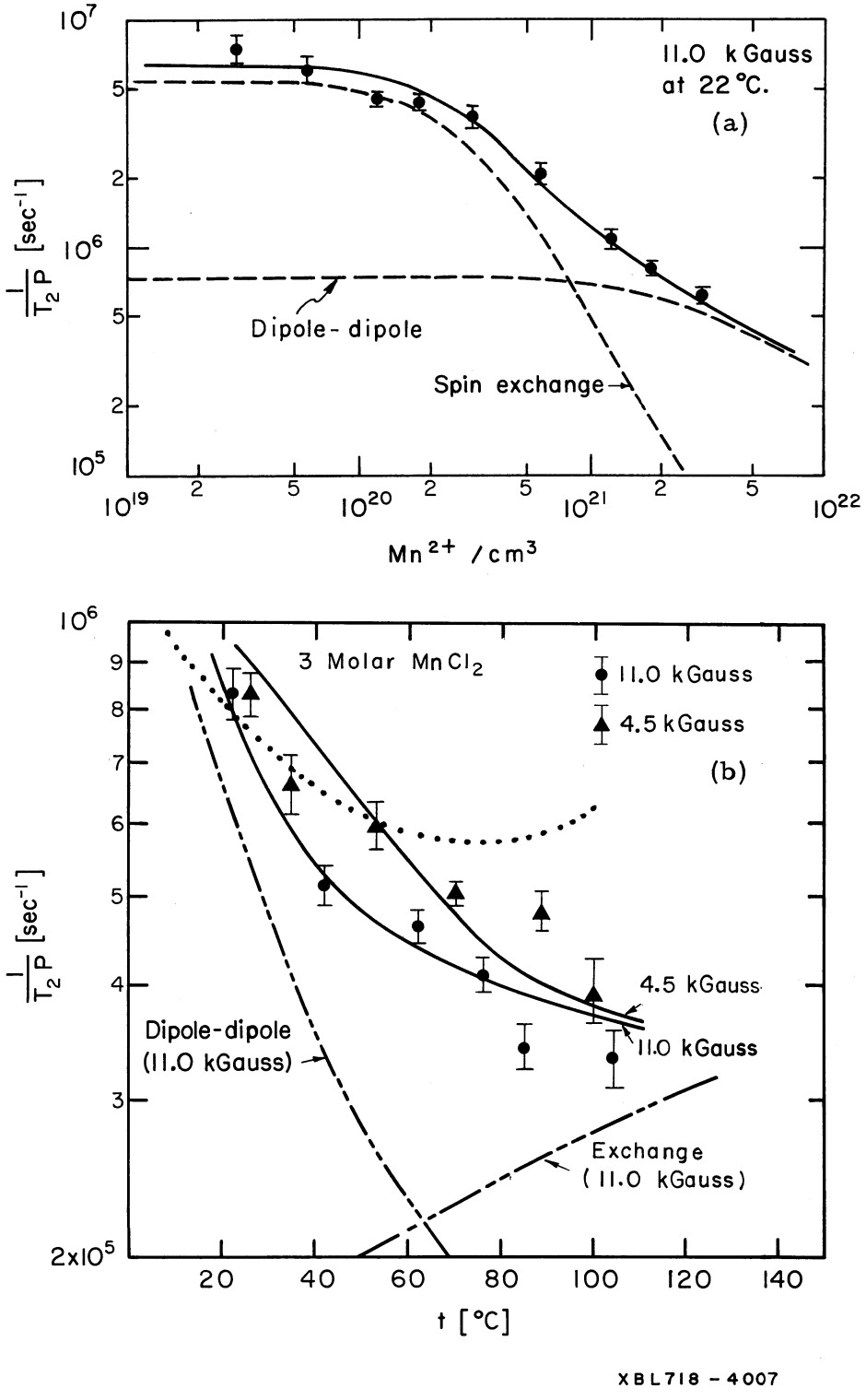
11.0 k Gauss
at 22 °C.
(a)
Dipole - dipole
Spin exchange
$\frac{1}{T_2 P}$ [sec^{-1}]
Mn^{2+} /cm^3
3 Molar MnCl$_2$
11.0 kGauss
4.5 kGauss
(b)
4.5 kGauss
11.0 kGauss
Dipole-dipole
(11.0 kGauss)
Exchange
(11.0 kGauss)
t [°C]
XBL718 - 4007

Fig. 20

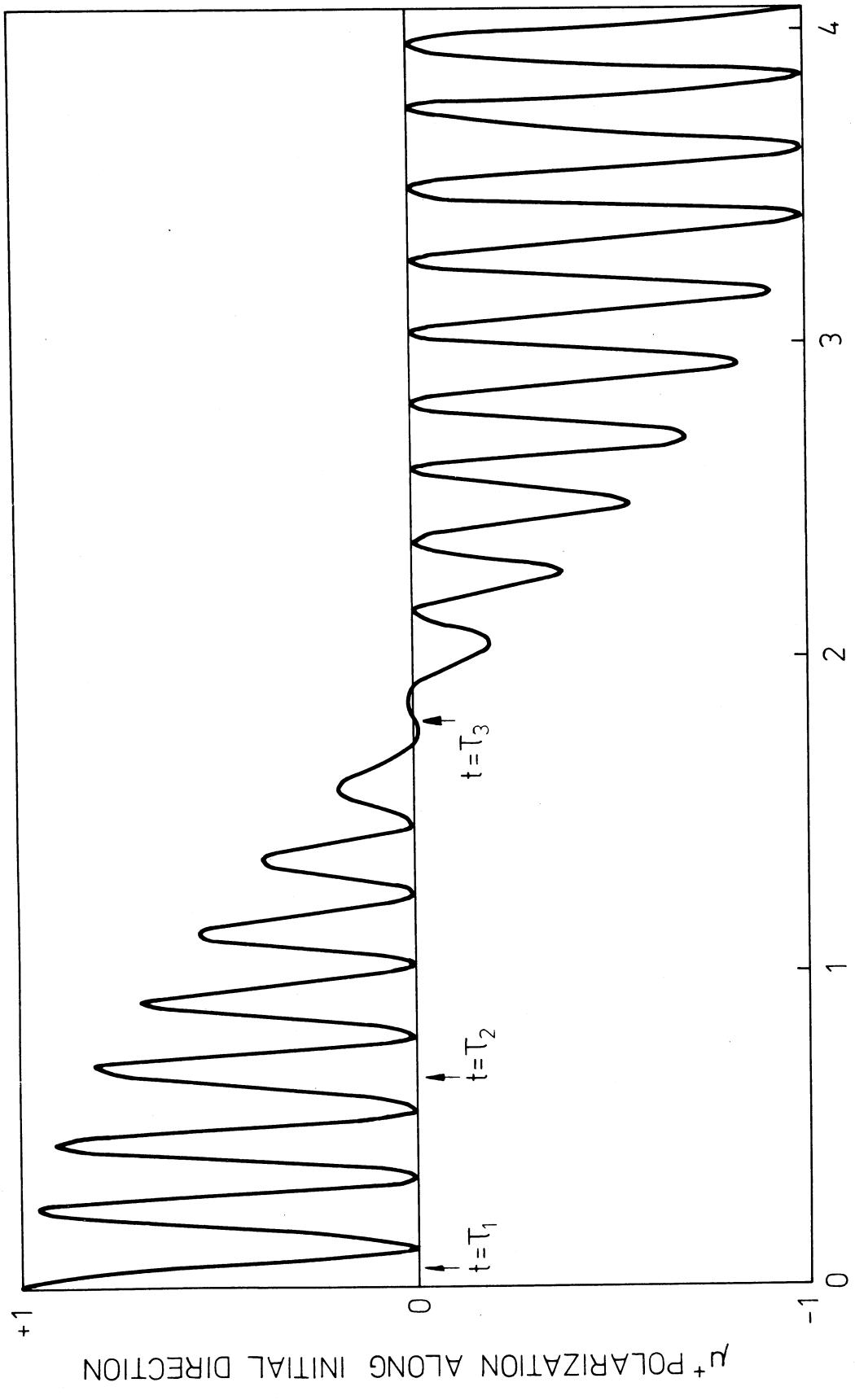
+1
0
-1
0
1
2
3
4
TIME (nsec)
$t=T_1$
$t=T_2$
$t=T_3$
μ^+ POLARIZATION ALONG INITIAL DIRECTION

Fig. 21

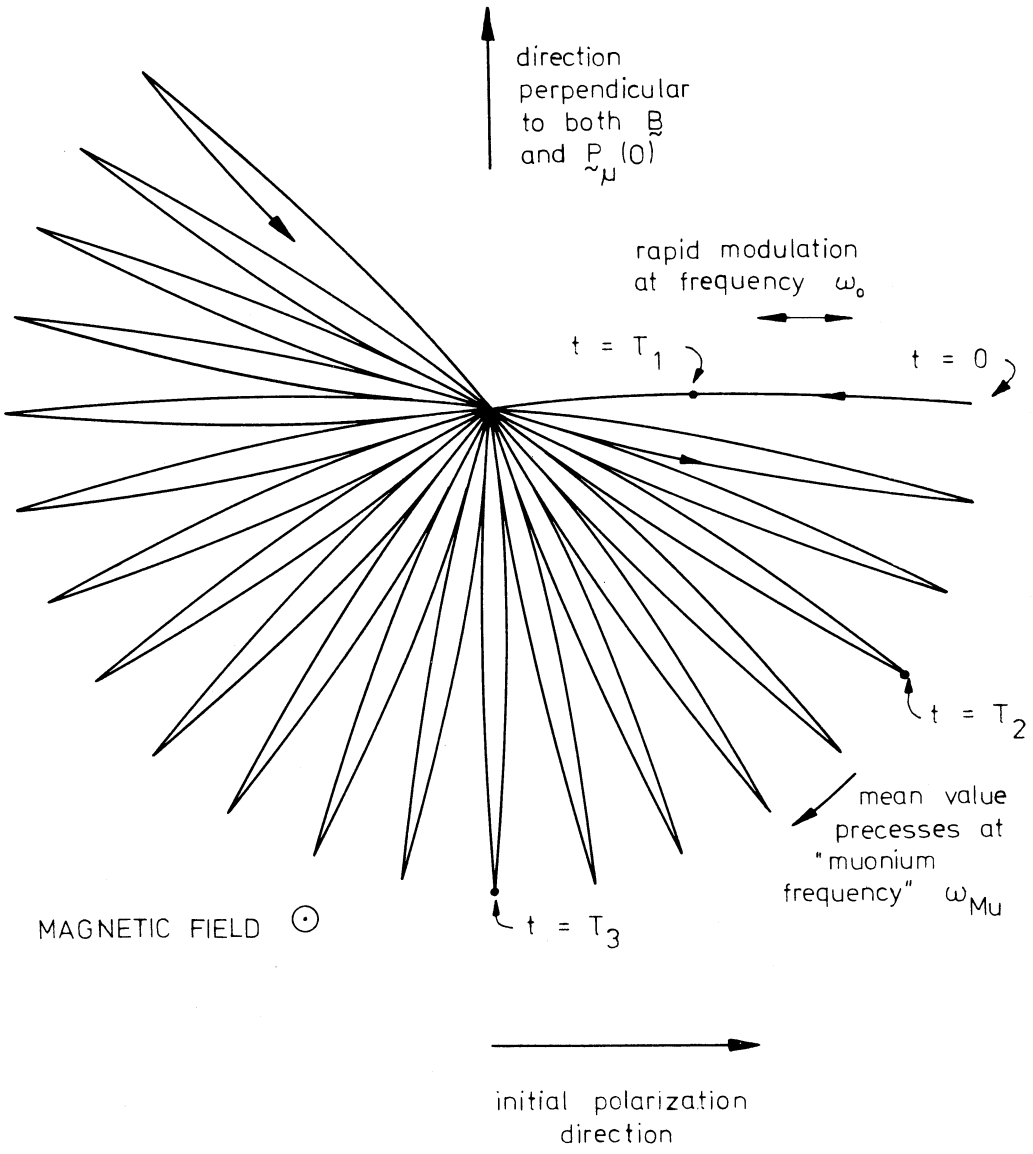
direction
perpendicular
to both B
and P_μ(0)
rapid modulation
at frequency ω₀
t = T₁
t = 0
t = T₂
mean value
precesses at
"muonium
frequency" ω_Mu
MAGNETIC FIELD ⊙
t = T₃
initial polarization
direction

Fig. 22

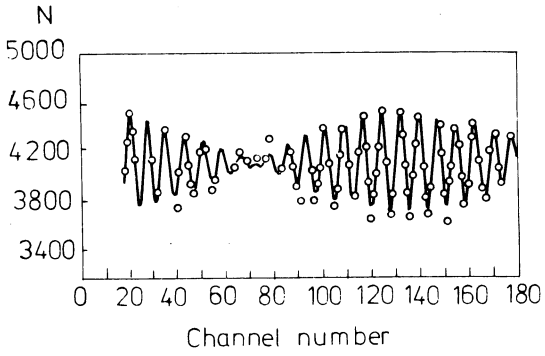
N
5000
4600
4200
3800
3400
0 20 40 60 80 100 120 140 160 180
Channel number

Fig. 23

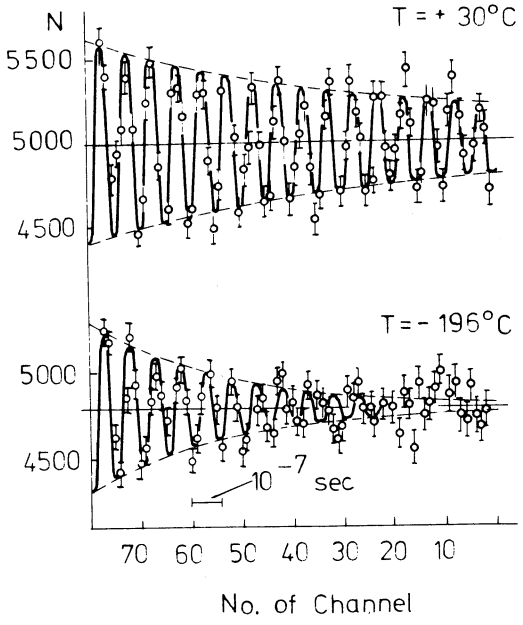
N
T = + 30°C
5500
5000
4500
T = - 196°C
5000
4500
10 -7 sec
70 60 50 40 30 20 10
No. of Channel

Fig. 24

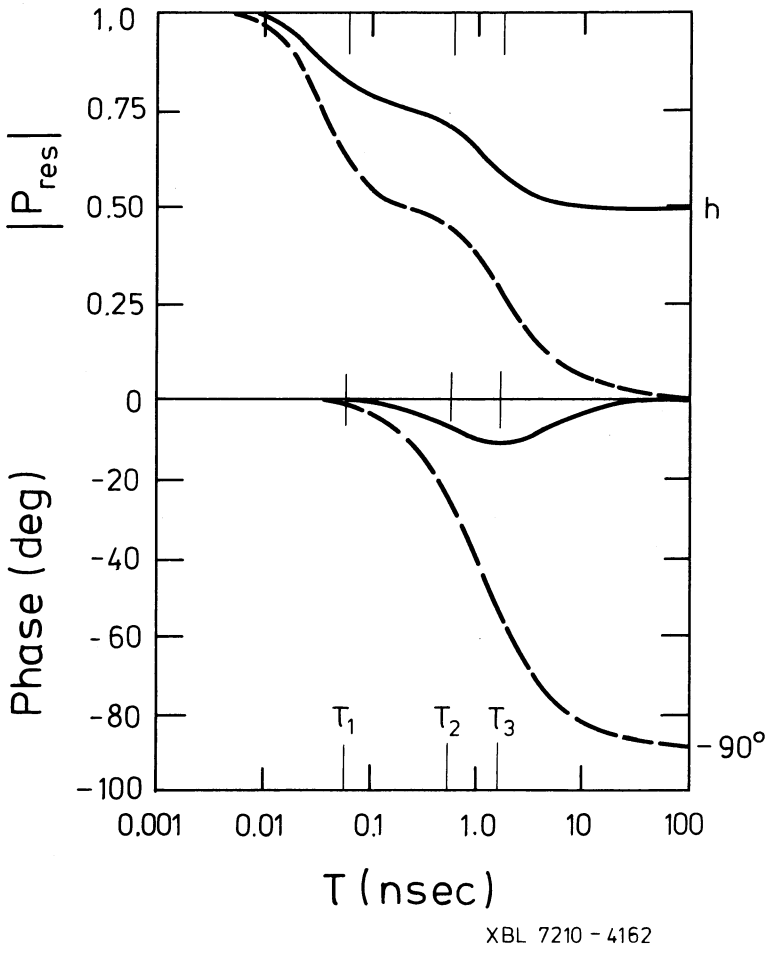

XBL 7210 - 4162

Fig. 25

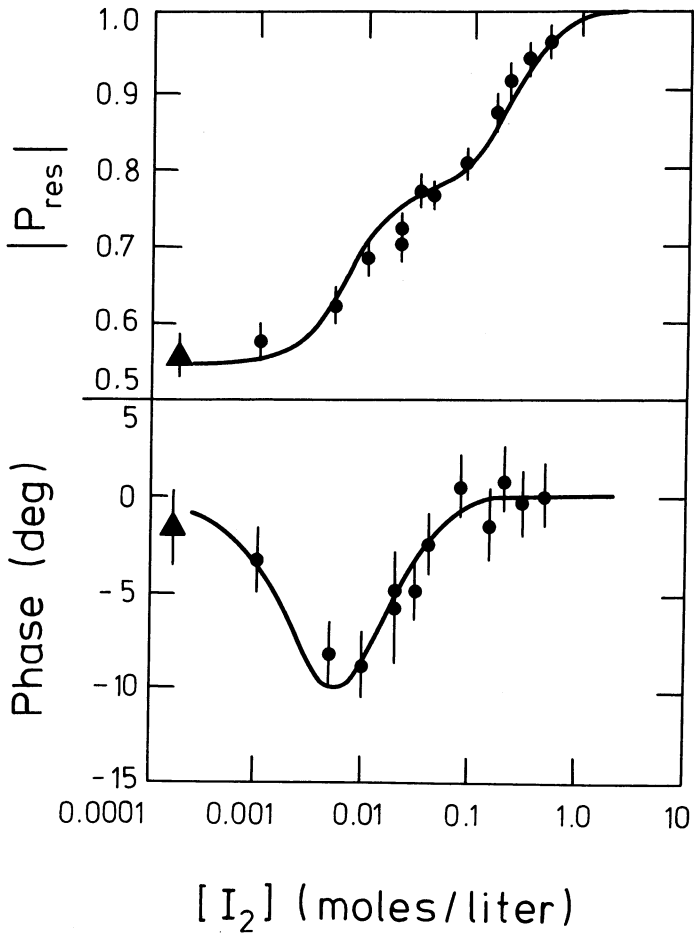

XBL 734 - 2763

Fig. 26

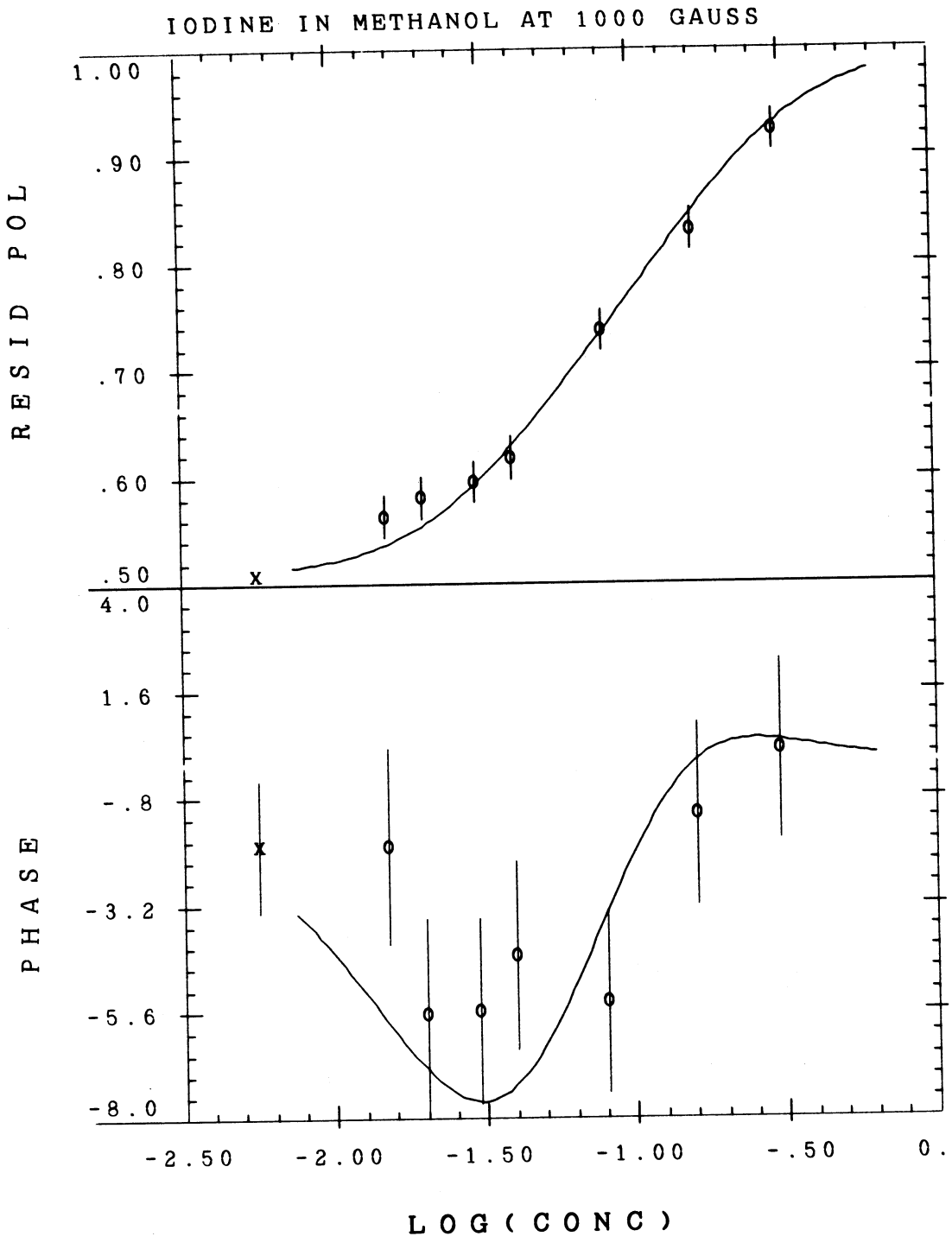

XBL 726-1122

Fig. 27

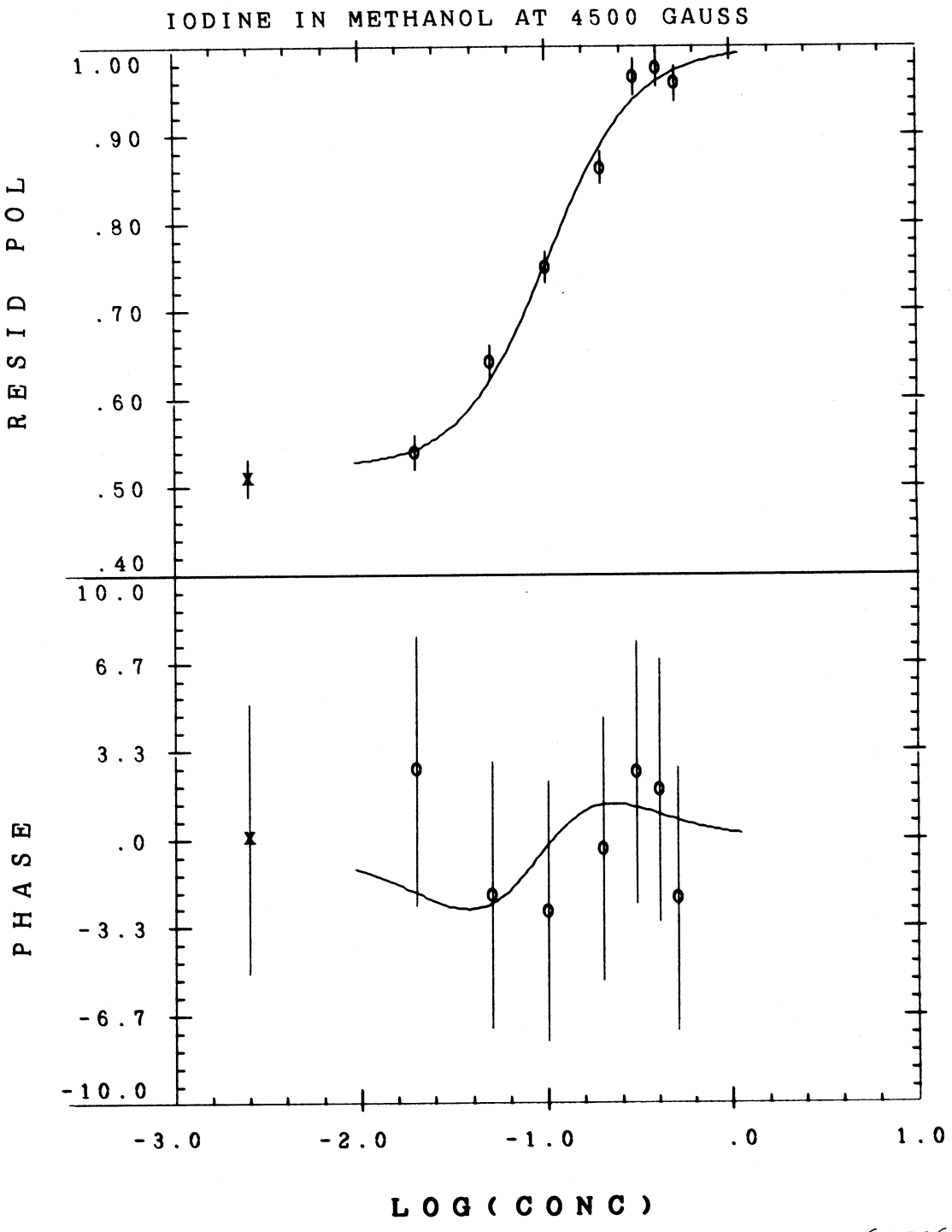

XBL 726-1106

Fig. 28

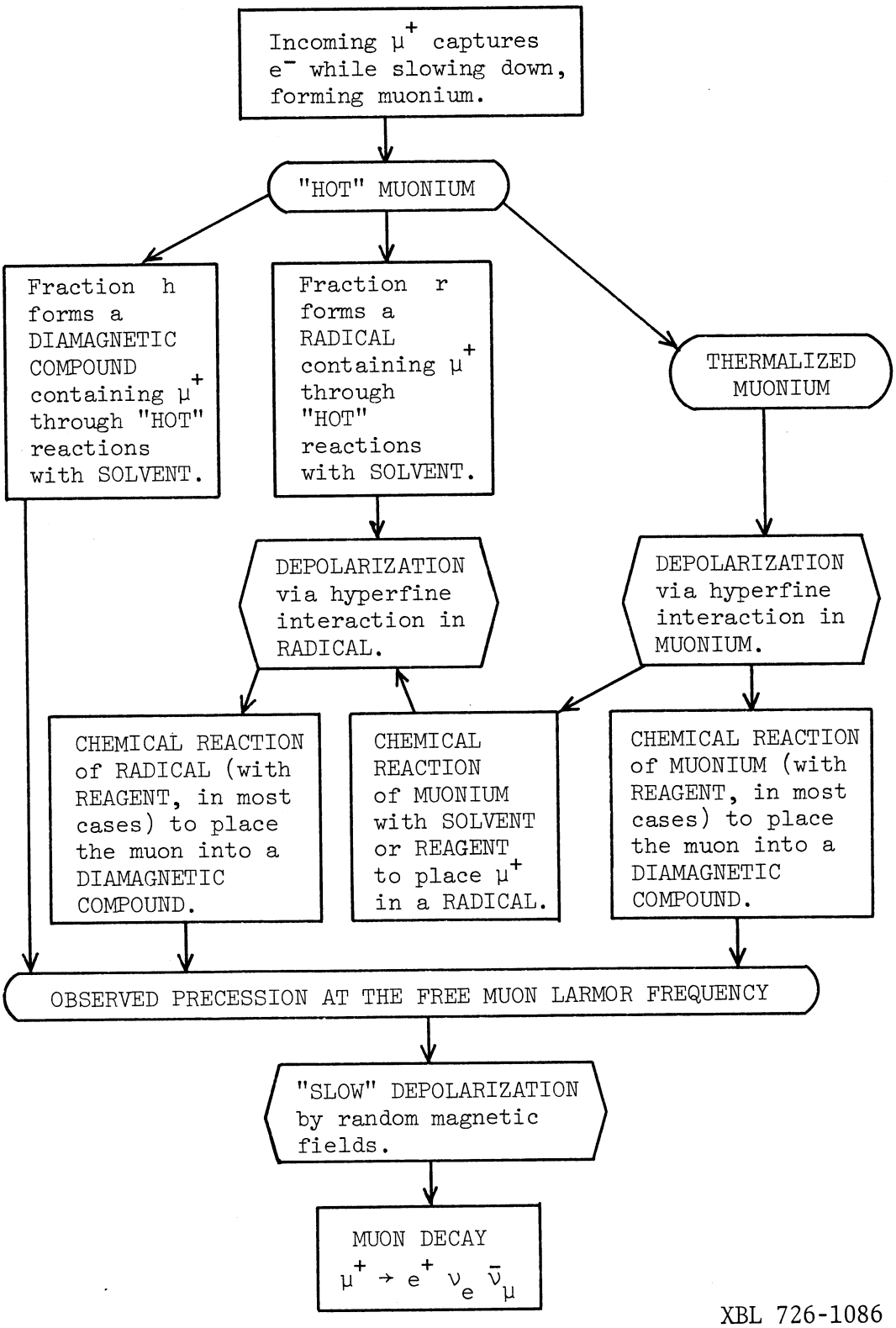

XBL 726-1086

Fig. 29

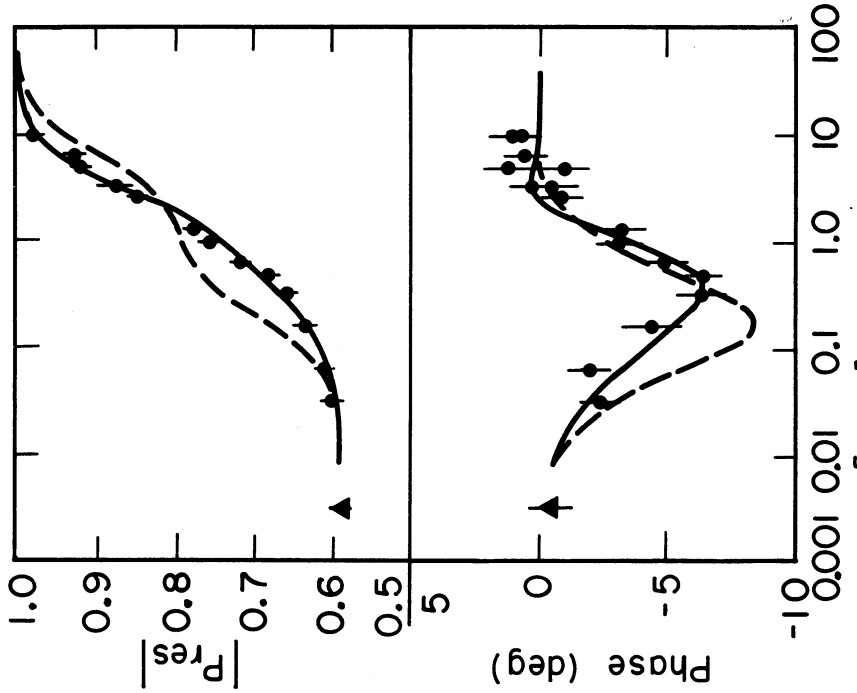

XBL 7210-4166

Fig. 31

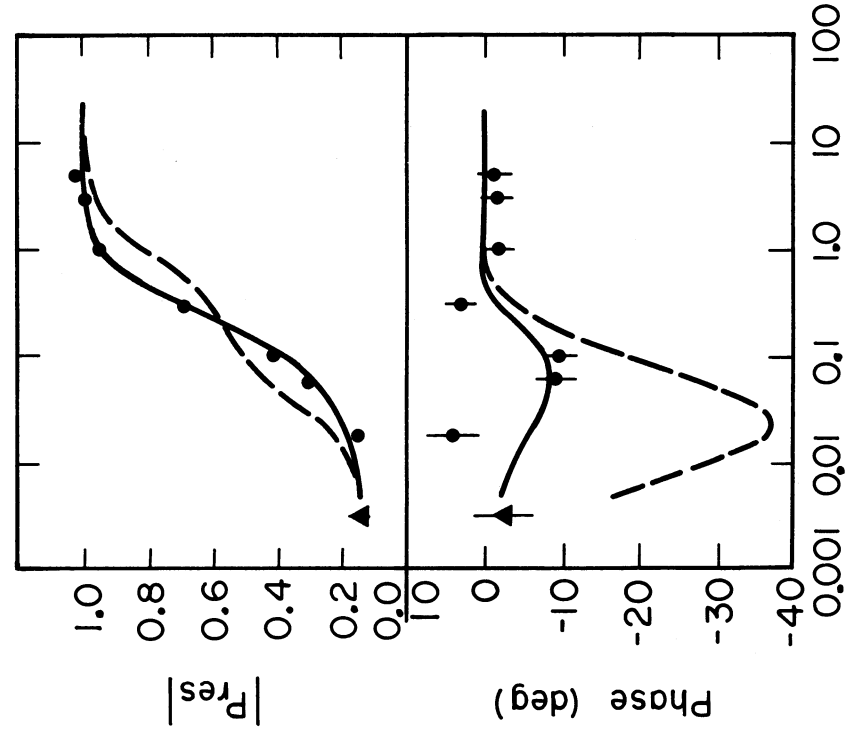

XBL 7210-4167

Fig. 30

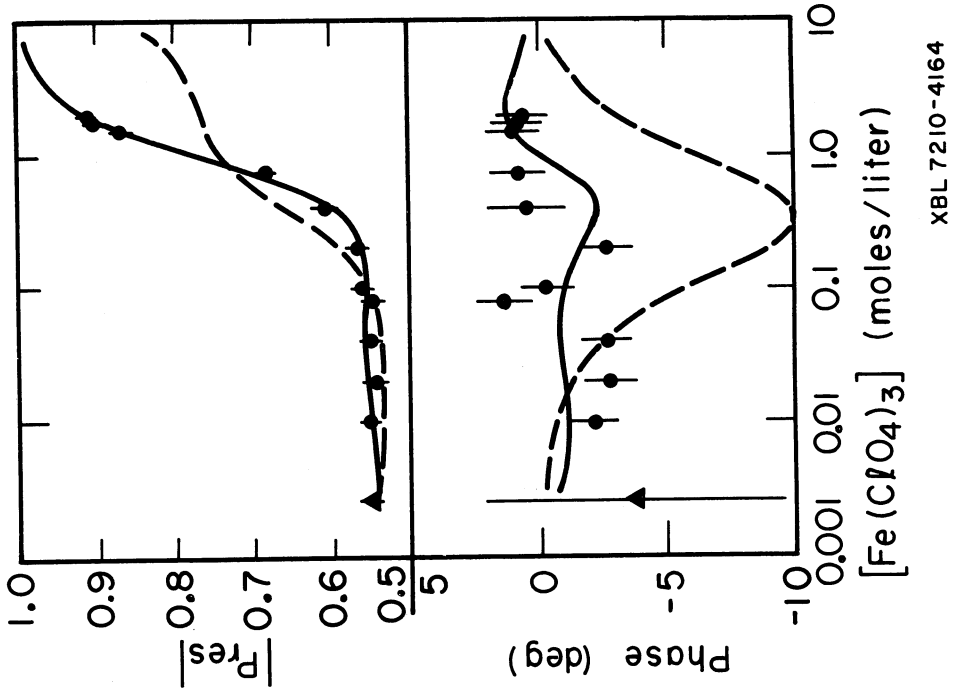

XBL 7210-4164

Fig. 33

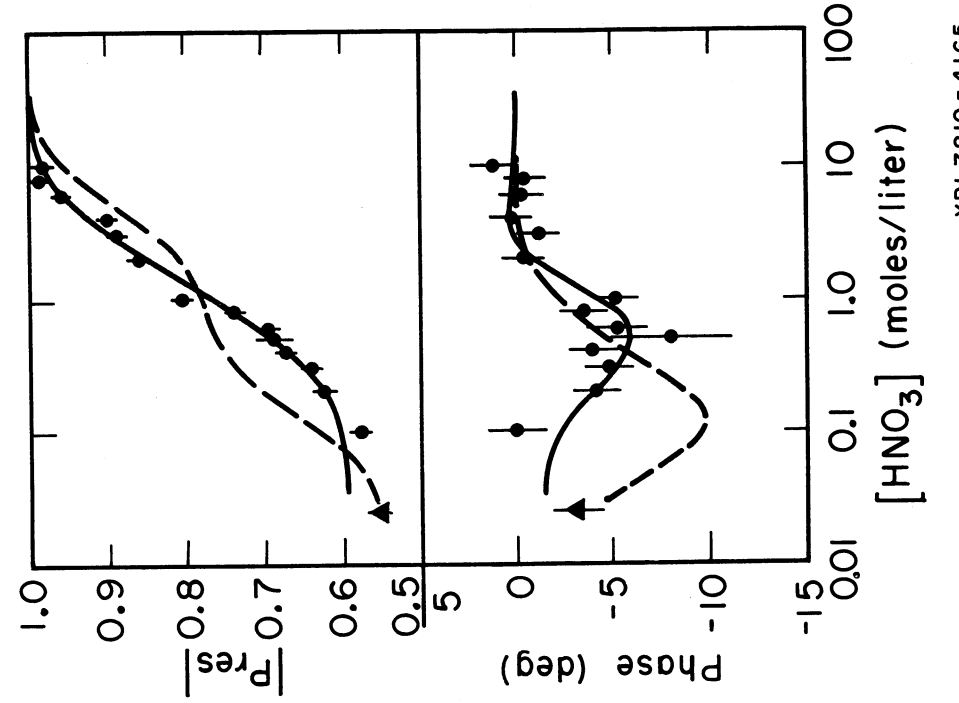

XBL7210-4165

Fig. 32

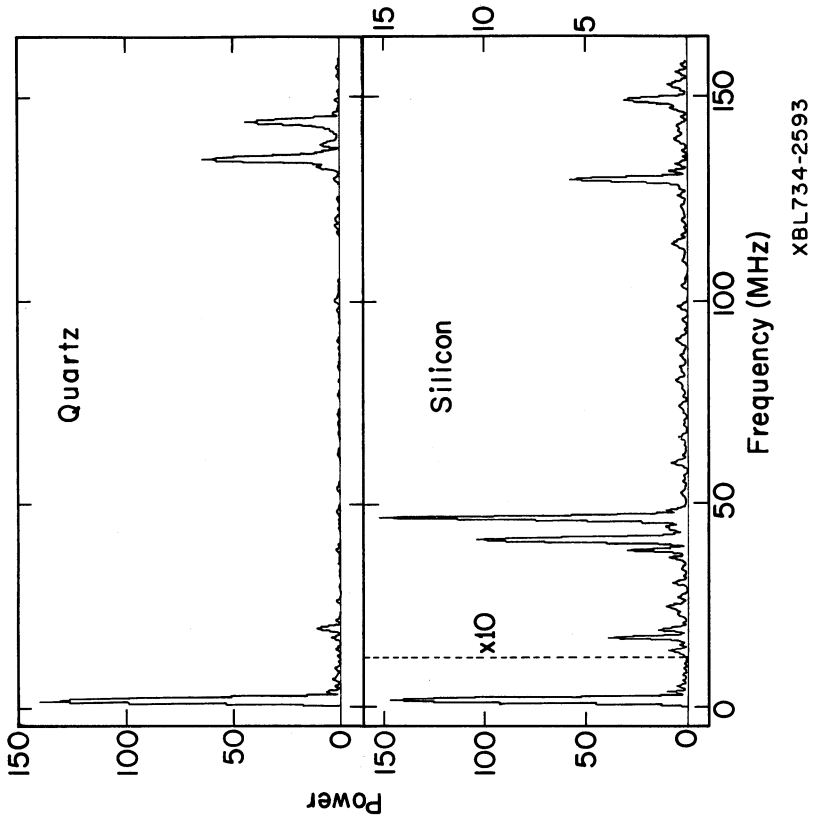
Quartz
Silicon
x10
Power
Frequency (MHz)
XBL734-2593

Fig. 35

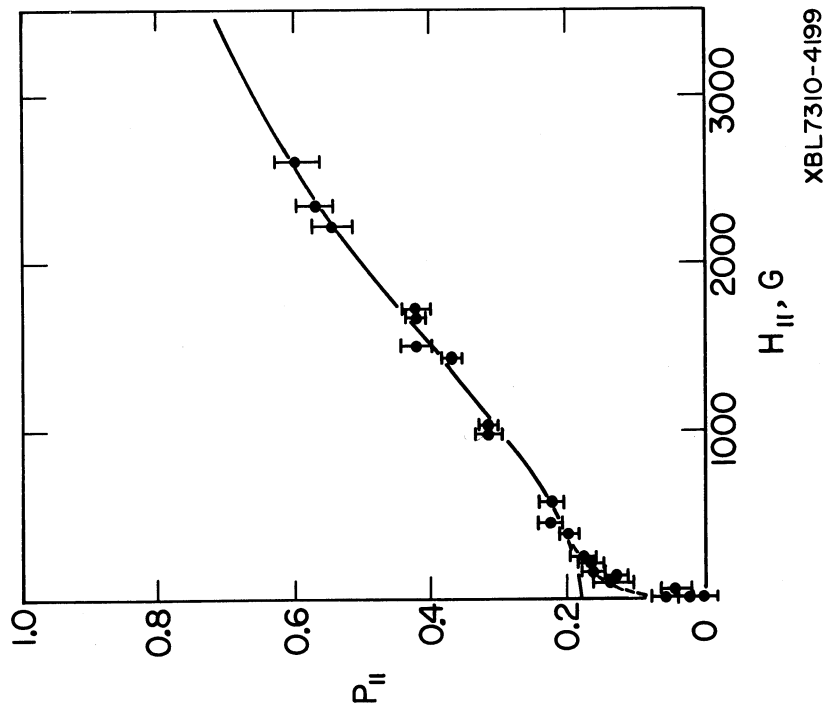
P_{II}
H_{II}, G
XBL7310-4199

Fig. 34

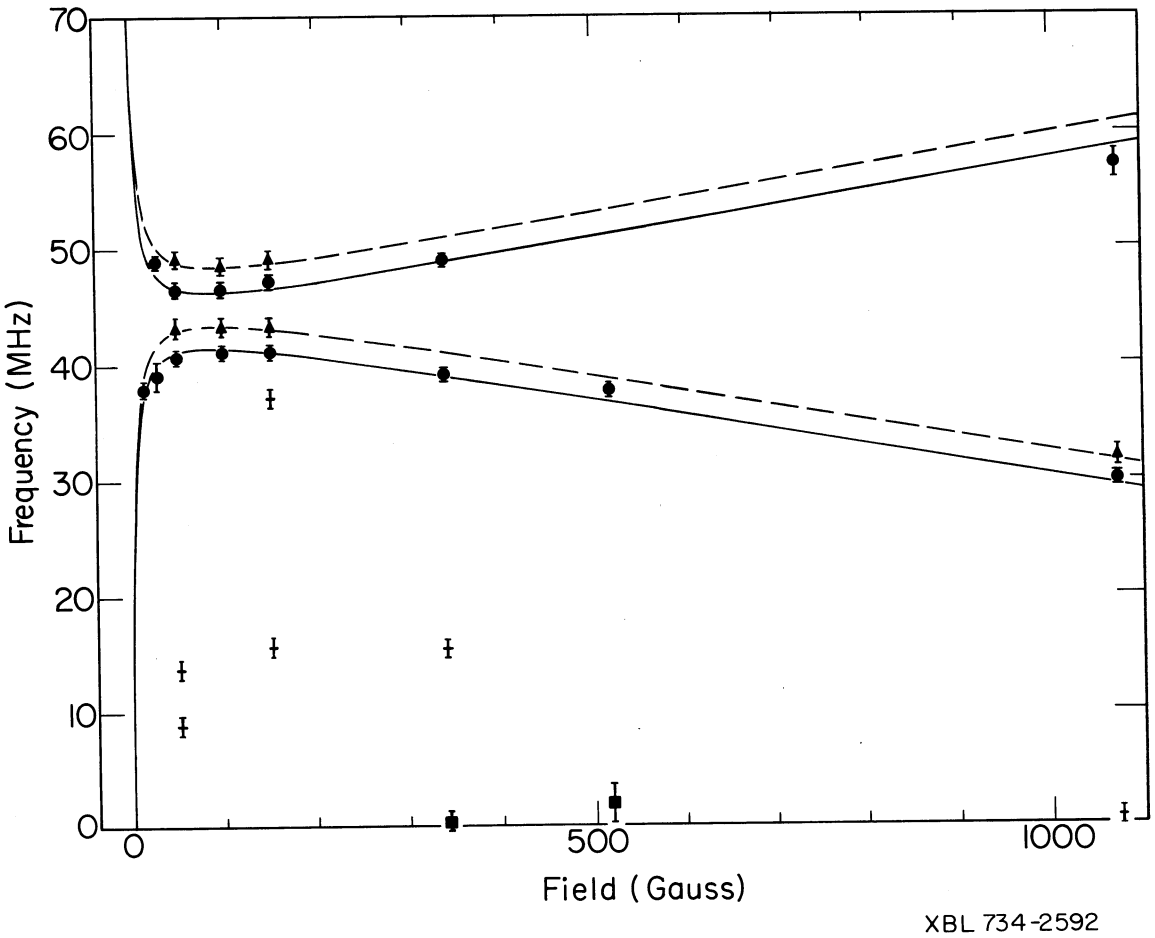
70
60
50
40
30
20
10
0
Frequency (MHz)
0
500
1000
Field (Gauss)
XBL 734-2592

Fig. 36

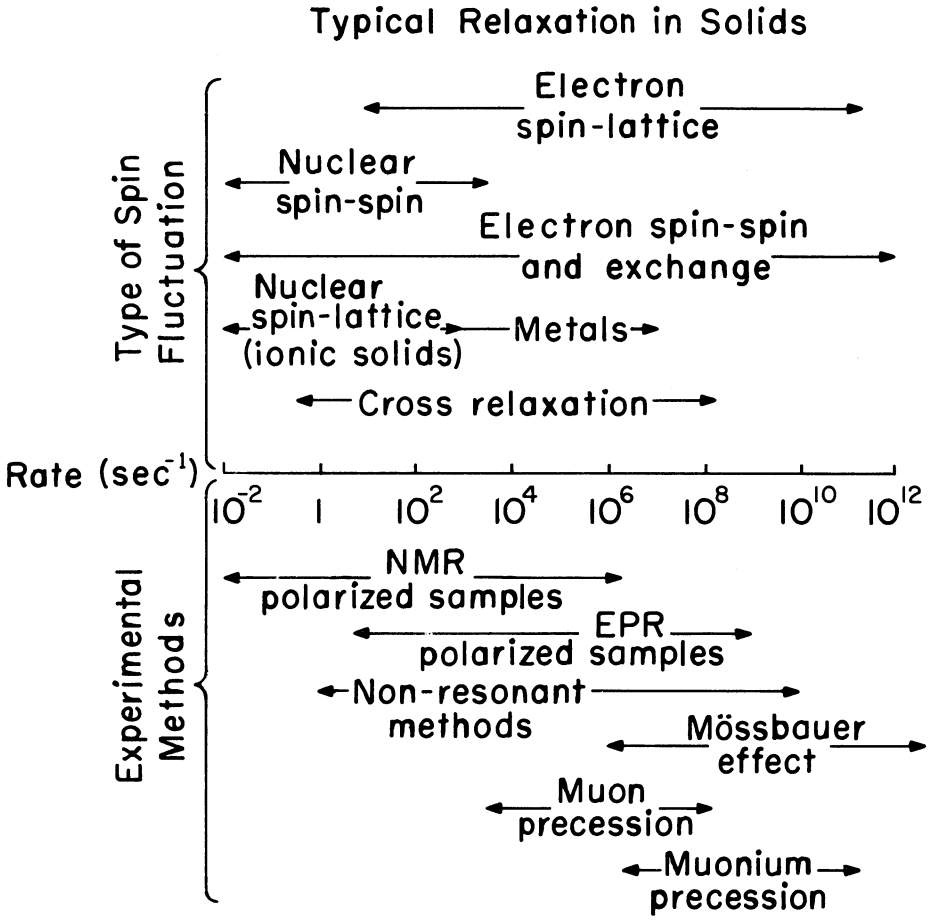
Typical Relaxation in Solids
Type of Spin Fluctuation
Electron spin-lattice
Nuclear spin-spin
Electron spin-spin and exchange
Nuclear spin-lattice (ionic solids)
Metals
Cross relaxation
Rate (sec^{-1})
10^{-2} 1 10^{2} 10^{4} 10^{6} 10^{8} 10^{10} 10^{12}
Experimental Methods
NMR polarized samples
EPR polarized samples
Non-resonant methods
Mössbauer effect
Muon precession
Muonium precession
XBL7310-4241

Fig. 37

PRECESSION EXPERIMENTS OF POSITIVE MUONS IN FERROMAGNETIC MATERIALS

W.J. Kossler
College of William and Mary, Williamsburg, Virginia, USA

A review of μ^+ precession experiments on ferromagnetic samples is made. In these experiments, the temperature and applied magnetic field were varied and the precession frequency, initial polarization, and depolarization rate were measured. Possible interpretations of the results are presented. Likely sources of the field felt at the muon are the contact hyperfine field from conduction electrons which shield the μ^+ and the dipole field sum for the case of Fe. Depolarization may in part be due to field inhomogeneities, defects, and single magnon interactions. Initial polarization may reflect domain alignment. Future experiments are discussed. A long list reviewed.

I. INTRODUCTION

That the muon can be a fundamentally important tool for condensed matter physics has recently begun to be recognized.[1] The work of Schenck, Crowe, and collaborators[2,3] has shown that the implanted positive muon behaves very much like a hydrogen nucleus, and that muon studies can provide information about lattice structure and chemical reactions. The behavior of hydrogen in metals is of intrinsic interest as one of the simplest alloy problems.[4] It is also a problem of considerable technological importance.[5] The behavior of the hydrogen like positive muons in ferromagnetic metals is of additional interest because of the interactions with the magnetic medium. Implanted muons cause minimal radiation damage, occur in infinitesimal concentration, leave no residual contamination, have no nuclear or quadrupole interactions, and do not possess a complicated ion core. Consequently the use of implanted muons can not only yield fundamental solid state information, but also contribute to the understanding of radioactive ion implantation[6], particularly in the case of ferromagnetic targets.[7]

The positive muon is also an excellent probe from the standpoint of experimental simplicity. High count rates are available with polarization approaching 100%. The muon mean life (2.2 μ sec) is long enough for easy timing and short enough for high count rates. The decay positrons are easily detected and the angular distributions of these positrons is highly anisotropic. The muon's magnetic moment has been determined to a few parts per million allowing high precision measurement of b_μ.

The experiments[8] on Ni and Fe by the author and collaborators have demonstrated the feasibility of the study of ferromagnetic material with μ^+.

It may well be wondered, if muons are indeed such marvelous probes of matter, why have these experiments not been done long ago. I think the answer to this question is that the early interest was in the properties of the muon itself or in muonium. In both of these, interesting solid state effects would be considered a nuisance.

II. A. REVIEW OF AN EXPERIMENT IN WHICH μ^+ WAS USED AS A PROBE OF FERROMAGNETIC METALS

Neil Heiman, M.L.G. Foy, C.E. Stronach and myself implanted polarized positive muons in nickel and iron. The magnetic fields at the sites of the muons (b_μ) were measured by observing the precession of the angular distribution of the decay positrons. The same data yielded the initial polarization (P) of the stopped muons and the time constant (τ) of the slow depolarization. Data were collected as function of temperature, from room temperature to 700^{o}K so that we observed the shift from the ferromagnetic to the paramagnetic state in nickel. This experiment demonstrated for the first time that the precession of muons stopped in ferromagnetic material can be observed and determined what the magnitude and direction of the internal fields are.

Some details of the experimental arrangement have been presented in a letter.[8] For here let it be noted that the magnetic field was transverse and positron detectors were at 0^o and 90^o with respect to the incident μ beam

direction. A time to amplitude converter followed by a multichannel analyzer was used to digitize the time between a μ stop and a decay positron.

Fig. 1 provides examples of data for paramagnetic nickel (at 670°K) and ferromagnetic nickel (at 551°K). Each set of data is the result of approximately 8 hours of counting. Note that the time scales differ by about a factor of 10. The data were fitted to the function:[1,2,6]

$$N(t) = N_c \exp(-\lambda t)[1 + aP\exp(-t/\tau)\cos(\omega t + \Phi)] + Bgnd.$$

N_o is for normalization. The term exp (-λt) accounts for the muon decay into a positron with a 2.2 μsec mean life. P is the initial polarization of the stopped muons and a is the positron anisotropy. τ is the time constant characterizing the relaxation of the transverse polarization of the precessing muons. The angular precession frequency $\omega = 2\mu_\mu b_\mu/h$, where μ_μ is the magnetic moment of the muon, provides direct measurement of the magnetic field at the muon site b_μ. ϕ is the initial phase angle and Bgnd is the background.

The solid lines in Fig. 1 are the fitted function.

II. B. RESULTS: PARAMAGNETIC NICKEL:

In this region $b_\mu \approx H_{external}$, the externally applied field, approximately 50G. The paramagnetic Knight shift was small, and significant variation of b_μ with temperature was not detected. The initial polarization P was equal to 0.8 P_c where P_c was the initial polarization observed in a carbon target of similar dimensions. Muons stopped in carbon re-

tain virtually 100% of their polarization.[9] Therefore carbon is useful for calibration. The depolarization time constant τ was 4 μsec. The parameters b_μ, P, and τ did not vary significantly over the temperature range: 630°K to 705°K, (T_c 630°K). Paramagnetic nickel thus behaves as a normal metal in that little or no muonium appears to have formed. Muonium formation would have resulted in reduced polarization and the appearance of frequency components about 100 times higher than the frequency observed. Our resolution was sufficient to detect such high frequency components, and none were present.

Ferromagnetic nickel results: In this region we were able to fit b_μ to a Brillouin function, see Fig. 2, with a saturation field of 1550 G. The circular data points were taken with a current of 1.5A in the electromagnet. This corresponded to a field in the small gap between the magnet and target of 1100 G at room temperature. Increasing the field to 2200 G in the gap or lowering the field to 500 G or even to zero had little effect on b_μ. In the runs with nickel below 385°K and in an external field of about 1100 G, we were not able to detect the precession of the angular distribution. On increasing the magnetic field in the gap to approximately 2200 G, we were able to observe the precession, (the square data point in Fig. 2). The internal field is in the same direction as the external field. This was determined by noting the relative phase of the data from the 4 and 5 detectors and also by noting that the initial phase for each detector was maintained during the transition from paramagnetic to ferromagnetic behavior.

Fig. 3 shows the behavior of P and τ. P/P_c increases from about 20% at room temperature to near 40% as T_c is approached.

τ was on the order of 0.25 μsec and increased slightly with temperature and to drop sharply as T_c was approached. The dashed line in Fig. 3 is intended only to illustrate this trend. Varying b_μ by changing temperature or varying the external field seemed to have little effect on τ, implying that the depolarization was not arising only from field inhomogeneity.

Ferromagnetic iron results: In the temperature range from room temperature to 675°K, b_μ decreased from approximately 4100 G to 3700 G. P/P_c was about 10% and τ was on the order of 0.5 μsec. It is interesting that the ratio of the field in Fe to that in Ni is not much different from the ratio of the magnetizations.

III. INTERPRETATION OF THE RESULTS

In these experiments we obtain the initial polarization: P, the internal field felt by the μ^+: b_μ, and the depolarization time constant: τ. It is, of course, possible that the data could manifest more complicated behavior than that characterizeable by these three constants but for the present we will ignore such complications.

The phenomena which correspond to each of these three are sufficiently distinct that they will be treated separately.

A. The Initial Polarization: P

The reduced initial polarization in our first run we believe is due to domain alignment. A muon will not precess if it stops in a domain where the magnetization or internal field is in the same direction as the polarization. The amplitude of the precession signal thus depends

upon the degree to which the domains are aligned transverse to the muon polarization. The solid line in Fig. 3 is a measure of this domain alignment extracted by dividing the measured permeability by the magnetization and normalizing to P. We were unable to saturate the sample, in this first run, however, in a subsequent experiment with approximately 2000 G external field, which should polarize the sample, an initial polarization was obtained which essentially equalled that from a copper sample. This tends to confirm this domain alignment explanation.

B. The magnetic field at the muon site: b_μ.

In any attempt to obtain explanation of b_μ the question of what the μ^+ site is arises. There is evidence that hydrogen atoms are implanted in the octahedral or body centered site in nickel.[10] It is reasonable to assume that the muon stops in the same site although it may not be as well localized due to its smaller mass. There also does exist a smaller site of tetragonal symmetry. For iron which is bcc one would expect the μ^+ to dominantly fill the available face sites.

The contribution to b_μ may be written:[11]

$$b_\mu = H_{appl} - DM + \frac{4\pi}{3} M + \sum H_{dipol}\,(\text{over a sphere}) + H_{Hyperfine}$$

H applied is the magnetic field produced by the external magnet. DM, the demagnetization arises from the macroscopic magnetization of the actual sample geometry. For our first experiment this was zero since the sample was part of a magnetic circuit. For a sphere the result would be $-DM = \frac{4\pi M}{3}$. For an oblate ellipsoid 3" Diameter 1/2" long DM $\frac{4\pi M}{10}$.

Σ H dipole is a sum over the contribution from the dipoles on the transition metal ions. For Ni this is zero, presuming the μ^+ is in the body centered site. For Fe the natural μ^+ sites would be the face center. The field would be +18.8kG or -9.4kG when the nearest neighbor are along or perpendicular to the magnetization respectively.[12]

In iron the hopping time is about $\leq 10^{-9}$ seconds at room temperature much less than the precession time 10^{-7} seconds hence one should average the fields weighted by the relative number if sites. This average: 4 x -9.4 kG + 2 x 18.8 = 0.

$H_{hyperfine}$ the field produced by electrons on the muon, may be written[13] $H_{hyperfine} = H_{cp} + H_v$. In this expression H_{cp} is due to the polarization of the inner core electron on the μ^+ by the magnetic electrons. A μ^+ ion has no core hence $H_{cp} = 0$. H_{cep} is due to the polarization of the conduction electrons by the moment of the transition metal atoms. H_v is a positive field due to the valence ns-like electrons which remain near the solute muon shielding the excess charge. These are polarized by an amount proporitional to the volume misfit of the solute muon. This term is thought to be small for the muon.

Keeping only those contributions which should be strong we have: $b_\mu = H_{applied} - DM + 4\pi M/3 + H_{cep}$. For our first experiment H applied and DM are small leaving only $4\pi M/3$ and H_{cep}.

Mary Beth Stearns[12] has used our results to obtain an extension of a "conduction electron polarization curve". The H_{cep} is thought to be "reasonable".

Another approach to the hyperfine fields has been that of J. Friedel and E. Daniel[14] who treat the shielding charge explicitly and then obtain $H_{HF} = \frac{8\pi}{3} \beta <|\chi(0)|^2>_f \delta\rho$.

When β is the Bohr magnetion $<|\chi(0)^2|>_f$ is the average density of conduction electrons at the μ^+ and $\delta\rho$ is the difference of spin density oscillations from the host atoms.

C. The depolarization time constant: τ.

Let us list and then discuss possible mechanisms which might depolarize (T_1) or dephase (T_2) the μ^+.

1. Inhomogeneities
   a. $H_{applied}$
   b. Internal
2. Creation or annihilation of single magnons
3. Magnon
4. Diffusion to impurities and/or defects
5. Paramagnetic ions, giant moments
6. Nuclear Moments
7. Muonium formation
8. Electron Scattering
9. Magnetization fluctuations

Not all of these occur at the same time and there exist dramatic differences in time scales.

1. Field Inhomogeneities

External fields and hence precession frequencies may vary over the target with some distribution $f(\omega)$ so that the detection rate with exponential lifetime factored out would be $\int(1 + P \cos \omega T)\, f(\omega)\, d\omega$.

For a frequency distribution which is Lorentzian $f(\omega) = \frac{A}{\sqrt{\pi}} \frac{1}{1/\tau^2 + (\omega - \omega_0)^2}$ the net transverse polarization falls as $\exp(-T/\tau)$.[15] Note that $1/\tau$ is the half width at half maximum. A fwhm field variation of 1 Gauss over the sample corresponds to about 5 μsec for τ. For most of our experiments external field inhomogeneities are probably smaller than this.

It is possible to scale the results from the gross line widths for NMR to obtain a comparison for μ^+ dephasing.

These line widths are sample dependant so one must be cautious in these comparisons.

Nucleus	Host	$\Delta\nu$[a]	$\rightarrow \tau = \frac{1}{\pi\Delta\nu}$	(G_{Fe}/G_μ)	$\rightarrow \tau_\mu$
Fe^{57}	Fe	30kHz	$10_\mu S$	.09/10	$1/10_\mu S$
Ni^{61}	Ni	150kHz	$2_\mu S$	15/10	$1/10_\mu S$

a. M. Weger, E.L. Hahn, and A.M. Portis, J. Appl. Phys. 32 1245 (1961). These relaxation times are shorter than observed for the μ^+ so one might argue that the samples used in μ^+ experiment, being larger might have smaller inhomogeneity broadening, or that since the NMR experiments are done in domain walls while the μ^+ is in the bulk, one should increase these depolarization times by the ratio of enchancement factors: domain wall/Bulk:

$$(5500/690)_{Fe} \longrightarrow \tau_\mu^{Fe} = 0.8\,\mu S$$

$$(4400/540)_{Ni} \longrightarrow \tau_\mu^{Ni} = 0.8\,\mu S$$

Now that we have a mechanism which can explain or at least produce relaxation rates of the right order of magnitudes it is fair to then ask why go on and consider other possibilities. A partial answer lies in the possibility that they may also contribute and be seperable from the inhomogneity contributions. The inhomogeneity field should be proportional to the sample contribution to b_μ.

2. Creation or Destruction of Single Magnons: τ_{sm}

This process produces a T type relaxation with

$$\frac{1}{\tau_{sm}} = \frac{2\pi}{\hbar} |K \langle I_f^z n_K \pm 1 | A \vec{I} \cdot \vec{S} | I_i^z n_K \rangle|^2 \rho(\varepsilon_K = \hbar\omega_0)$$

Where I^z is the z component of the μ spin n_k is the number of magnons present of wave number $\vec{k}$, $\rho(\varepsilon_k)$ is the spectral density of magnon modes of energy ε_k and $\hbar\omega$ is the transition energy associated with a muon spin flip). One would expect by scaling:

$$\tau_{sm}^{\mu} = \tau_{sm}^{Fe} (A_{Fe}/A_\mu)^2 (\varepsilon_{Dw}/\varepsilon_{Bulk}) \rho(Fe)/\rho(\mu)$$

$$= 140\mu s \, (0.5 \cdot 10^8/4.4 \cdot 10^9)^2 (5500/690)^2 \cdot 1$$

$$\tau_{sm}^{\mu}(Fe) = 1.1\,\mu s$$

$$\tau_{sm}^{\mu}(Ni) = 100\mu s \, (0.4 \cdot 10^8/4.4 \cdot 10^9)^2 (4000/5400)^2 \cdot 1$$

$$\tau_{sm}^{\mu}(Ni) = 0.45\,\mu s$$

From this result it seems at least plausible that single magnon interacting might play some role in the depolarization of the muons in our samples.

It would be expected that this depolarization mechanism would be such that $T \cdot \tau_{sm}$ = constant where T is the temperature.

3. Magnons

In principle multiple magnon processes including scattering and magnon phonon interaction should also take part expecially at elevated temperatures. Description of these processes for insulators[17] seems to indicate much longer times than would be observable in times on the order of the μ lifetime.

4. Diffusion to Impurities or Defects

The muon at room temperature and above should diffuse rapidly through material. The hopping time for hydrogen in Fe is about 10^{-9}sec[6], and somewhat longer in Ni. Muons due to their lighter mass should hop on the order of ($m_p/m_\mu = 10$) times faster. Thus in a lifetime of a muon 10^4 sites are sampled each with at least four atoms not previously nearest neighbors.

Trapping centers for hydrogen and hence μ^+ with relative abundance of one part per million could have a noticable effect on the local fields.

Raising the temperatures should increase the number of sites, while lowering it should be able to prevent diffusion altogether, the hopping rate is exponentially dependant on the temperature relative to the excitation energy. Further discussion of diffusion will be given under future experiments.

5. Paramagnetic Ions

Paramagnetic ions in solution cause depolarization of the μ^+ as has been demonstrated by Schenck, Crowe et al.[2,3] This sort of depolarization mechanism is appropriate for the paramagnetic region of our samples. An estimate for such time might be obtained by extrapolating T_2 curves for Mn^{2+} in solution up to solid densities of about 10^{23}. If no correction is applied for changes in correlation times this yields a $\tau_{pi} \approx 10^{-7}$sec. However, at these concentrations electron exchange should enter to reduce the correlation times. The fastest correlation time given for the solution is on the order of 10^{-11}sec. An estimate for the correlations with exchange can be obtained by considering $kTc=h/\tau_c$. This yields $\tau_c \approx 10^{-13}$sec and hence a 10μS T_2.

6. Nuclear Moments

The nuclear moments of a sample can interact with the μ^+. Because the correlation times are much longer the effect of the nuclei is greater than one would expect from the ratio of nuclear to electronic moments. I.I. Gurevich et al.(18) have studied dipole interaction and diffusion of μ^+ mesons is copper. They find depolarization rates which reach 2×10^5/sec for cold samples and which go to nearly zero at room temperature and above where one could speak of diffusion narrowing. Neither Ni nor Fe have abundant isotopes with nuclear moments.

7. Muonium Formation

A large literature exists on this subject.[19] In metals where the electron spin relaxes rapidly relation to the hyperfine interval Nosov and Yakovleva[20] give

$$\frac{1}{T} = \frac{\omega_0^2}{4\alpha}$$

where $\frac{\omega_o}{2\pi} = \Delta\nu = 4.4 \times 10^9$ H the muon hyperfine interval and α^{-1} is the correlation time for the electron spins, which is on the order of $(kT_c)^{-1}$ or 10^{-13}sec. thus

$$\frac{1}{T} = 1.5 \cdot 10^{7}\, s^{-1}$$

$T_{relax} \approx 10^{-7}$ sec. which would imply considerable depolarization in metals. Yakovleva[21] has made the remark that since $T_{relax} \sim r.^6$ where r is the radius of the system a small change in r would produce a large T_{relax} as observed for ordinary metals.

8. Electron scattering from μ^+

In this process the electrons of the metal scatters from the μ^+ to cause its spin to flip. An estimate for the rate is given by

$$\frac{1}{T_1} = \frac{64}{9}\pi^3\hbar^3\gamma_e\gamma_{\mu^+}\left|\langle|u_k(0)|^2\rangle\right|^2_{E_f} \cdot \rho^2(E_f)\,kT$$

this expression has many factors in common with the Knight shift

$$\frac{\Delta H}{H} = \frac{8\pi}{3}\langle|u_k(0)|^2\rangle\chi_e^s$$

which leads to the Korringa relation

$$T_1\left(\frac{\Delta H}{H}\right)^2 = \left[\frac{\chi_e^s}{\rho(E_f)}\right]\frac{1}{\pi kT}\frac{1}{\gamma_{\mu^+}^2\gamma_e^2\hbar^3} \qquad \chi_e^s \approx \frac{\gamma_e^2\hbar^2}{2}\rho(E_f)$$

$$\longrightarrow \quad T_1\left(\frac{\Delta H}{H}\right)^2 = -\frac{\hbar}{4\pi kT}\frac{\gamma_e^2}{\gamma_{\mu^+}^2}$$

Hutchinson et al.[22] report $\frac{\Delta H}{H} \approx 10^{-4}$ H for μ^+ in Cu. Using the Korringa relation this yields 8ms for the relaxation time. μ^+ should be clear that this process is not dominant. In general one expects

$$T_{relax} = \frac{10^{-8}}{T/T_{room\ Temp}\left(\frac{\Delta H}{H} = \text{Knight shift}\right)}$$

9. Magnetization Fluctuations

Near the Curie Temperature one expects time fluctuations of local fields. The detailed time dependance of the polarization should be able to generate several moments in the time correlation spectrum of the field fluctuations.

If one assumes an extra field H producing an extra precession rate ω, on for a time τ and then switched randomly to $\pm H$ for another interval τ, one obtains a relaxation rate

$$\frac{1}{T} = \frac{(\omega\tau)^2}{\tau}$$

Extensive theoretical discussion of time dependent magnetic fields exists.[23]

IV. FUTURE EXPERIMENTS

I list below a series of experiments which may be interesting: this list is not meant to be exhaustive except in the sense that to do all of them would be exhausting. For each of these let me make a few brief comments on why they might be interesting:

1. The ferromagnetic elements

The experiments which we have done so far on Ni and Fe leave many open questions. For instance what effects are sample dependent? How do the parameters observed vary as one goes through the Curie point? As diffusion is inhibited by low temperature does one see more than one frequency of precession? The rare earths have helical ferromagnetic structure; what does that do to the observed fields and depolarization roles can one see precession in all of these elements? (We have seen precession in Gd but not in Dy in a recent run). Comparison may be most interesting.

2. Ferromagnetic Insulators

Here one is likely having muonium formation, hence in some sense this is outside the realm of this paper. If the internal fields are no higher than in Ni then it still should be possible to see precession. One should look for cases where one would expect low internal fields.

3. Ferromagnetic Alloys

In a weak sense these have been investigated since both Ni and Fe certainly had some impurities, however, what is meant here are random alloys with a sizeable $\geq$ 10% admixture. It may be that the μ^+ will feel some average field. Depolarization rates should be sensitive to internal field variations.

4. Paladium and several other metals have the capability of soaking up an incredible amount of hydrogens. Paladium itself is only paramagnetic. If one fills the paladium placing with 0.8 H for each Pd atom. The system is superconducting at $8^{o}K$. It would be interesting to study the behavior of this system with the μ^+

as a function of temperature, H concentration and applied field.

5. Paladium with a slight admixture of Ni (2% becomes ferromagnetic). Again it would be interesting to study this ferromagnetic system again as a function of H concentration, temperature, and applied field.

6. Ordinary metals. The depolarization mechanisms in these materials cannot be field inhomogeneities, presuming the external field magnet is of sufficient quality. One then has electron, phonon and nuclear interactions.

7. Alloys with local moments and enhanced paramagnets; when material which is nearly ferromagnetic such as Pd, or Rh has Fe or Ni added often larger local moments build around these admixed ions. These giant moments should produce fields at an implanted μ^+ for which the precession rate would be a measure and the depolarization rate a means of studying the internal field fluctuations.

8. Ferromagnetic and ordinary metals with varying defect concentration. In a ferromagnetic material defects should produce local magnetic field inhomogeneities which will in turn depolarize the μ^+. The sensitive of a μ^+ to defect concentration should be investigated. If a μ^+ is quite sensitive then practical applications of μ^+ precession may develop in studying hydrogen induced defects, embrittlement and corrosion.

Defects in non magnetic metals may allow muonium formation and hence enhanced depolarization. Again practical application on materials research might develop.

9. Oriented Ferromagnetic and Normal Metal Crystals

The field at the μ^+ may depend upon the orientation of the external field to the crystaline axes. M.B. Stearns for instance notes that in an Fe crystal, with the external field along an edge of the bcc lattice the top and botton focus of the acbc see a+18.8kG field from the dipoles, while the side face positions have -9.4kG.

Generally the field induced inside the sample should depend upon whether or not the applied field is along the easy magnetization axis of the crystal.

In non cubic lattices the field should depend upon external field - crystal lattice orientation.

Relaxation processes involving magnons may also depend upon crystaline axis.

Inhomogeneity depolarizations with crystal defects may depend upon the orientation of the defects with respect to the crystal or on the external field.

10. Strained Ferromagnetic Crystals

Strain certainly effects the susceptibility, χ, of ferromagnetic material. The saturation magnetization tends not to charge. The field we measure is thought to be proportional to the saturation magnetization and hence should be unaffected. Is this really so?

11. Depolarization Near the Curie Point

Fluctuation phenomena should dominate the depolarization process. Study t through the curie point should provide information on the fluctuation spectrum.

12. Insulators

Muonium is possibly formed. External rf fields can penetrate the sample and interact with the μ^+e system as a whole. The fields at the site of the muonium produce effects 200 times more strongly. The properties of the bound electron are solid state dependant.

13. Semiconductor

These are a special technologically interesting case of insulators.

14. Superconductors

It may be possible to observe trapped flux. Phenomena near the critical temperature might be interesting.

15. Metal Insulator Transitions

Certain material undergoes transition from a metal (conducting) state to an insulating state. The relative probability of muonium formation is affected by the availability of electrons, hence depolarization phenomena should occur near the transition.

16. Various material, e.g. La Ni_5 and La Co_5, pick up larger quantities of H. The properties of such systems might be studied with hydrogen like μ^+.

REFERENCES

1) Meeting on Muons in Solid, Schweizerisches Institut für Nuklearforschung (SIN, Zurich (1971))

2) A. Schenck and K.M. Crowe, Phys. Rev. Letters 26, 57 (1971)

3) J.H. Brewer, K.M. Crowe, R.F. Johnson, A. Schenck and R.W. Williams, Phys. Rev. Letters 27, 297 (1971)

4) J. Friedel, Berichte der Bunsen-Gesellschaft 76, 828 (1972)

5) Proceedings of the International Conference on Hydrogen in Metals, Julich, (1972)

6) Hyperfine Structure and Nuclear Radiations, E. Matthias and D.A. Shirley ed., North Holland Publishing Co., Amsterdam (1968), Chaps. VI and VIII

7) B. Herskind, R.B. Borchers, J.D. Bronson, D.E. Murnick, L. Grodzins, and R. Kalish, in Hyperfine Structure and Nuclear Radiation, E. Matthias and D.A. Shirley ed., North Holland Publishing Co., Amsterdam (1968), p. 735

8) M.L.G. Foy, Neil Heiman, W.J. Kossler, C.E. Stronach, Phys. Rev. Letters 30, 1064 (1973)

9) R.A. Swanson, Phys. Rev. 112, 580 (1958)

10) F. Brotzen, Private Communication

11) D.A. Shirley, S.S. Rosenblum and E. Matthias, Phys. Rev. 170, 363 (1968)

12) Mary Beth Stearns, submitted to Phys. Rev. Letters

13) Mary Beth Stearns, submitted to Phys. Rev. Letters

14) E. Daniel and J. Friedel, J. Chem. Solids 24, 1601 (1963)

15) A. Abragam, The Principles of Nuclear Magnetism, Oxford University Press, London (1961), p33

16) Mary Beth Stearns, Phys. Rev. 187, 648 (1969)

17) D. Beeman and P. Pincus Phys. Rev. 166, 359 (1968)

18) I.I. Gurevich, E.A. Meleshko, L.A. Muratova, B.A. Nikolsky, V.S. Roganov, V.I. Selivanov and B.V. Sokolov Phys. Letters 40A, 143 (1972)

19) References this extensive literature may best be found in the talks of Crowe, Schenck and Telegdi at this meeting

20) V.G. Nosov and I.V. Yakovleva, Nucl. Phys. 68, 609 (1965)

21) V.G. Yakovleva JETP 34, 70 (1958)

22) David P. Hutchinson, Jack Menes, G. Shapiro and A.M. Patlach, Phys. Rev. 131, 1351 (1963)

23) See; e.g., Charles P. Slichter Principles of Magnetic Resonance, Haprer and Row, Publishers Inc. New York, (1963) pp. 115-160

FIGURE CAPTIONS

Fig. 1 Data for paramagnetic nickel at about 670°K and ferromagnetic nickel at 551°K. Note that time scales differ by a factor of 10

Fig. 2 B_μ as a function of temperature. Circular data points were obtained with 1.5 amperes in the electromagnet. The square data point was taken at room temperature with 3.0 amperes.

Fig. 3 Initial polarization P and depolarization time constant τ as functions of temperature. The solid line is a measure of domain alignment: the measured sample permeability divided by B_μ. The dashed line is only to guide the eye

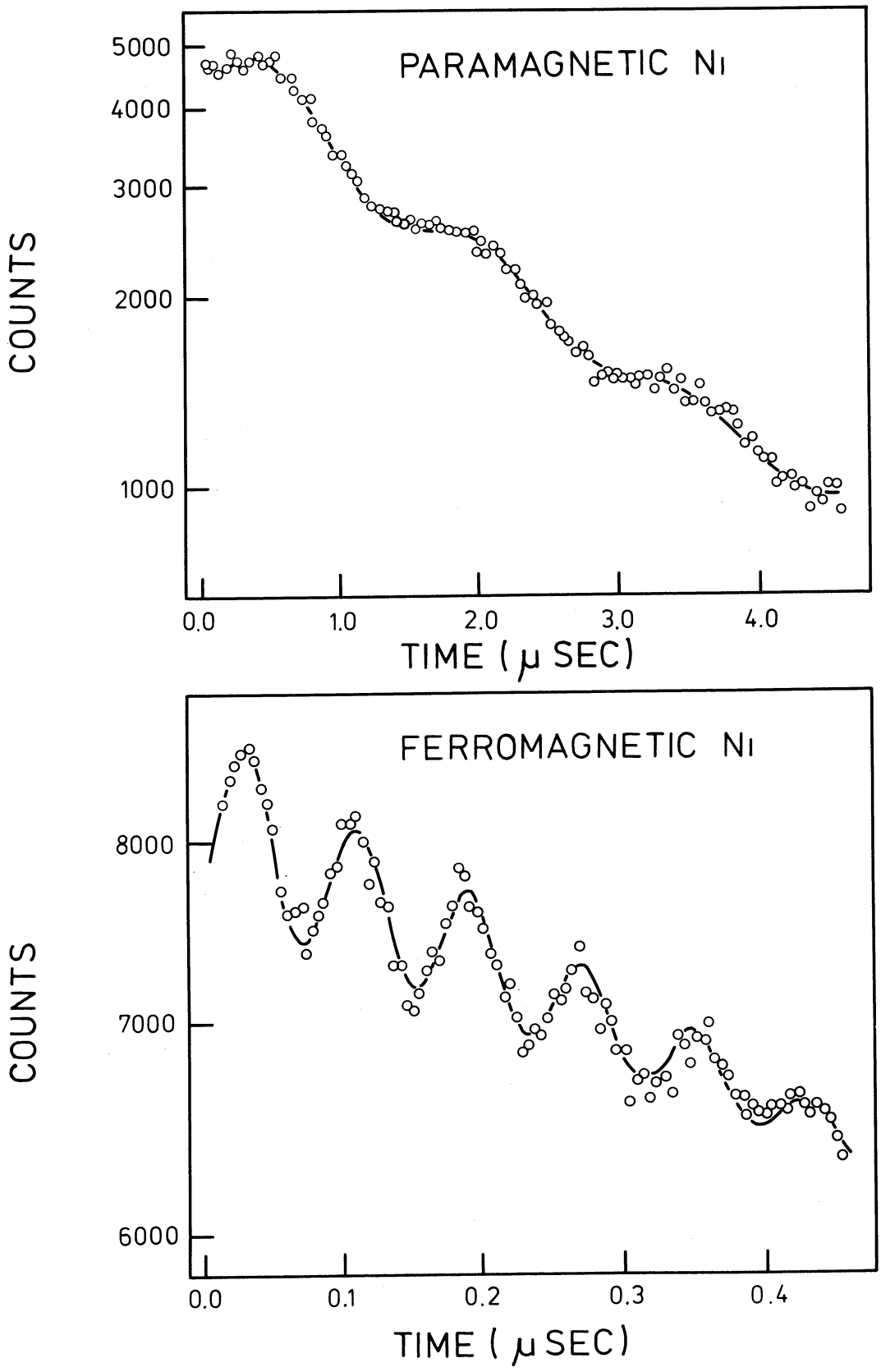
PARAMAGNETIC Ni
COUNTS
5000
4000
3000
2000
1000
0.0
1.0
2.0
3.0
4.0
TIME (μ SEC)
FERROMAGNETIC Ni
COUNTS
8000
7000
6000
0.0
0.1
0.2
0.3
0.4
TIME (μ SEC)

Fig. 1

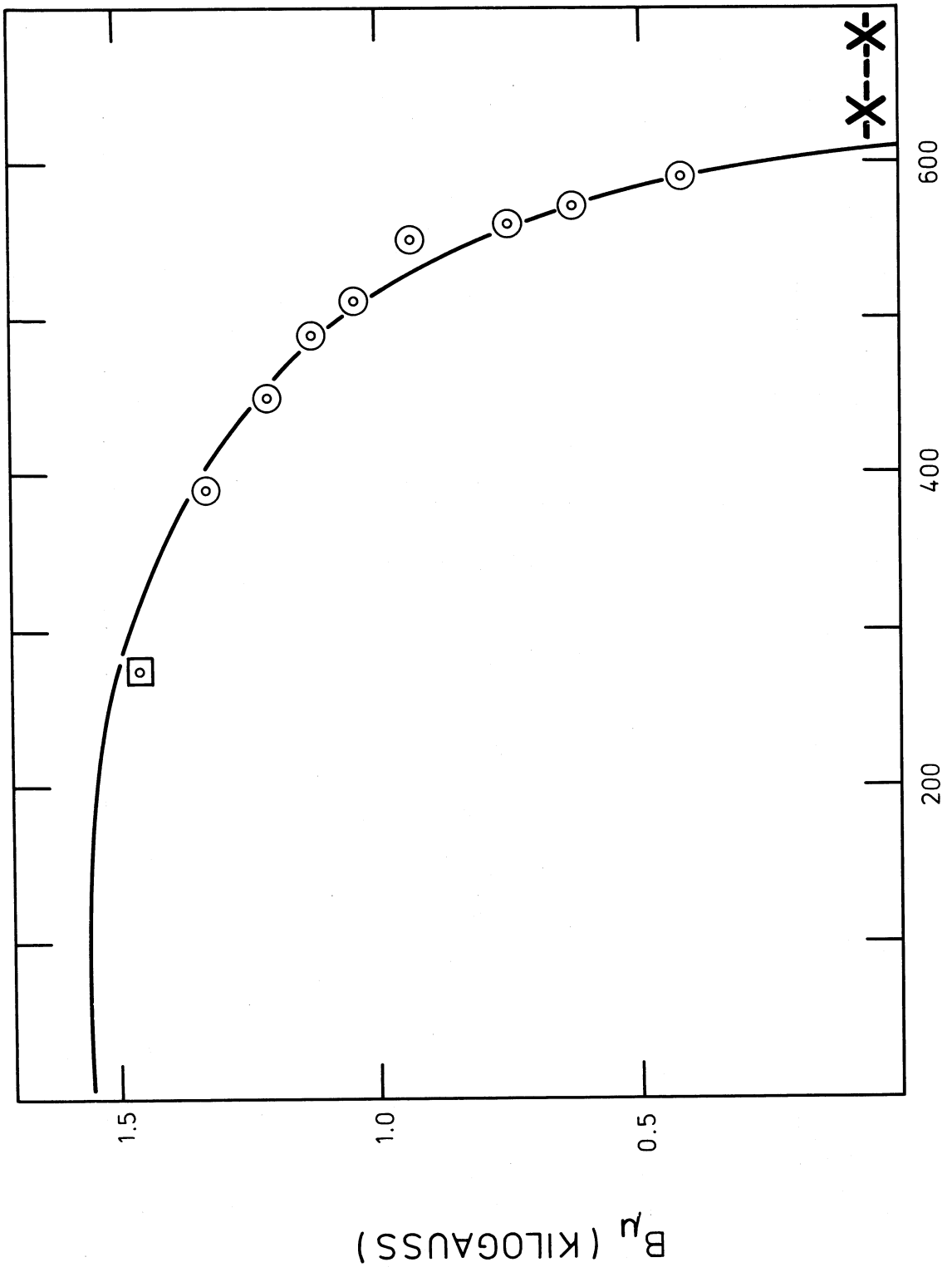

Fig. 2

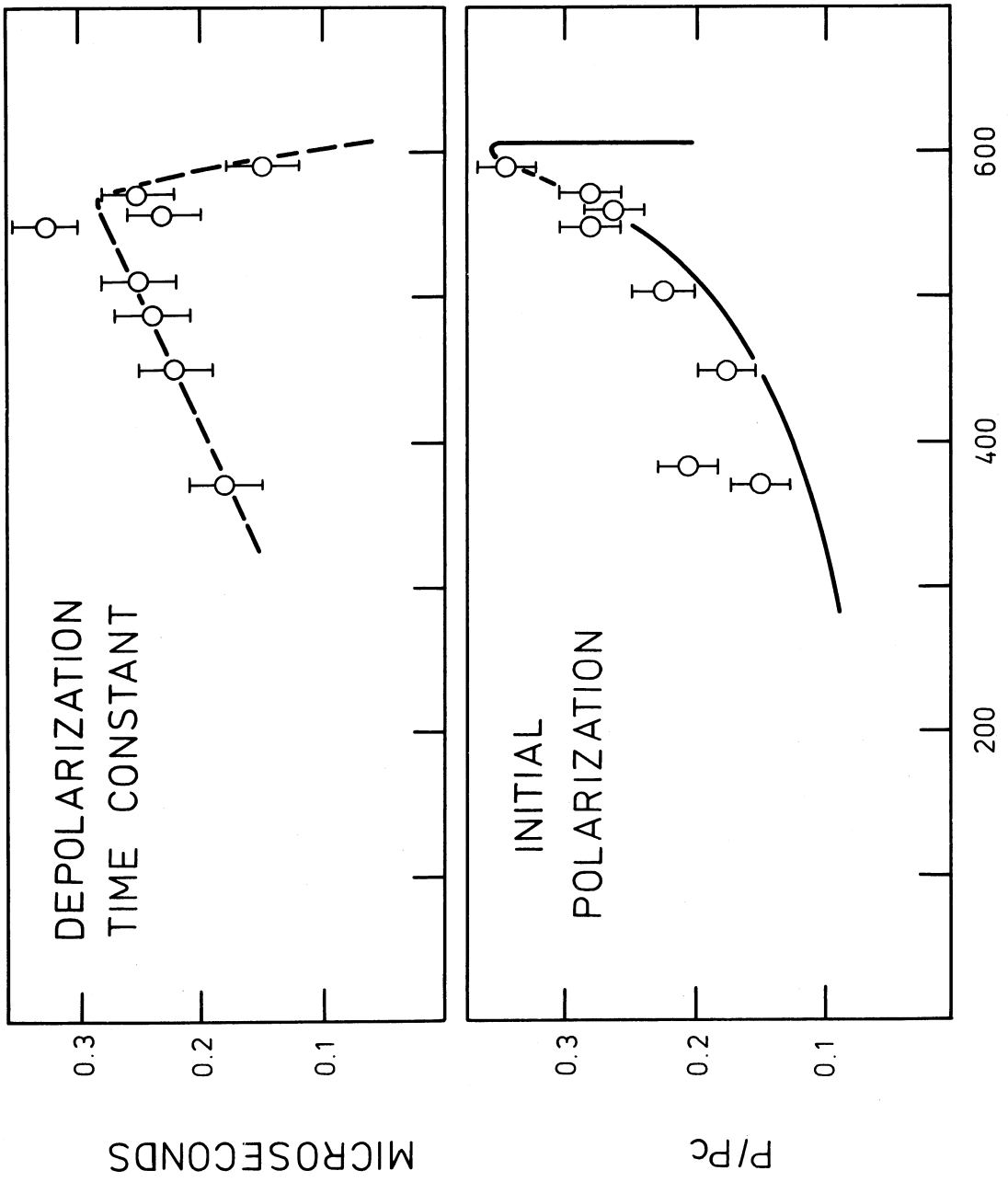
DEPOLARIZATION
TIME CONSTANT
MICROSECONDS
0.3
0.2
0.1
INITIAL
POLARIZATION
P/Pc
0.3
0.2
0.1
200
400
600
TEMPERATURE (°K)

Fig. 3

LIST OF PARTICIPANTS

AAS B., ETH Zürich, Switzerland
AEBISCHER D., University of Geneva, Switzerland
AKIMOV Y., Joint Institute for Nucl.Res.,Moscow, USSR
AMSLER C., ETH Zürich, Switzerland
ASHERY D., University, Tel Aviv, Israel
BAIER J., University of Vienna, Austria
BAILEY J., Daresbury Nucl. Physics Lab., Daresbury, GB
BEINER J., Institute of Physics of Neuchâtel, Switzerland
BEVERIDGE J.L., Lawrence Berkeley Lab. of Berkeley, U.S.A.
BOSCHITZ E., University of Karlsruhe, Germany
BOUYSSY A., C.N.R.S. Orsay, France
BREUNLICH W., University of Vienna, Austria
BRYMAN D.A., University of Victoria, B.C., Canada
CAMANI M.,ETH Zürich, Switzerland
CANNATA F., University of Bologna, Italy
CHRISTILLIN P., University of Pisa, Italy
CLOUGH A., University of Surrey, Great Britain
CORFU R.,University of Neuchâtel, Switzerland
CROWE K.M., University of California, Berkeley, U.S.A.
VAN DANTZIG R., IKO of Amsterdam, Netherlands
DAUM M., SIN, Villigen, Switzerland
DELLAFIORE A., University of Pisa, Italy
DEUTSCH J., University of Louvain, Louvain-la-Neuve, Belgium
DIEPERINK A., IKO of Amsterdam, Netherlands
DILLING M., University of Erlangen, Germany
DOMINGO J., CERN, Geneva, Switzerland
EATON G.H., SIN, Villigen, Switzerland
EDINGTON J.A., Queen Mary College of London, Great Britain
EGGER J., CERN, Geneva, Switzerland
EICHLER R., ETH Zürich, Switzerland
ENGELHARDT H.D., CERN, Geneva, Switzerland
ENGFER R., CERN, Geneva, Switzerland
FAURE J.-L., CEN Saclay, Gif-sur-Yvette, France
VON FELLENBERG H., University of Zürich, Switzerland
FETSCHER W., University of Karlsruhe, Germany
FISCHER U., Max-Planck-Institute of Freiburg, Germany
FISCHER W., SIN, Villigen, Switzerland
FRICKE G., University of Mainz, Germany
FROSCH R., SIN, Villigen, Switzerland
GABATHULER K., SIN, Villigen, Switzerland
GERBER H.-J., SIN, Villigen, Switzerland
GILLESPIE J., University of Grenoble, France
GRAF H., University of Zürich, Switzerland
GROSSMANN Z., SIN, Villigen, Switzerland
GUSTAFSON Ch., CEA, Paris, France
HARTMANN R., ETH Zürich, Switzerland
HIRT W., SIN, Villigen, Switzerland

HORLACHER G., University of Mainz, Germany
HUEFNER J., University of Freiburg, Germany
HUGUENIN P., Institute of Physics, Neuchâtel, Switzerland
INGRAM Q., U.B.C., Vancouver, Canada
JANETT A., SIN, Villigen, Switzerland
KIM C.W., CEN Saclay, Gif-sur-Yvette, France
KOCH H., CERN, Geneva, Switzerland
KOSSLER W., College of William and Mary, Williamsburg,U.S.A.
KUENDIG W., University of Zürich, Switzerland
LAMBERT E., University of Neuchâtel, Switzerland
LANG J., ETH Zürich, Switzerland
LECHANOINE C., University of Geneva, Switzerland
LEHMANN L., University of Freiburg, Germany
LEISI H.J., ETH Zürich, Switzerland
LENZ F., SIN, Villigen, Switzerland
LESNIAK H., Institute Fizyki Jadrowej, Krakow, Poland
LESNIAK L., Institute Fizyki Jadrowej, Krakow, Poland
LOCHER M.P., SIN, Villigen, Switzerland
LUNKE C., University of Neuchâtel, Switzerland
LYNEN U., CERN, Geneva, Switzerland
MAHLER H.J., ETH, Zürich, Switzerland
MARTIN J., CEN, Gif-sur-Yvette, France
MARTIN P.W., University of B.C., Vancouver, Canada
MEYER J., TU München Garching, Germany
MILLER J., CEN Saclay, Gif-sur-Yvette, France
PEARCE R.M., TRIUMPF, Vancouver, B.C. Canada
PEDRONI E., ETH, Zürich, Switzerland
PETITJEAN C., SIN, Villigen, Switzerland
PICCIOTTO C.E., University of Victoria, B.C., Canada
PIFFARETTI J., University of Neuchâtel, Switzerland
PILKUHN H., University of Karlsruhe, Germany
POWERS R., California Institute of Tech., Pasadena, Cal.U.S.A.
RENBERG P., University of Uppsala, Sweden
RHO M., CEN Saclay, Gif-sur-Yvette, France
RITTER H., CERN, Geneva, Switzerland
ROESSLE E., University of Freiburg, Germany
ROSA-CLOT M., University of Pisa, Italy
ROSSEL J., University of Neuchâtel, Switzerland
RUNGE K., University of Freiburg, Germany
SALOMON M., University of Vancouver, B.C., Canada
SAPP W., ETH Zürich, Switzerland
SAPP B., ETH Zürich, Switzerland
SAUDINOS J., CEN Saclay, Gif-sur-Yvette, France
SCHALLER L., University of Fribourg, Switzerland
SCHECK F., SIN, Villigen, Switzerland
SCHELLENBERG H., University of Fribourg, Switzerland
SCHENCK A., ETH Zürich, Switzerland
SCHMID C., ETH Zürich, Switzerland

SCHMIDT-ROHR U., Max-Planck-Institute of Heidelberg,Germany
SCHNEUWLY H., University of Fribourg, Switzerland
SCHUCAN T., SIN, Villigen, Switzerland
SCHWALLER P., SIN, Villigen, Switzerland
SCHWARZ E., University of Neuchâtel, Switzerland
SCHWITTER A., CERN, Geneva, Switzerland
SEVGEN A., University of Fribourg, Switzerland
SHUSTER M., University of Karlsruhe, Germany
STEINMANN O., SIN, Villigen, Switzerland
STRAUMANN N., SIN, Villigen and University of Zürich,Switz.
STRINI G., Institute of Physics, Milan, Italy
STROHBUSCH U., University of Freiburg, Germany
TANNER N., Nuclear Physics Lab., Oxford, Great Britain
TELEGDI V.L., University of Chicago, U.S.A.
THIES M., University of Heidelberg, Germany
TRUOEL P., University of Zürich, Switzerland
TSCHALAER C., SIN, Villigen, Switzerland
WALTER H.C., ETH, Zürich, Switzerland
WARREN J.B., CERN, Geneva, Switzerland
WARSZAWSKI J., University of Tel Aviv, Israel
WILKIN C., CERN, Geneva, Switzerland
WULLSCHLEGER A., ETH, Zürich, Switzerland
ZAVATTINI E., CERN, Geneva, Switzerland
ZEHNDER A., ETH Zürich, Switzerland
ZINOV V., Joint Institute for Nuclear Reseach, Moscow,USSR
ZUPANCIC C., University of München, Germany